The Role of Redox-dependent Reactions with Kras Cysteine 118 in Tumorigenesis

by

Lu Huang

Department of Pharmacology and Cancer Biology
Duke University

Date:_____

Approved:

_____
Christopher M. Counter, Supervisor

_____
Xiao-Fan Wang

_____
Jeffrey C. Rathmell

_____
Dennis J. Thiele

_____
David G. Kirsch

Dissertation submitted in partial fulfillment of
the requirements for the degree of Doctor
of Philosophy in the Department of
Pharmacology and Cancer Biology
in the Graduate School
of Duke University

2015

ABSTRACT

The Role of Redox-dependent Reactions with Kras Cysteine 118 in Tumorigenesis

by

Lu Huang

Department of Pharmacology and Cancer Biology
Duke University

Date:_____

Approved:

_____
Christopher Counter, Supervisor

_____
Xiao-Fan Wang

_____
Jeffrey C. Rathmell

_____
Dennis J. Thiele

_____
David G. Kirsch

An abstract of a dissertation submitted in partial
fulfillment of the requirements for the degree
of Doctor of Philosophy in the Department of
Pharmacology and Cancer Biology
in the Graduate School of
Duke University

2015

Abstract

The Ras family of small GTPases, comprised of the *KRAS*, *NRAS,* and *HRAS* genes, are mutated to encode constitutively-active, GTP-bound, oncogenic proteins in upwards of one quarter or more of all human cancers, which is well established to promote tumorigenesis. Despite the prominent role these genes play in human cancer, the encoded proteins have proven difficult to pharmacologically inhibit. Therefore, it is important to understand how Ras proteins are activated.

RAS proteins cycle between a GDP-bound inactive state and a GTP-bound active state through guanine nucleotide exchange factors (GEFs) and GTPase activating proteins (GAPs). GEFs facilitate the GDP-to-GTP exchange of RAS and promote RAS activation. Similar to GEFs, reactive oxygen/nitrogen species can also promote RAS activation through reactions with the thiol residue of cysteine 118 (C118). This residue may therefore play a role in RAS activation in cancer. To test this possibility, I investigated the effect of mutating C118 to serine (C118S) in Kras on (1) carcinogen-induced lung tumorigenesis, and (2) xenograft tumor growth of $HRAS^{12V}$-transformed cells.

To explore the impact of the C118S mutation in Kras on carcinogen-induced lung tumorigenesis, I introduced a C118S mutation into the endogenous murine *Kras* allele and exposed the resultant mice to the carcinogen urethane, which induces *Kras* mutation-positive lung tumors. $Kras^{+/C118S}$ and $Kras^{C118S/C118S}$ mice developed fewer and

smaller lung tumors than *Kras*$^{+/+}$ mice. Although the *Kras*^{C118S} allele did not appear to affect tumorigenesis when the remaining *Kras* allele was conditionally oncogenic (Kras^{G12D}), there was a moderate imbalance of oncogenic mutations favoring the native *Kras* allele in tumors from *Kras*$^{+/C118S}$ mice treated with urethane. Therefore, mutating C118 of *Kras* impedes urethane-induced lung tumorigenesis.

To explore the the impact of the C118S mutation in Kras on xenograft tumor growth of HRAS^{12V}-transformed cells, I tested and found that redox-dependent reactions with cysteine 118 (C118) and activation of wild type KRAS are critical for oncogenic HRAS-driven tumorigenesis. Such redox-dependent activation of KRAS affected both PI3K-AKT and RAF-MEK-ERK pathways. These findings were confirmed in the endogenous mouse *Kra*s gene. Speicfically, oncogenic HRAS-transformed *Kras*$^{C118S/C118S}$ MEFs grew in soft agar and as xenograft tumors more slowly than similarly transformed *Kras*$^{+/+}$ MEFs, suggesting that redox-dependent reactions with C118 of Kras promotes transformation and tumorigenesis.

Taken together, I have demonstrated a critical role of redox-dependent reactions with Kras C118 in tumorigenesis.

Contents

List of Tables

List of Figures

Acknowledgements

First of all, I would like to sincerely thank my advisor Dr. Christopher Counter for all his support and mentoring during my graduate studies. Without his effort, this dissertation would not have been completed. I would also thank my thesis committee members Dr. Xiao-Fan Wang, Dr. Jeffrey Rathmell, Dr. Dennis Thiele, and Dr. David Kirsch for all their valuable suggestions on my progress throughout my PhD training.

Furthermore, I want to thank Dr. Benjamin Lampson for assistance in the design of the *Kras*^{C118S} targeting vector and the Transgenic Mouse Facility at Duke Cancer Institute for aid in generating mice with a *Kras*^{C118S} allele, which laid the foundation for the work on *Kras*^{C118S} mice. I would also thank Dr. John Carney and Dr. Diana Cardona for their assistance in the histological analysis of the lung tumor sections, and Dr. Sharon Campbell, Dr. Aaron Hobbs, Dr. Donita Brady, and Matt Crowe for review of my manuscript on *Kras*^{C118S} mice. Moreover, I would like to thank Dr. Kian-Huat Lim for generation of important constructs used in this study, Dr. Nicole Pershing for her technical assistance with lung tumor models, Dr. David Kashatus for his help with the IKKα project, Jianqi Zhang for her assistance with statistical analysis and all members of Counter lab for their valuable advice and support throughout my time in the lab.

Finally, I am very grateful to all my friends and family, especially my parents Mr. Xiaoqing Huang and Ms. Xiaoqin Jiao, and my husband Dr. Zhiqiang Wang for their encouragement during my tough times and always showing me love and passion.

1. Introduction

1.1 RAS

1.1.1 RAS family of small GTPases: overview

1.1.1.1 RAS small GTPases: introduction

The RAS family of small GTPases functions as molecular switches, cycling between the GDP-bound inactive states and the GTP-bound active states (Takai, Sasaki et al. 2001). Upon receptor activation by upstream signals, guanine nucleotide exchange factors (GEFs) are activated, which stimulate the dissociation of GDP from RAS, promting the binding of free GTP (Quilliam, Rebhun et al. 2002). Binding of GTP activates RAS by inducing a conformational change in the protein structure that fosters the interaction with downstream effectors (Karnoub and Weinberg 2008). GTPase acting proteins (GAPs) bind to GTP-bound RAS and enhance the low intrinsic GTPase activity of RAS, accelerating GTP hydrolysis into GDP. This process returns RAS to the GDP-bound inactive state and terminates RAS signaling (Donovan, Shannon et al. 2002).

1.1.1.2 RAS signaling pathways

RAS proteins function as signal transducers to convert upstream extracellular signals to diverse downstream intracellular effects, thus playing critical roles in a variety of cellular phenotypes, such as cell growth, proliferation, and survival. Extracellular signals (such as growth factors) activate cell surface receptor tyrosine kinases such as epidermal growth factor receptor (EGFR) (Malumbres and Barbacid 2003), leading to their autophosphorylation and binding to adaptor proteins such as growth factor receptor bound protein 2 (Grb 2). RasGEFs, such as son of sevenless (SOS), are then recruited from the cytosol to the plasma membrane by these adaptor proteins. The recruited GEFs stimulate the release of GDP from on RAS proteins, which are anchored in the plasma membrane, promoting GTP-binding and activation of RAS (Malumbres and Barbacid 2003). Upon activation, RAS proteins can trigger many downstream pathways. Three most well-characterized downstream signaling pathways are the RAF/MEK/ERK, PI3K/AKT and RalGEF/Ral pathways, which promote cell proliferation, cell survival, and cell adhesion/motility (Karnoub and Weinberg 2008).

With regards to the RAF/MEK/ERK pathway, activated RAS recruits the MAP kinase kinase kinases (MAPKKK) of the RAF serine/threonine kinase family, composed of C-RAF, A-RAF and B-RAF, to the plasma membrane (Roberts and Der 2007). This recruitment allows RAFs to phosphorylate the MAP kinase kinase (MAPKK) MEK1/2.

MEK1/2, in turn, phosphorylate and activate the MAP kinases (MAPK) ERK1/2, which can phosphrylate and activate many downstream targets either in the cytoplasm or after translocating into the nucleus. Once translocated into the nucleus, ERK1/2 phosphorylates and activates transcription factors, activating many mitotic genes to promote cell proliferation (Deschenes-Simard, Kottakis et al. 2014).

With regards to the PI3K/AKT pathway, activated RAS binds and activates PI3K (phosphatidyl-inositol-3 kinase), a family of heterodimeric lipid kinases composed of a regulatory subunit (p85) and a catalytic subunit (p110) (Cully, You et al. 2006). Once activated, PI3K catalyzes conversion of PIP_2 (phophatidylinositol 4,5-biphosphate) into PIP_3 (phophatidylinositol 3,4,5-triphosphate) at the plasma membrane (Castellano and Downward 2011). PDK1 then binds to PIP_3 through a PH (pleckstrin homology) domain, leading to the activation of AKT serine/threonine kinase through phosphorylation at threonine 308 (Thr 308) (Engelman 2009). Active AKT phosphorylates a number of downstream targets that play roles in cell proliferation, cell growth and cell survival. For example, AKT phosphorylates BAD and caspase-9 to inhibit their pro-apoptotic functions and promote cell survival; it also phosphorylates glycogen synthase kinase-3β (GSK-3β) to inactivate it and prevent it from degrading cyclin D1, which regulates cell cycle. AKT phosphorylates and activates the mammalian target of rapamycin (mTOR) kinase, leading to an increase in cell growth. AKT also phosphorylates endothelial nitric

oxide synthases (eNOS) on serine 1177, leading to the activation of eNOS and production of nitric oxide (NO), which modifies and regulates numerous proteins to affect many cellular processes (Fulton, Gratton et al. 1999) (see 1.3.1 Nitric oxide and nitric oxide synthases).

With regards to the RalGEF/Ral pathway, activated RAS recruits RalGEFs (Ral guanine nucleotide exchange factors) to the plasma membrane, which then promote the exchange of GDP-to-GTP on the RAS-like small GTPases RalA and RalB. Ral proteins activate downstream effectors like SEC5, EXO84 and RalBP1, which are involved in filopodia formation, endocytosis, and actin dynamics (Feig 2003), thus playing important roles in cell adhesion, motility, and morphology. RalA has also been shown to play an important role in oncogenic RAS-induced tumor initiation, while RalB has been shown to play a more prominent role in RAS-mediated metastasis (Lim, O'Hayer et al. 2006).

1.1.1.3 RAS isoforms

The mammalian RAS family of small GTPases is composed of three genes: *HRAS*, *NRAS*, and *KRAS*. In the case of *KRAS*, the transcript can be spliced into two different products to generate KRAS 4A and KRAS 4B (Castellano and Santos 2011). Therefore, three *RAS* genes encode four proteins: HRAS, NRAS, KRAS 4A, and KRAS 4B. The

amino acid sequences of these proteins are very similar in the N-terminus, but variable in the C-terminus. The differences in C-terminal sequences confer isoform-specific C-terminal posttranslational modifications that regulate their specific cellular localizations (Arozarena, Calvo et al. 2011). All four proteins have a C-terminal CAAX motif (C is cysteine, A is aliphatic and X is any amino acid) that helps target RAS proteins to the membrane. The cysteine in the CAAX motif is farnesylated, followed by -AAX-proteolysis and methylation of the cysteine (Ahearn, Haigis et al. 2012). In addition to the irreversible farnesylation of this cysteine, stable membrane association of RAS also requires a second targeting signal. Specifically, HRAS and NRAS are additionally palmitoylated on one (NRAS) or two (HRAS) cysteines adjacent to the farnesylcysteine, and palmitoylated HRAS and NRAS localize to the plasma membrane and the surface of the Golgi apparatus (Hancock 2003). KRAS 4A is thought to be modified and trafficked similar to NRAS (Henis, Hancock et al. 2009). In constrast, KRas 4B instead contains a polybasic region and is primarily confined to the plasma membrane (Hancock 2003).

The isoform-specific lipid post-translational modifications and membrane localization of the the different RAS proteins may lead to their different preference for downstream effectors. For example, when ectopically expressed in COS-1 cells, KRAS 4B activates RAF more potently than the other RAS isoforms (Voice, Klemke et al. 1999). HRAS has been shown to more potently activate PI3K activity than KRAS (Yan, Roy et

al. 1998). Therefore, although the four RAS proteins may have redundant roles in cell proliferation, survival, and adhesion/motility, there is some functional specificity between the different isoforms.

1.1.2 The role of RAS in development

To understand the functional specificity of different RAS isoforms in normal development, the different genes have been knocked out in mice. These studies revealed that both *Nras* and *Hras* are dispensable for normal development (Umanoff, Edelmann et al. 1995, Ise, Nakamura et al. 2000). $Nras^{-/-}$; $Hras^{-/-}$ double knock-out mice are also viable, but are born at a reduced frequency (Esteban, Vicario-Abejon et al. 2001). In contrast, *Kras* is embryonic lethal, with $Kras^{-/-}$ embryos exhibiting heart dysfunction (Johnson, Greenbaum et al. 1997, Koera, Nakamura et al. 1997). Much of this may be due to loss of Kras 4B expression, as selective knockout of the Kras 4A splice variant is dispensable for development (Plowman, Williamson et al. 2003). Although *Kras* is the only isoform essential for mice development, the other *Ras* genes appear to have functional overlap with *Kras* in development. First, while $Nras^{-/-}$ mice are viable, $Nras^{-/-}$; $Kras^{+/-}$ mice are embryonic/neonatal lethal (Johnson, Greenbaum et al. 1997). Second, introduction of a human *HRAS* transgene can rescue the lethal phenotype of mice lacking *Kras* or other combinaitons of the three *Ras* genes (Nakamura, Ichise et al. 2008).

Besides null mutation, activating mutations of *RAS* genes also affect normal development. Germline activating mutations in *KRAS* (weak activating mutations such as V14I, T58I, D153V or N116S) have been found in patients with Noonan Syndrome, which is characterized by short statue, facial dysmorphism, cardiac defects, and susceptibility to develop juvenile myelomonocytic leukemia (Kratz, Schubbert et al. 2006, Schubbert, Shannon et al. 2007, Razzaque, Komoike et al. 2012). In agreement, knock-in mice with an activating $Kras^{G12D}$ mutant allele exhibit abnormal brain development and embryonic lethality by E11.5 (Tuveson, Shaw et al. 2004). Similarly, activating mutations in *HRAS* (strong activating mutations at glycine 12 or weak activating mutations such as K117R or A146T) are found in patients with Costello Syndrome, which is characterized by short stature, heart and facial abnormalities, mental retardation, and a susceptibility to rhabdomyosarcomas and neuroblastomas (Aoki, Niihori et al. 2005, Schubbert, Shannon et al. 2007). Consistent with this, knock-in mice with a germline activating $HRAS^{G12V}$ allele have high perinatal lethality, high susceptibility to cancer, and craniofacial abnormalities (Schuhmacher, Guerra et al. 2008, Chen, Mitsutake et al. 2009). Interstingly, germline activating mutations in *NRAS* are not associated with developmental disorders, except in one case in which an activating germline $NRAS^{G13D}$ mutation was identified in a patient with an autoimmune lymphoproliferative syndrome and a history of childhood leukemia (Oliveira, Bidere et al. 2007).

In summary, among the three *Ras* genes, *Kras* is the only isoform that is essential for development, as evidenced by the embryonic lethality of both *Kras* knock-out mice and $Kras^{G12D}$ (strong activating mutation) knock-in mice. Those findings not only suggest a unique role of wild-type *Kras* in development, but also indicate the importance of a well-controlled regulatory mechanism to regulate the activation of Kras. Therefore, it is necessary to investigate on the regulation of KRAS activity *in vivo*.

1.1.3 The role of RAS oncogenes in cancer

1.1.3.1 Oncogenic mutations in RAS genes are found in cancer

In a quarter or more of all human cancers, one of the three *RAS* genes harbor an activating "oncogenic" mutation, which is well established to drive tumorigenesis (Downward 2003). These oncogenic mutations usually occurr at amino acid G12, G13, or Q61 (Prior, Lewis et al. 2012), altering the intrinsic as well as GAP/GEF mediated GTP hydrolysis or GDP-to-GTP exchange activity, thereby locking RAS in an active GTP-bound state and leading to constitutive activation of the protein (Smith, Neel et al. 2013). Usually only one of the three *RAS* isofroms bears an oncogenic mutation depending on the type of cancer, athough the frequency is not equally distributed among the three *RAS* isoforms. More specifically, about 85% of all *RAS* mutations in cancer are in *KRAS*, about 15% in *NRAS*, and 1% in *HRAS*. Mutations in the *KRAS* gene have been shown to

occur in 95% of pancreatic tumors, 50% of colon tumors, and 30% of lung adenocarcinomas, whereas mutations in the *NRAS* gene are the predominant form in myeloid leukemia and melanomas (Pylayeva-Gupta, Grabocka et al. 2011, Prior, Lewis et al. 2012, Cox, Fesik et al. 2014).

1.1.3.2 Oncogenic RAS proteins drive cellular transformation

A wealth of studies demonstrate that introduction of oncogenic mutations into any of the three *RAS* isoforms imparts transformed and tumorigenic phenotypes to cells, as assessed by focus formation or anchorage-independent growth *in vitro* (in soft agar) and tumorigenicity *in vivo* (in immunocompromised mice) respectively (Malumbres and Barbacid 2003). There are, however, isoform-specific differences in terms of the ability of the different oncogenic RAS protein to drive cellular transformation that are extremely context dependent. For example, $NRAS^{G12V}$ and $KRAS4A^{G12V}$ are the most transforming oncoproteins when ectopically expressed in RIE-1 rat epithelial cells, as assessed by anchorage-independent growth (Voice, Klemke et al. 1999). $HRAS^{G12V}$ and $KRAS4A^{G12V}$, when expressed in multiple rodent epithelial cells, were reported to be the most potently transforming RAS isforms as assessed by focus formation assay (Voice, Klemke et al. 1999). Another study showed that ectopic expression of $HRAS^{G12V}$ in NIH3T3 mouse fibroblasts was the most transforming isoform compared with $KRAS^{G12V}$ and $NRAS^{G12V}$

in both anchorage-independent growth and focus formation assays (Maher, Baker et al. 1995). More recently, oncogenic $HRAS^{G12V}$ was shown to be more effective at promoting soft agar growth and tumorigenesis of SV40-transfromed human embryonic kidney cells (Lampson, Pershing et al. 2013).

1.1.3.3 Targeting oncogenic RAS in cancer

Despite the prominent role *RAS* oncogenes play in human cancer, the encoded RAS oncoproteins have proven difficult to pharmacologically inhibit. As such, efforts have focused on targeting downstream pathways. Drugs targeting these individual pathways show limited clinical efficacy in the treatment of RAS mutation-positive cancers as monotherapies. Therefore, combinations of multiple drugs that target different points within the RAS signaling network are being explored (Gysin, Salt et al. 2011), but whether the toxicity of multiple drugs can be tolerated remains to be determined .

Besides targeting RAS downstream pathways, there are other approaches to inhibit RAS signaling and block tumorigenesis. The most straightforward method is to decrease the levels of oncogenic RAS. Inducible knockdown of $HRAS^{G12V}$ or $KRAS^{G12V}$ in mice caused tumor regression (Chin, Tam et al. 1999, Lim and Counter 2005) . These studies suggest that ablating RAS signaling could be useful in treating RAS-driven

cancers, but genetic ablation of oncogenic RAS is difficult to achieve in human cancer patients.

Another approach is to suppress RAS activity. As mentioned in **1.1.1.3**, post-translational modification of RAS, particularly farnesylation at the cysteine within the CAAX motif, is essential for RAS localization and activity. Substitution of this critical cysteine with serine makes RAS proteins unable to be farnesylated, and this RAS mutant turned out to be inactive and cannot transform cells (Willumsen, Norris et al. 1984). In this regard, farnesyltransferase inhibitors (FTIs) were developed, and proven to lead to the regression of oncogenic HRAS-driven tumors in mice (Kohl, Omer et al. 1995) . However, these results could not be recapitulated in human clinical trials, probably because most human cancers are driven by oncogenic KRAS/NRAS rather than HRAS, and KRAS or NRAS can undergo alternative geranylgeranylation when the farnesyltransferase is inhibited (James, Goldstein et al. 1995, Whyte, Kirschmeier et al. 1997, Zhang, Kirschmeier et al. 1997).

As mentioned in **1.1.1.1**, RAS activity can be regulated by GEFs and GAPs, so targeting RAS GEFs may be another way to block RAS activation. Similar to GEFs, NO can promote the RAS GDP-to-GTP exchange through its reactions with RAS C118 and thereby activating RAS (will be discussed in **1.3.4 Redox dependent activation of RAS**

through C118). Therefore, understanding this regulation of RAS activity may be helpful in developing new methods to inhibit RAS-driven tumors.

1.1.4 The role of wild-type RAS in cancer

1.1.4.1 Tumor-suppressive vs. tumor promoting role of wild-type RAS

Beyond the oncogenic versions of the *RAS* genes, accumulating evidence also supports an important role for the remaining non-mutated RAS proteins in cancer. The non-mutated wild-type RAS proteins appear to suppress or promote tumorigenesis in a context-dependent manner. In terms of a tumor-suppressive role, loss of one wild-type *Kras* allele in mice increases their susceptibility to tumorigenesis driven by the carcinogen urethane, which induces oncogenic mutations in *Kras* that leads to lung adenomas (Zhang, Wang et al. 2001). Furthermore, loss of one or both of any of the wild-type *Ras* alleles in mice increases the sensitivity to tumorigenesis in the same carcinogen-induced *Kras* mutation-positive lung tumor model (To, Rosario et al. 2013). These findings suggest wild-type RAS proteins suppress tumorigenesis in some settings.

In terms of a tumor-promoting role, loss of one or both of *Hras* or *Nras* allele(s) renders mice more resistant to DMBA and TPA treatment, which induces skin papillomas with an oncogenic mutation in *Hras* (To, Rosario et al. 2013). Wild-type

KRAS has also been shown to promote tumorigenesis through counteracting mutant KRAS-induced apoptosis in colorectal cancer (Matallanas, Romano et al. 2011). Similarly, a number of recent studies have demonstrated a tumor-promoting role of wild-type HRAS and NRAS in oncogenic KRAS-driven tumorigenesis by mediating RTK (Receptor Tyrosine Kinases) signaling (Young, Lou et al. 2013) or modulating the DNA damage response (Grabocka, Pylayeva-Gupta et al. 2014). These findings suggest wild-type RAS proteins can promote tumorigenesis in some settings.

1.1.4.2 Activation of wild-type RAS in oncogenic RAS-driven tumors

It is becoming increasingly clear that wild-type RAS proteins can be activated in the presence of an oncogenic protein. Indeed, wild-type HRAS and NRAS were found to be activated through oncogenic KRAS-dependent stimulation of the RasGEF member SOS in *KRAS* mutation-positive cancer cells (Jeng, Taylor et al. 2012). Activation of wild-type HRAS and NRAS proteins can also occur through endothelial nitric oxide synthases (eNOS), which generates nitric oxide (NO) and mediates the *S*-nitrosylation at RAS cysteine 118 (C118) and activation of the protein. More specifically, NO as well as other free radical oxidants can facilitate *S*-nitrosylation or *S*-glutathiolation and activation of RAS in a manner dependent upon the thiol residue of C118 (Lander, Milbank et al. 1996, Raines, Bonini et al. 2007, Hobbs, Bonini et al. 2013). Substitution of C118 for serine

(C118S), a very minor modification in which the thiol residue of this cysteine is replaced with a hydroxyl group, renders RAS completely insensitive to activation by free radical oxidants, with no measureable effect on the protein structure, GTPase activity, intrinsic and GEF-mediated guanine nucleotide dissociation rate, or the ability to bind an effector (Lander, Milbank et al. 1996, Lander, Hajjar et al. 1997, Mott, Carpenter et al. 1997, Williams, Pappu et al. 2003, Adachi, Pimentel et al. 2004, Heo and Campbell 2004, Clavreul, Adachi et al. 2006, Raines, Cao et al. 2006, Hobbs, Bonini et al. 2013). In cancer cells, activation of PI3K-AKT pathway downstream of oncogenic KRAS results in phosphorylation of S1177 on eNOS and activation of the enzyme, which leads to elevated *S*-nitrosylated and GTP-bound wild-type HRAS and NRAS (Lim, Ancrile et al. 2008). Reducing the expression of these wild-type RAS proteins by shRNA impedes oncogenic RAS-driven tumorigenesis, an effect rescued by re-expressing wild-type HRAS or NRAS, but not the C118S mutant variants (Lim, Ancrile et al. 2008). These results support a role for redox-dependent reactions with C118 of wild-type HRAS and NRAS in oncogenic KRAS-driven tumorigenesis. However, it remains unclear whether wild-type KRAS is also important for mediating oncogenic RAS signaling in cells through redox-dependent reactions on C118. Thus, we explored the effect of mutating C118 to serine in KRAS on oncogenic HRAS-driven tumorigenesis in Chapter 4.

1.2 Mouse models to study RAS tumorigenesis

1.2.1 Carcinogen-induced tumorigenesis

A number of carcinogens can induce an oncogenic mutation in one of the *Ras* genes, which drives the formation and growth of primary tumors at a certain organ site (Nuzum, Malkinson et al. 1990, Ichikawa, Yano et al. 1996). Two of the most well characterized mouse tumor models will be discussed here: urethane-induced lung tumor model and DMBA/TPA-induced skin tumor model.

1.2.1.1 Urethane chemical carcinogenesis in the lung

Urethane, also known as ethyl carbamate, is a carcinogen that causes DNA adducts and thus somatic mutation during nucleotide repair (Barbin 2000). A single intraperitoneal (IP) injection of urethane into mice primarily initiates *Kras* mutations in the lung, leading to lung adenomas or adenocarcimas (Barbin 2000). Most of the oncogenic mutations in *Kras* occur at codon 61, resulting in Q61R or Q61L mutations (You, Candrian et al. 1989). Given the prevalence of *KRAS* mutations in human lung cancer (Ding, Getz et al. 2008), this approach models a *Kras* mutation-positive cancer spontaneously arising from an environmental insult (You, Candrian et al. 1989) in the lung.

Different mouse strains may have different susceptibility to urethane-induced tumorigenesis, and several genomic loci have been identified to be associated with this strain-specific difference. One such locus, *Pulmonary Adenoma Susceptibility 1(Pas1)*, maps to a region containing six genes, one being *Kras* (Malkinson 1989, Matzinger, Chen et al. 1997, Manenti, Galbiati et al. 2004). Therefore, it is critical to ensure that the *Kras* alleles of mice in a study using this carcinogen arise from the same genetic background.

1.2.1.2 DMBA/TPA chemical carcinogenesis in the skin

The mouse model of DMBA/TPA chemical carcinogenesis in the skin is a two-stage application of chemicals to the murine skin for the initiation and promotion of skin tumors, including a single topical administration of the chemical mutagen 7,12-dimethylbenz[*a*]anthracene (DMBA) followed by repeated topical applications of a pro-inflammatory phorbol ester 12-O-tetradecanoylphorbol 13-acetate (TPA) (Filler, Roberts et al. 2007). DMBA function as an initiator, which initiates an irreverable oncogenic mutation in *Hras* within the skin, yielding "potential tumor cells" or "initiated cells" (Hecker 1987). When exposed to promoters such as TPA, these "initiated cells" may obtain a second additional genomic or epigenomic insult and therefore exhibit a selective advantage of growth over surrounding normal cells. This will eventually lead to the development of either Squamous Cell Carcinoma (SCC) or benign papillomas that

may or may not later progress to SCC (Filler, Roberts et al. 2007). Over 90% of the DMBA-initiated skin tumors, including premalignant papillomas, were found to have a specific A→T transversion at the second nucleotide of codon 61, resulting in a Q61L mutation in *Hras* (Quintanilla, Brown et al. 1986).

Using this DMBA/TPA chemical carcinogenesis model on genetically engineered mice could help identify important molecular pathways involved in skin tumorigenesis and provide an opportunity to monitor early and late events in cancer development and progression (Filler, Roberts et al. 2007). Again, the susceptibility to DMBA/TPA induced skin tumorigenesis varies among different mouse strains. For example, the FVB/n strain is particularly susceptible, while the C57BL/6 strain is relatively resistant to tumor formation (Hennings, Glick et al. 1993, Elmets, Athar et al. 1998, Woodworth, Michael et al. 2004).

1.2.2 Tumorigenesis driven by conditional expression of oncogenic RAS

Besides carcinogen-induced spontaneous mutations in *Ras* genes and *de novo* tumorigenesis, mice can also be genetically engineered to express a conditionally oncogenic *Ras* allele that can lead to tumorigenesis upon Cre-mediated recombination and expression of an oncogenic *Ras*. The most well characterized genetically engineered mice for use in this model are mice in which a *LSL-Kras*^{G12D} allele, with two *loxP* sites

flanking a transcriptional/translational STOP sequence (LSL) upstream of *Kras* harboring a G12D oncogenic mutation, are knocked into the endogenous *Kras* locus (Johnson, Mercer et al. 2001). Cre recombinase, expressed in a specific vector or under a specific promoter, mediates recombination of the two *loxP* sites in the targeted tissue, excising the transcriptional/translational STOP sequence and inducing the expression of the oncogenic $Kras^{G12D}$ allele under the endogenous promoter, resulting in tumorigenesis. Adeno-Cre-induced lung tumorigenesis and Pdx1-Cre-induced pancreatic tumorigenesis will be discussed here.

1.2.2.1 Lung tumorigenesis driven by Ad-Cre induced conditional expression of oncogenic Kras

In mice with a *LSL-*$Kras^{G12D}$ allele, infection of lung tissue upon intranasal administration of a recombinant adenovirus expressing Cre recombinase (Ad-Cre) induces recombination of two *loxP* sites flanking STOP sequence (LSL), thereby allowing the expression of the $Kras^{G12D}$ allele in the lung and driving lung tumorigenesis (Jackson, Willis et al. 2001). This mouse lung tumor model allows control of the multiplicity and timing of tumor initiation by controlling the dose of Ad-Cre and the time of the administration. The ability to synchronize tumor initiation in these mice can help characterize the stages of lung tumor progression (Jackson, Willis et al. 2001).

1.2.2.2 Pancreatic precancerous lesions driven by Pdx1-Cre induced conditional expression of oncogenic Kras

Mice with a *LSL-Kras^{G12D}* allele can also be crossed with transgenic mice expressing *Pdx1-Cre*, which encodes Cre recombinase driven by *Pdx1* promoter specific for pancreatic tissues. In *Pdx1-Cre; LSL-Kras^{G12D}* mice, Cre recombinase is expressed mainly in the progenitor cells of pancreas, and mediates the recombination of *loxP* sites and expression of oncogenic *Kras^{G12D}* in pancreatic tissues early in development (Hingorani, Petricoin et al. 2003). Physiological levels of *Kras^{G12D}* induce ductal lesions that recapitulate human pancreatic intraepithelial neoplasias (PanINs), precursors to invasive pancreatic cancer (Hingorani, Petricoin et al. 2003). At low frequencies, these PanIN lesions can progress spontaneously to invasive and metastatic pancreatic ductal adenocarcinomas (PDAC) (Hingorani, Petricoin et al. 2003). This mouse model allows the study on molecular pathways that are important for pancreatic tumor development.

1.2.3 Xenograft tumor growth of cancer cell lines

In addition to mouse models of *de novo* tumorigenesis, RAS oncogenesis can also be studied as xenografts whereby cell lines are transplanted into immunocompromised mice. This approach has the advantage of being rapid and genetically manipulable, as the injected cells, rather than the mouse can be genetically manipulated. The drawback of this approach is that cell lines are the source of the tumor, which can differ genetically

from the original cancer. Furthermore, the model can only be used to model later stages of tumorigenesis, because the injected cells would be either established cancer cell lines or primary cells immortalized with SV40 early region (including large T and small t antigen), which inactivates tumor suppressors such as p53 and p16 and activates c-Myc (Pipas 2009).

1.3 Nitric oxide signaling and cancer

1.3.1 Nitric oxide and nitric oxide synthases

Nitric oxide (NO) is a diffusible free radical gas that was originally identified as a signaling molecule that is produced in endothelial cells and mediates vascular smooth muscle cells relaxation and blood vessel dilation (Harrison 1997). Subsequent studies have discovered that NO plays diverse and important roles in normal physiology (Hirst and Robson 2011), including immunity (Wink, Hines et al. 2011), neurotransmission (Hirst and Robson 2011), and vascular homeostasis (Dudzinski and Michel 2007). NO is generated by nitric oxide synthases (NOS), which include three isoforms: neuronal NOS (nNOS or NOS 1), inducible NOS (iNOS, or NOS 2) and endothelial NOS (eNOS, or NOS 3) (Foster, Hess et al. 2009). All three isoforms of NOS enzymes function as homodimers to couple reduction of NADPH with oxidation of L-arginine to generate L-citrulline and NO.

The three isoforms of NOS, while all generating NO, are regulated in different manners. iNOS is expressed in certain tissues upon induction by inflammatory cytokines (Nathan and Xie 1994). Once expression is induced, iNOS is primarily localized to cytosolic particulate fractions such as vesicles in macrophages (Michel and Feron 1997). iNOS binds to activated calmodulin (Ca^{2+} bound) with resting levels of intracellular Ca^{2+},

and can be activated upon induction of iNOS expression. nNOS and eNOS, however, are constitutively expressed at low levels in many tissues, and are primarily localized to membranes (Alderton, Cooper et al. 2001). Their localization and activity are regulated by posttranslational modifications and interactions with other molecules (Michel and Feron 1997, Geller and Billiar 1998, Alderton, Cooper et al. 2001). Both nNOS and eNOS can be activated through their interaction with activated (Ca^{2+} bound) calmodulin (which require upregulated intracellular Ca^{2+}) and the resulting NOS conformational change that promotes their catalytic activity (Nathan and Xie 1994). In the case of eNOS, phosphorylation at serine 1177 (S1177) by AKT at the plasma or Golgi membranes activates this enzyme (Michell, Griffiths et al. 1999, Gonzalez, Kou et al. 2002). A phospho-mimetic S1177D mutation in eNOS renders this enzyme constitutively active, while an S1177A mutation renders it inactive (Dimmeler, Fleming et al. 1999).

1.3.2 Nitric oxide signaling

1.3.2.1 Nitric oxide signaling through cGMP (Cyclic guanosine monophosphate)

In response to acetylcholine stimulation, NO generated by endothelial nitric oxide synthase (eNOS) in endothelial cells is released from the endothelium, leading to relaxation of neighboring vascular smooth muscle and dilation of blood vessels

(Moncada and Higgs 1993). This is achieved through NO-stimulated sGC/cGMP signaling pathway. More specifically, NO released from endothelial cells diffuses into neighboring vascular smooth muscle cells, where it binds to the haem iron of soluble guanylate cyclase (sGC) and activates sGC, resulting in increased production of cGMP and activation of protein kinase G, which can signal to myosin kinases and cause a relaxation in smooth muscle tissue (Hess, Matsumoto et al. 2005, Dudzinski, Igarashi et al. 2006).

1.3.2.2 Nitric oxide signaling through *S*-nitrosylation

In addition to the sGC/cGMP signaling pathway, NO can also regulate cell signaling through a type of protein post-translational modification termed *S*-nitrosylation (Stamler, Lamas et al. 2001). During *S*-nitrosylation, an NO group is covalently attached to the thiols (-SH) of cysteine (Cys) residues to allow the formation of *S*-nitrosothiol (SNO). *S*-nitrosylation can affect the functions of many proteins, thus playing important roles in cell signaling and normal physiology, and dysregulated *S*-nitrosylation is related with human diseases, including cancer (Stamler, Lamas et al. 2001, Mannick and Schonhoff 2002, Hess, Matsumoto et al. 2005, Foster, Hess et al. 2009). Therefore, it is critical to study how *S*-nitrosylation influences protein functions and how dysregulated *S*-nitrosylation results in certain diseases.

Up to now, many studies have shown that *S*-nitrosylation can affect protein functions in a variety of ways, including: 1) promoting formation of disulfide bonds between molecules and dimerization of proteins (Akhand, Pu et al. 1999, Cho, Nakamura et al. 2009), 2) inactivating proteins with cysteines at the active site (e.g. caspases, phosphatases, and possibly deubiquitinases (Mannick, Schonhoff et al. 2001, Yu, Li et al. 2005), and 3) promoting the activation of small GTPases such as RAS and DRP1 (Lander, Milbank et al. 1996, Lim, Ancrile et al. 2008, Cho, Nakamura et al. 2009). In terms of RAS *S*-nitrosylation and activation, however, some studies argued that it is the process of *S*-nitrosylation in redox environment rather than the *S*-nitrosylated RAS end product that promotes RAS activation (Raines, Bonini et al. 2007). This will be discussed in **1.3.4 Redox-dependent activation of RAS through C118**.

1.3.3 Nitric oxide, NOS and cancer

1.3.3.1 The role of nitric oxide in cancer

The role of nitric oxide in cancer is context-dependent and quite complex. NO has been shown to either promote or inhibit tumorigenesis depending on tumor type, the initiating oncogene, tumor suppressor mutation, tumor cell intrinsic versus stromal source of NO, perturbation of different NOS isoforms, and assessment of *de novo*

tumorigenesis versus xenograft tumor growth of established tumor cell lines (Fukumura, Kashiwagi et al. 2006). Another important factor is the dose of NO (Bonavida and Baritaki 2011), with high doses promoting cell death and low doses being more likely to promote tumorigenesis (Singh and Gupta 2011).

NO could influence tumorigenesis through protein *S*-nitrosylation. Numerous proteins that influence cancer, including RAS, HIF-1α, dynnamin, COX-2, PTEN, p53, BCl-2 and NF-κB p65, have been found to be targets of *S*-nitrosylation (Foster, Hess et al. 2009). It is important understand how the *S*-nitrosylation or denitrosylation of a protein affects its activity and the influence of such a change on cancer.

1.3.3.2 The role of nitric oxide in lung cancer

The role of nitric oxide in lung cancer is also complex. Human lung cancer patients have been found to be more likely to exhale high levels of NO and nitrite (Masri, Comhair et al. 2005, Kallianos, Tsimpoukis et al. 2013), with elevated levels of nitrated serum proteins indicative of nitrosative stress (Pignatelli, Li et al. 2001). The production of NO in chronic inflammation may contribute to the carcinogenesis (Yang, Taboada et al. 2009). In another study, however, high levels of immunohistochemical staining of NOS in human lung cancer samples were associated with better prognosis (Puhakka, Kinnula et al. 2003). In mouse models of *de novo* lung tumorigeneis, *iNOS*

knockout mice have shown decreased lung tumorigenesis after exposure to the carcinogen urethane, which induces $Kras^{Q61R/L}$ mutations (Nuzum, Malkinson et al. 1990, Kisley, Barrett et al. 2002). Interestingly, NO can be generated from urethane derivatives in the appropriate conditions *in vitro* (Sakano, Oikawa et al. 2002). These studies indicate that NO may play an important role in urethane-induced *de novo* lung tumorignesis.

1.3.3.3 The role of eNOS in cancer

Among the three NOS isoforms, only eNOS has been shown to mediate tumor maintenance. Upon activation by oncogenic RAS-PI3K-AKT signliang cascade, eNOS generates NO that can promote the *S*-nitrosylation and activation of the endogenous wild-type RAS proteins, thereby promoting tumorigenesis (Lim, Ancrile et al. 2008). This role of eNOS was implicated in at least two types of cancer: skin tumors and pancreatic cancer. First, upon initial treatment with DMBA followed by repeated application with TPA, which are known to induce oncogenic Hras-driven skin tumors, $eNOS^{-/-}$ mice had an approximate three-fold drop in the number of skin papillomas per mouse compared to the control $eNOS^{+/+}$ mice (Lim, Ancrile et al. 2008), suggesting a tumor-promoting role of eNOS in skin tumor development. Second, knockdown of eNOS in certain human pancreatic cancer cells reduced tumor growth, demonstrating a

requirement for eNOS in the tumor growth of human pancreatic cancer cells (Lim, Ancrile et al. 2008). Furthermore, either pharmacological inhibition of NOS by L-NAME or genetic ablation of *eNOS* by shRNA slowed disease progression in a mouse model of *de novo* $Kras^{G12D}$-driven pancreatic cancer (Lampson, Kendall et al. 2012), indicating a critical role of eNOS in pancreatic cancer progression. To better understand the role of eNOS in tumorigenesis, it is important to find more potential targets of *S*-nitrosylation downstream of eNOS.

1.3.4 Redox-dependent activation of RAS through C118

1.3.4.1 Redox-dependent reactions with RAS C118 promotes RAS activation

As mentioned above, *S*-nitrosylation and activation of wild-type RAS proteins mediated by eNOS-generated NO can promote tumorigenesis (Lim, Ancrile et al. 2008). Thus, it is important to understand how NO can promote RAS activation.

NO and other reactive nitrogen or oxygen species (RNS or ROS) derived from NO can react with the thiol residue of the surface-accessible cysteine 118 (C118) of GDP-bound RAS to promote the release of the nucleotide (GDP), generating a covalent bond of nitrogen with the thiol residue of C118, in a process termed *S*-nitrosylation (Lander, Hajjar et al. 1997, Heo and Campbell 2004, Raines, Bonini et al. 2007). Release of GDP

then favors binding of GTP, rendering RAS active (Lander, Hajjar et al. 1997, Raines, Bonini et al. 2007). Similarly, reactive nitrogen or oxygen species can react with glutathione (GSH) (Hill and Bhatnagar 2012), which in turn can covalently bond with the thiol residue of C118 in RAS (Adachi, Pimentel et al. 2004), in a process termed *S*-glutathiolation (Hill and Bhatnagar 2012), which can also lead to elevated levels of GTP-bound RAS (Adachi, Pimentel et al. 2004, Clavreul, Adachi et al. 2006). Actually, in addition to NO and glutathione, the thiol group of RAS C118 can react with many other thiol oxidants, including superoxide, hydrogen dixode, cystamine, diamide, NO-drived oxidants (such as nitrogen dixode and peroxynitrite) and oxidized glutathione (such as glutathione disulfate and *S*-nitroglutathione) (Mallis, Buss et al. 2001, Lancaster 2008). These reactions happen in redox environment and are termed redox-dependent reactions with RAS C118.

Studies on how redox-dependent reactions with RAS C118 promote RAS activation suggest a radical-based mechanism for the free radical oxidants to promote RAS *g*uanine *n*ucleotide *e*xchange (GNE). More specifically, NO could react with O_2 and form $\cdot NO_2$, which then reacts with the thiol of RAS C118 to form a RAS C118 thiyl radical intermediate (RAS $S^{118\cdot}$). This RAS thiyl radical intermediate will convert to a RAS-GDP guanine radical ($G^{\cdot+}DP$), which is particularly sensitive to reaction with free radicals ($\cdot NO_2$), with the end products being nitrothiols (S-nitrosylated RAS). In this

process, the formation of this guanine radical is likely to alter interactions with Ras, resulting in dissociation of Ras bound GDP and binding of GTP to RAS, thereby promoting RAS GNE and thus RAS activation (Heo and Campbell 2004, Raines, Bonini et al. 2007). Similarly, RAS C118 thiyl radical intermediate (RAS $S^{118\cdot}$) can also interact with oxidized glutathione to form RAS GSS· radical, which then generates the end product glutathiolated RAS (Hobbs, Bonini et al. 2013). In this process, the formation of this radical promotes GDP release and subsequent GTP loading, thus facilitating RAS activation. As an important note, the end product of *S*-nitrosylated RAS or *S*-glutathiolated RAS does not promote GDP-to-GTP exchange of RAS. Actually, the *S*-nittrosylated RAS or *S*-glutathiolated RAS can protect the protein from radical-based nucleotide dissociation (Hobbs, Bonini et al. 2013).

1.3.4.2 Redox-dependent reactions with RAS C118 promotes RAS signaling, cell proliferation and tumorigenesis

Accumulating evidence suggests that this redox-dependent activation of RAS through C118 has cellular consequences. Specifically, expressing activated eNOS increases the level of *S*-nitrosylated and GTP-bound NRAS in a manner dependent upon C118 in T-cells. Such activation stimulates the MAPK pathway upon conjugation with APC cells, although MAPK activation is not always the product *S*-nitrosylated RAS (Raines, Cao et al. 2006). Both an increase in iNOS protein levels upon cytokine

stimulation, and stimulation of ATP-sensitive potassium channels by NO, appear to be dependent upon C118 of HRAS (Lin, Raab-Graham et al. 2004, Lee and Choy 2013). Furthermore, angiotensin II stimulation of smooth muscle cells, or treatment of endothelial cells with peroxynitrite, results in *S*-glutathiolation and an increase in the levels of GTP-bound HRAS (Adachi, Pimentel et al. 2004, Clavreul, Adachi et al. 2006). With regards to cancer, treating a variety of cells with NO donors or agents to increase NO levels increases the level of *S*-nitrosylated and activated RAS, and when examined, MAPK signaling (Lander, Jacovina et al. 1996, Switzer, Cheng et al. 2012, Batista, Ogata et al. 2013), which has been linked to increased proliferation (Switzer, Cheng et al. 2012, Batista, Ogata et al. 2013). Finally, the levels of *S*-nitrosylated and GTP-bound wild-type HRAS and NRAS are reduced upon knockdown of endogenous eNOS, and xenograft tumor growth of some cancer cell lines can be suppressed by replacing these RAS proteins with mutants defective in *S*-nitrosylation (Lim, Ancrile et al. 2008).

1.3.4.3 Characterization of RAS C118S mutant

Despite accumulating data, the effect of specifically blocking these redox-dependent reactions with RAS C118 on the physiological functions of RAS remains to be demonstrated in mammals. This is especially important in terms of cancer, as tumor initiation appears to be incredibly sensitive to the level of activated RAS (Sarkisian,

Keister et al. 2007). Fortunately, there is a very precise separation-of-function mutation of RAS to apportion the effects of these modifications. Specifically, substitution of C118 with serine (C118S), a very minor modification in which the thiol residue of this cysteine is replaced with a hydroxyl group, renders RAS completely resistant to modification and activation by NO (Lander, Hajjar et al. 1997, Batista, Ogata et al. 2013). As an important note, without stimulation with NO, the C118S mutation of RAS proteins does not affect the protein structure, as assessed by multidimensional heteronuclear NMR (Mott, Carpenter et al. 1997). Furthermore, the mutation does not have a measureable effect on GTPase activity, intrinsic and GEF-mediated guanine nucleotide dissociation rate, or the ability to bind RAS-binding domain of the effector RAF (Lander, Milbank et al. 1996, Mott, Carpenter et al. 1997, Williams, Pappu et al. 2003). In contrast, stimulation of cells with NO donors could activate the wild-type RAS protein, thereby promoting downstream MAPK signaling and cell proliferation, but does not have any effect on cells expressing the RAS C118S mutant (Lander, Hajjar et al. 1997, Batista, Ogata et al. 2013). More specifically, in one study, analysis of ERK1/2 activity by immunoblot in Jurkat cells treated without/with SNAP (an NO donor) for 10 minutes showed that mock transfected cells had increased ERK1/2 activity upon addition of the NO donor in a dose-dependent manner, while ERK1/2 activity of cells stably transfected with the p21 RAS C118S mutant remain insensitive to stimulation with NO (Lander, Hajjar et al. 1997). In another

study, cell proliferation was increased upon stimulation with GSNO (an NO donor) in Hela cells transfected with vector or wild-type HRAS, but did not change upon stimulation with GSNO in those transfected with HRAS C118S mutant. These experiments suggest that the RAS C118S mutant is insensitive to RAS activation upon stimulation with NO.

Therefore, the RAS C118S mutant is a useful tool to study both the biochemical and functional roles of redox-dependent reactions with RAS C118. This mutant has been demonstrated *in vitro* to have almost no difference with wild-type RAS proteins unless NO or other redox free radicals are present. In the presense of free radical oxidants, this RAS C118S mutant does show a defect in RAS activation, downstream signaling and the ability to stimulate cell proliferation. Considering reactive oxygen/nitrogen species (including NO and glutathione in an oxidized environment) are often present *in vivo*, especially in tumor microenvironment, I assessed the consequence of introducing the C118S mutation into the murine *Kras* gene on tumorigenesis *in vivo* in Chapter 3.

1.3.5 Other targets of *S*-nitrosylation in cancer

1.3.5.1 Components of NF-κB pathway: targets of *S*-nitrosylation

Since NO is a diffusible gas, it is highly likely that eNOS-derived NO has other downstream targets besides wild-type RAS. Therefore, in order to better understand the role of eNOS in tumor initiation and maintenance, it has become increasingly important to search for additional targets of *S*-nitrosylation by eNOS that are involved in cancer.

NF-κB (nuclear factor kappa-light-chain-enhancer of activated B cells) is a group of transcription factors that transduce a variety of noxious or inflammatory stimuli into the coordinated activation of multiple genes, including genes involved in the immune response as well as genes that influence cell survival, differentiation and proliferation. The mammalian NF-κB family of proteins is composed of five members: Rel (c-Rel), RelA (p65), RelB, NF-κB1 (p50 and its precursor p105) and NF-κB2 (p52 and its precursor p100) (Rothwarf and Karin 1999, Ghosh and Karin 2002, Gilmore 2006, Hayden and Ghosh 2008, Sethi, Sung et al. 2008, Shen and Tergaonkar 2009). NF-κB can be activated not only through the well-established canonical pathway but also through a non-canonical pathway (Gilmore 2006). In the canonical pathway, the inhibitory κB α (IκBα), which usually binds to and retains the p50-RelA dimer in the cytoplasm, are phosphorylated by an IκB kinase (IKK) and degraded upon stimulation with pro-inflammatory cytokines, thus freeing the p50-RelA dimer and allowing its translocation

into the nucleus, where it binds to κB sites and activates the transcription of a wide variety of genes (Gilmore 2006). Alternatively, NF-κB can be activated through the non-canonical NF-κB pathway. Upon stimulation of certain members of the TNF cytokine family such as lymphotoxin β, IKKα is selectively activated by the NF-κB-inducing kinase (NIK), leading to phosphorylation of NF-κB2 (p100/p52) and subsequent processing of p100 to p52, which then results in the formation of the p52-RelB heterodimer that enters the nucleus and regulates NF-κB responsive gene expression (Gilmore 2006).

Several components of the NF-κB pathway have been found to be regulated by *S*-nitrosylation. For example, *S*-nitrosylation of NF-κB by exogenous NO or induction of iNOS has been shown to inhibit NF-κB-DNA binding and gene transcription activity both *in vitro* and in intact cells. p50 is *S*-nitrosylated at Cys-62, which is conserved in other NF-κB subunits, including p65, p52 and c-Rel (Marshall, Hess et al. 2004). IKKβ, the predominant component of the inhibitory κB (IκB) kinase (IKK) complex responsible for the phosphorylation and degradation of IκBα upon cytokine stimulation, has also been found to be *S*-nitrosylated. The S-nitrosylation of Cys-179 on IKKβ can inhibit IκB phosphorylation by repressing IKKβ kinase activity, and TNF-α activation of IKKβ is coordinated with denitrosylation (Marshall, Hess et al. 2004, Reynaert, Ckless et al.

2004). It is possible that other components of the NF-κB pathway could also be *S*-nitrosylated.

1.3.5.2 IKKα: a potential target of *S*-nitrosylation?

Another component of the IKK complex, IKKα, is highly homologous with IKKβ. Alignment of IKKα and IKKβ shows a 52% homology in their overall sequences and 65% homology in their kinase domains (Zandi, Rothwarf et al. 1997). It is not yet known whether IKKα is a target of *S*-nitrosylation. Since IKKβ kinase activity was found to be inhibited by this modification (Reynaert, Ckless et al. 2004), it is possible that IKKα could also be *S*-nitrosylated and negatively regulated by this modification.

Besides its cytoplasmic role in the NF-κB canonical and noncanonical pathways, IKKα also has important functions in the nucleus. IKKα activates NF-κB responsive gene expression in the nucleus usually through some modifications of proteins around promoters, including the phosphorylation and acetylation of histone H3 on the chromatin and NF-κB p65 around the gene promoters. For example, activated IKKα interacts with CREB-binding protein and in conjunction with Rel A/p65 is recruited to the promoters of NF-κB responsive genes and mediates the phosphorylation of histone H3 Ser-10 and subsequent acetylation of Lys-14 in histone H3, leading to sustained transcription of these genes (Yumi Yamamoto and Gaynor 2003). IKKα has also been

found to induce the phosphorylation of Rel A/p65 at Ser-536, which displaces SMRT-HDAC3 corepressor activity and allows p300-mediated acetylation of RelA/p65 and subsequent activation of NF-κB responsive genes (Hoberg, Popko et al. 2006). These findings demonstrate a novel nuclear role of IKKα, which involves inducible chromatin modification leading to the activation of NF-κB responsive genes. Furthermore, IKKα is critical for normal physiology. It has been identified as a critical regulator of epidermal differentiation as well as a suppressor of skin cancer (Descargues, Sil et al. 2008). Therefore, it is important to study how IKKα activity is regulated.

2. Materials and Methods

2.1 Decreased tumorigenesis in mice with a Kras point mutation at C118

2.1.1 Plasmids

pBabeNeo-SV40-T/t-Ag (encoding the early region of SV40) was described previously (O'Hayer and Counter 2006, Lim, Ancrile et al. 2008). pBabeBleo-eNOS^{S1177D}-HA was generated by introducing a mutation resulting in a S1177D amino acid change into C-terminal HA-epitope tagged eNOS cDNA (Lim, Ancrile et al. 2008). pBabePuroFlag-Kras^{Q61L} and pBabePuroFlag-Kras^{G13D} were generated by introducing a mutation resulting in a Q61L or G13D amino acid change into N-terminal FLAG-epitope tagged human Kras cDNA (Lim, Ancrile et al. 2008). pBabePuroFlag-Kras^{Q61L,C118S} and pBabePuroFlag-Kras^{G13D,C118S} were generated by introducing a mutation resulting in a C118S amino acid change into the aforementioned pBabePuroFlag-Kras^{Q61L} or pBabePuroFlag-Kras^{G13D} plasmid.

2.1.2 Animals and generation of *Kras^{C118S}* mice

All animal experiments were approved by an Institutional Animal Care and Use Committee at Duke University. 129S6/SvEvTac mice were from Taconic. C57BL/6 mice

(C57BL/6NJ), CMVCre transgenic mice (B6.C-Tg (CMV-cre)1Cgn/J), and *Kras*$^{LSL\text{-}G12D}$ transgenic mice (129S/Sv-*Kras*^{tm4Tyj}/J) were obtained from Jackson Laboratory.

Kras^{C118S} knock-in mice were generated at Transgenic Mouse Facility of Duke Cancer Institute. The *Kras*^{C118S} targeting vector was linearized with NotI and electroporated into W4 Embryonic Stem (ES) cells from 129S6/SvEvTac mice, followed by positive selection with G418 and negative selection with ganciclovir. RNA was isolated from individual ES cell clones, and RT-PCR was performed with primers P1 and P2 to amplify *Kras* cDNA (Table 8). PCR products were resolved in 2% agarose gels, purified by a gel purification kit (QIAGEN), and sequenced to confirm the *Kras*^{C118S} mutation. One successfully targeted clone was injected into C57BL/6 blastocysts, which were then implanted into pseudo-pregnant females to generate chimeras. Male chimeras were bred with female C57BL/6 mice, and offspring with germline transmission of the *Kras*$^{C118S\ (Neo)}$ allele were identified by PCR of genomic DNA with primer pairs P3+P4 specific for the *Kras*$^{C118S\ (Neo)}$ allele and P3+P5 specific for the wild type allele (Table 8) as well as direct sequencing of *Kras* RT-PCR products from lung tissues. Male *Kras*$^{+/C118S\ (Neo)}$ mice were bred with female *CMVCre* transgenic mice to excise the *Neo* cassette. The genotypes of offspring were identified by PCR of genomic DNA using the primer pair P3+P5 to identify the wild type *Kras* allele and the *Kras*^{C118S} allele lacking the *Neo* cassette. Absence of the *Neo* cassette was also confirmed with primer pair P3+P4, which does not generate a product when the *Neo* cassette is deleted. *CMVCre; Kras*$^{+/C118S}$

mice were then crossed with *Kras*$^{+/+}$ mice to generate *Kras*$^{+/C118S}$ mice without *CMVCre* for use in all the animal studies. *Kras*$^{+/C118S}$ mice were crossed to generate *Kras*$^{+/+}$, *Kras*$^{+/C118S}$, and *Kras*$^{C118S/C118S}$ mice, whose genotypes were again identified by PCR of genomic DNA using the primer pair P3+P5. *Kras*$^{+/C118S}$ mice were further crossed into *Nras*$^{-/-}$; *Hras*$^{-/-}$ background to generate *Nras*$^{-/-}$; *Hras*$^{-/-}$; *Kras*$^{+/C118S}$ mice.

2.1.3 Genotyping PCR

Mouse tissue (toes or tails) samples were incubated in 25 mM NaOH / 0.2 mM EDTA at 95°C for 30 minutes, followed by neutralization with one volume of 40 mM Tris HCl, generating crude genomic DNA extraction.

Genotyping for *Kras*^{C118S} allele was performed using Red Taq polymerase (Sigma) with supplied buffer, 2 mM dNTP, and 1 μM of each primer. Reactions were run using standard PCR reactions: initial denaturation at 95°C 5 minutes, followed by 35 cycles of denaturation at 94°C for 30 seconds, annealing at 62°C for 45 seconds, and elongation at 72°C for 1 minute, and finally elongated at 72°C for 5 minutes. Bands were resolved in 2% agarose gel electrophoresis stained with ethidium bromide. Genotyping PCR procedures for *Kras*$^{LSL-G12D}$ allele were described previously (Jackson, Willis et al. 2001).

2.1.4 Semi-quantitative RT-PCR

RNA was extracted from ES cells, MEFs, lung tissue, or lung tumors with the RNA-BEE reagent according to the manufacture's protocol (Fisher Scientific). For isolation of RNA from lung tumors, RNA was co-precipitated with pellet paint (Covagen) using isopropanol. 0.5 - 2 μg RNA was reverse transcribed using Omniscript RT kit (QIAGEN) and Oligo dT (QIAGEN) as primers. The reactions were incubated at 37°C for 60 minutes and 70°C for 10 minutes. Resultant cDNA was used as templates to PCR amplify targets of interest using the primers listed in Table 8. For cDNA from cells and lung tissues, PCR amplification was performed using Red Taq polymerase with the supplied buffer, 1 mM dNTPs, and 1 μM forward and reverse primers. Reactions were run using standard PCR reactions: initial denaturation at 94°C 5 minutes, followed by 35 cycles of denaturation at 94°C for 30 seconds, annealing at 60°C for 1 minute, and elongation at 72°C for 1 minute, and finally elongated at 72°C for 10 minutes. For cDNA from lung tumors, PCR amplification was performed using Platinum Taq polymerase with the supplied buffer used at 0.7X the suggested final concentration, 1 mM dNTPs, 2 mM $MgCl_2$, and 0.4 μM forward and reverse primers (P6 and P7, Table 8). Reactions were run using standard PCR reactions: initial denaturation at 94°C 2 minutes, followed by 35 cycles of denaturation at 94°C for 30 seconds, annealing at 55°C for 45 seconds, and elongation at 72°C for 2 minutes, and finally elongated at 72°C for 7 minutes. Bands were resolved in 2% agarose gel electrophoresis stained with ethidium bromide.

2.1.5 Generation of MEFs and cell culture

All the cells were maintained in Dulbecco's modified Eagle's medium (DMEM) supplemented with 10% FBS and incubated at 37°C in a 5% CO_2 incubator. *Kras*$^{+/+}$ and *Kras*$^{C118S/C118S}$ MEFs were prepared from embryos from *Kras*$^{C118S/+}$ females bred with a *Kras*$^{C118S/+}$ male. Embryos (E13-E16) were dissected from pregnant *Kras*$^{C118S/+}$ females and washed with sterile PBS. The head of each embryo were removed for isolation of genomic DNA and identification of genotypes by PCR using primers P3+P5 as described above. The remaining embryos were cut into pieces in a sterile dish and incubated with 1 ml 0.25% trypsin at 37°C in a 5% CO_2 incubator for 30-45 minutes. The trypsinized cells were then mixed with 10 ml 10% FBS DMEM and incubated at 37°C in a 5% CO_2 incubator for further experiments. *Nras*$^{-/-}$; *Hras*$^{-/-}$; *KrasC118S*$^{/C118S}$ MEFs were prepared as above from embryos from an *Nras*$^{-/-}$; *Hras*$^{-/-}$; *KrasC118S*$^{/+}$ female bred with an *Nras*$^{-/-}$; *Hras*$^{-/-}$; *KrasC118S*$^{/+}$ male. Primary MEF lines were immortalized by stable infection (O'Hayer and Counter 2006) with retroviruses derived from pBabeNeo-SV40-T/t-Ag. In some cases these cells were further stably infected (O'Hayer and Counter 2006) with retroviruses derived from pBabeBleo, pBabeBleo-eNOS^{S1177D}-HA, pBabePuroFlag-Kras^{Q61L}, or pBabePuroFlag-Kras^{Q61L,C118S}, pBabePuroFlag-Kras^{G13D}, or pBabePuroFlag-Kras^{G13D,C118S}. Where indicated, immortalized MEFs were serum starved by incubating with 0.5% FBS DMEM overnight and harvested the next day. Where indicated,

immortalized MEFs were also treated with 100 ng/μl Epidermal Growth Factor (EGF, from Sigma) for 5 minutes at 37°C in a 5% CO_2 incubator before being harvested on ice.

2.1.6 Immunoblot analysis

Cells or lung tissue were lysed with RIPA buffer (1% NP-40, 20 mM Tris pH 8.0, 137 mM NaCl, 10% glycerol, 2mM EDTA) and protein concentrations quantified by Bradford assay (Bio-Rad). Equal amounts of protein lysates (50 μg) were resolved by SDS-PAGE, transferred to a PVDF membrane, and immunoblotted with primary antibodies anti-Kras F234 (Santa Cruz sc-30, diluted 1:200), anti-Flag M2 (Sigma F1804, diluted 1:500), anti-HA (Covance, diluted 1:1000), anti-β-actin (Sigma A2228, diluted 1:10000), anti-β-tubulin (Sigma T5201, diluted 1:2000), anti-Erk1/2 (Santa Cruz sc-94, diluted 1:2000), or anti-P (Thr 202/Tyr 204)-Erk1/2 (Santa Cruz sc-7383, diluted 1:500), followed by incubation with either goat anti-rabbit (Santa Cruz sc-2004, diluted 1:5000) or anti-mouse (Invitrogen G21040, diluted 1:10000) IgG-HRP conjugated secondary antibodiesand detected by ECL (GE healthcare). Bands of targeted protein in scanned images were quantified using Image J software and normalized.

2.1.7 Urethane carcinogenesis

Kras$^{+/C118S}$ mice (without CMVCre) were bred with *Kras*$^{+/+}$ mice in 129S6/SvEvTac background. Resultant *Kras*$^{+/C118S}$ mice were then crossed to generate *Kras*$^{+/+}$, *Kras*$^{+/C118S}$,

and *Kras*$^{C118S/C118S}$ littermates in which both *Kras* alleles originated from a 129S6/SvEvTac background. 25 to 27 male and female mice of each genotype were ultimately compared to detect a measurable difference in tumor parameters between control and experimental cohorts. 38 male and 39 female mice at two months of age were intraperitoneally injected with urethane (1 mg/g body weight) (Zhang, Wang et al. 2001). Weight and behavior were monitored twice weekly starting at three months post-injection. Eight months after injection, mice were euthanized, and lungs were inflated with PBS and harvested for analysis. Lung surface tumors were counted under a dissecting microscope. Tumor diameter was determined using micro-calipers. Mice that reached moribundity endpoints before eight months were excluded from the final analysis. I was blinded to the genotype when injecting urethane as well as when assessing tumor number and size.

2.1.8 Ad-Cre-induced lung tumorigenesis

Kras$^{+/C118S}$ mice in which both *Kras* alleles originated from a 129S6/SvEvTac background were bred with *LSL-Kras*$^{G12D/+}$ mice to generate *Kras*$^{LSL\text{-}G12D/+}$ and *Kras*$^{LSL\text{-}G12D/C118S}$ mice. 17 to 21 male and female mice of each genotype were ultimately compared to detect a measurable difference in tumor parameters between control and experimental cohorts. 9 male and 29 female mice were infected with 6x10E^{6} pfu of AdCre virus at two months of age (Jackson, Willis et al. 2001). Weight and behavior

were monitored twice weekly starting at three months post-AdCre. Four months after AdCre administration, mice were euthanized and lungs were inflated with PBS and harvested for analysis. Surface tumors were counted under a dissecting microscope. Tumor diameter was determined using micro-calipers. Mice that reached moribundity endpoints before four months were excluded from the final analysis. I was blinded to the genotype when administrating AdCre as well as when assessing tumor number and size.

2.1.9 Histological analysis

Left lobes of lungs from the indicated mice (*see* above) were fixed in 10% neutral buffered formalin overnight, dehydrated in 70% ethanol, and paraffin embedded. 5 μm-thick sections were cut from each sample, mounted on glass slides, and stained with Hematoxylin and Eosin (H&E). A total of 77 lung sections were reviewed by two pathologists (DMC, JC) who were masked to the study design and blinded to the genotype. The number and type (atypical adenomatous hyperplasia (AAH), adenoma (AD), and/or adenocarcinoma (AC)) of lesions were quantified in each sample. Adenomas were further classified by size (≤1 mm, 1-3 mm or ≥3 mm) and histological subtype (solid, papillary, or mixed solid-papillary) (Avanzo, Mesnil et al. 2004).

2.1.10 Immunohistochemistry

Left lobes of lungs from the indicated mice (*see* above) were fixed in 10% neutral buffered formalin overnight, dehydrated in 70% ethanol, and paraffin embedded. 5 μm-thick sections were cut from each sample, mounted on glass slides, and subjected to epitope retrieval and stained with anti-P (Thr 202/Tyr 204)-Erk1/2 (Cell Signaling 4376), anti-P (Ser473)-Akt (Cell Signaling 4060), or anti-Ki67 (Thermo Scientific RM9106) antibodies followed by peroxidase-based detection with Vectastain Elite ABC Kits (Vector Labs) and counterstained with haematoxylin. Photographs were taken of four to six high-power (20X) random fields with tumor areas on an Olympus Vanox S microscope. Images were blinded and tumors were circumscribed in stained tissue images with the freehand selection tool in Image J, and the total area of the tumor in pixels was recorded. Tumor images were copied and pasted to new, blank images and color threshold was applied to determine positive-staining areas, using the same parameters for each tumor image. Areas staining positive by these parameters were selected and the positive staining area in pixels was recorded. The percentage of positive-staining area was calculated by dividing the positive-staining area of the tumor in pixels by the total area of tumors in pixels.

2.1.11 *Kras* mutation analysis

Lung tumors arising in urethane-treated *Kras*$^{+/C118S}$ mice (*see* above) were removed with the aid of a dissection microscope. 500 ng of RNA isolated from the

tumors were RT-PCR amplified (*see* above) using the primer pair P6+P7 containing HindIII and SacI sites, respectively (Table 8). Resultant products were cloned into the HindIII and SacI sites of pBluescript vector (from Addgene), after which 12 positive clones from each ligation reaction were sequenced using T7 promoter (Eton Bioscience) to determine whether the clone corresponded to the native or C118S allele of *Kras*, and whether the clone had an oncogenic mutation (at position G12, G13 and Q61).

2.1.12 Statistical analysis

Data were presented as mean values ± standard error of the mean (SEM). Most statistical analyses were performed with Graphpad Prism 5 software. The two-tailed unpaired student's *t* test was used to compare two groups. The one-way ANOVA plus post-hoc Bonferroni's multiple comparison tests were used to compare three or more groups. The MANOVA test was used to compare mice weight change over time between two groups, while the long-rank test was performed to compare the survival between two groups. The Chi-square test was used to analyze the difference in frequency (between the observed vs. the expected or between two groups) based on contingency tables. P values < 0.05 were considered significant.

2.2 Reduced HRAS^{G12V}-driven tumor growth of cells expressing KRAS^{C118S}

2.2.1 Plasmids

pBabePuro, pBabeNeo-SV40-T/t-Ag (encoding the early region of SV40), pBabePuro-Flag-HRAS^{G12V}, pBabeBleo-p110-CAAX, pBabeBleo-eNOS^{S1177D}-HA, and pBabeBleo-eNOS^{S1177A}-HA were described previously (O'Hayer and Counter 2006, Lim, Ancrile et al. 2008). pSuperRetroGFP/Neo-*KRAS*-shRNA were created with the target sequence being GTTGGAGCTGGTGGCGTAG. pSuperRetroGFP/Neo-scramble shRNA was created with the sequence being: GATTTGGGAATCTTATAAGTTCCCTATCAGTGATAGAGATGGTCAGCGCACTCTT GCCTTTTTA. pBabeHygro-Flag-KRAS^{C118S}, -KRAS*^{C118S}, and -KRAS$^{G12V, C118S}$ were created by introducing C118S and/or G12V mutations by site directed mutagenesis into the previously described vectors pBabeHygro-Flag-KRAS (Lim, Ancrile et al. 2008) and -KRAS* (Lampson, Pershing et al. 2013), which encode shRNA-resistant and N-terminal Flag epitope-tagged human *KRAS* cDNA, either comprised of the wild-type sequence (KRAS) or one in which a number of rare codons were converted to common codons to increase protein expression (KRAS*).

2.2.2 Cell lines

HEK-TtH cells (primary human embryonic kidney cells transduced with vectors encoding the early region of SV40 and hTERT) were previously described (Kashatus, Lim et al. 2011). Mouse embryonic fibroblasts (MEFs) were prepared using standard approaches (Xu 2005) from embryos from *Kras*$^{C118S/+}$ females bred with a *Kras*$^{C118S/+}$ male. Each primary MEF line was immortalized by stably infection (O'Hayer and Counter 2006) with a retrovirus derived from pBabeNeo-SV40-T/t-Ag. Genotypes of resultant MEF cell lines were determined by PCR with the primer pair P3+P5 (Table 8) that distinguishes the wild-type and C118S *Kras* alleles by amplification of a 621 bp versus a 517 bp product, respectively, as previously described (Huang, Carney et al. 2014). HEK-TtH cells or SV40-immortalized *Kras*$^{+/+}$ or *Kras*$^{C118S/C118S}$ MEFs were stably infected (O'Hayer and Counter 2006) with retroviruses derived from vectors encoding no transgene as a control or the indicated transgenes or shRNA.

2.2.3 Immunoblot analysis

The indicated cells were lysed with RIPA buffer (1% NP-40, 20 mM Tris pH 8.0, 137 mM NaCl, 10% glycerol, 2mM EDTA) and protein concentrations determined by Bradford assay (Bio-Rad). Equal amounts of protein lysates (50 μg) were resolved by SDS-PAGE, transferred to a PVDF membrane, and immunoblotted with primary antibodies anti-Kras F234 (Santa Cruz sc-30, diluted 1:200), anti-Flag M2 (Sigma F1804,

diluted 1:1000), anti-HA (Covance MMR-101R, diluted 1:1000), anti-β-actin (Sigma A2228, diluted 1:10000), anti-β-tubulin (Sigma T5201, diluted 1:2000), anti-Erk1/2 (Santa Cruz sc-94, diluted 1:2000), anti-P (Thr 202/Tyr 204)-ERK1/2 (Santa Cruz sc-7383, diluted 1:500), anti-AKT (Cell Signaling, diluted 1:1000), or anti-P(Thr 308)-AKT (Cell Signaling, diluted 1:200), followed by incubation with either goat anti-rabbit (Santa Cruz sc-2004, diluted 1:5000) or anti-mouse (Invitrogen G21040, diluted 1:10000) IgG-HRP (Horseradish peroxidase) conjugated secondary antibodies and detected by ECL (GE healthcare).

2.2.4 Ras-GTP analysis

Cell lysates were prepared and protein concentrations determined as above from the indicated cells cultured over night in medium supplemented with 0.5% fetal bovine serum. Equal amounts (0.5-2 mg) of lysates were incubated with recombinant glutathione *S*-transferase protein fused with the Ras-binding domain of Raf (GST-RBD) that was bound to glutathione agarose beads (GE healthcare) and then rotated for 45 minutes at 4°C as previously described (de Rooij and Bos 1997). The beads were washed with 0.5 ml of RIPA buffer three times for 10 minutes each at 4°C, boiled in sample buffer, resolved using SDS-PAGE, and immunoblotted with anti-Kras or anti-Flag antibodies, as described above.

2.2.5 Semi-quantitative RT-PCR

RNA was extracted from cells with the RNA-BEE reagent according to the manufacture's protocol (Fisher Scientific). 0.5 – 2.0 μg of RNA was reverse transcribed using Omniscript RT kit (QIAGEN) with an Oligo dT (QIAGEN) primer. Resultant cDNA was used as a template to amplify targets of interest using the primers listed in Table 8 using the protocol described in **2.1.3**.

2.2.6 Tumor xenograft analysis

All animal experiments were approved by an Institutional Animal Care and Use Committee at Duke University. For xenograft studies, $5x10^6$ of the indicated HEK-TtH-derived cell lines or $1x10^6$ of the indicated SV40-immortalized MEF-derived cell lines were each mixed with 500 μl Matrigel (BD Biosiences) and injected subcutaneously into each flank of five 8-week-old female immunocompromised SCID-Bg mice (Charles River). Seven days later, the length (L) and width (W) of tumors were measured with a caliper three times a week. Tumor volumes were calculated by $0.5*L*W^2$. When the average tumor volume in one mouse in a group reached 1.5 cm^3, all mice were euthanized and the tumors removed, photographed, and weighed. For survival studies, mice were injected and monitored as above, except that each individual mouse was euthanized when tumors reached 1.5 cm^3 or if a moribundity endpoint was reached, and

time to reach endpoint was recorded. Kaplan-Meier survival curves were generated with Graphpad Prism 5 software.

2.2.7 Soft agar growth analysis

The indicated SV40-immortalized *Kras*$^{+/+}$ and *Kras*$^{C118S/C118S}$ MEFs stably infected with a retrovirus encoding no transgene (vector) or HAS^{G12V} were plated in triplicate in 6-well plates in soft agar, as previously described (Brady, Crowe et al. 2014). Four weeks later, colonies were quantified by Image J software based on the scanned images of the wells.

2.2.8 Statistical analysis

Data were presented as mean values ± standard error of the mean (SEM). Statistical analyses were performed with Graphpad Prism 5 software. The two-tailed unpaired student's *t* test was used to compare two groups. The one-way ANOVA plus post-hoc Bonferroni's multiple comparison tests were used to compare three or more groups. The long-rank test was performed to compare the survival between two groups. *P* values < 0.05 were considered significant.

2.3 eNOS inhibits NF-κB signaling through S-nitrosylation of IKKα

2.3.1 Plasmids

pBabeBleo-p110CAAX were described previously (Lim, Ancrile et al. 2008). pSuperRetro-Puro-scramble shRNA was described previously (Lim, Baines et al. 2005). pSuperRetro-Puro-eNOS1819i (eNOS shRNA) was created with the target sequence being: AAGAGTTATAAGATCCGCTTC. pGEX-GST-IKKα was a kind gift from Dr. Albert Baldwin. HA-IKKα was PCR amplified from this plasmid using primer pair P24+P25 (Table 8), cut with EcoR I and Sal I and cloned into pBabe-Hygro vector. HA-IKKα amino acid 1-300 fragment was PCR amplified using primer pair P26+P27 (Table 8), cut with EcoR I and Xho I and cloned into pCDNA3 vector. HA-IKKα^{C178S} mutant and mutants of HA- IKKα amino acid 1-300 fragment were made by site-directed mutagenesis.

2.3.2 Cells, transient transfection and stable infection

All the cells were maintained in Dulbecco's modified Eagle's medium (DMEM) supplemented with 10% FBS and incubated at 37°C in a 5% CO_2 incubator. HEK-TtH cells (primary human embryonic kidney cells transduced with vectors encoding the early region of SV40 and hTERT) were previously described (Kashatus, Lim et al. 2011). HEK-TtH cells were transiently transfected with pcDNA3-HA-IKKα (1-300) or its

mutants using the Fugene reagent (Promega E2691) according to the manufacture's protocol and harvested two days later for the analysis of S-nitrosylation. For generation of stable cell lines, HEK-TtH cells were stably infected (O'Hayer and Counter 2006) with retroviruses derived from pBabe-Bleo vectors encoding p110CAAX, pSuperRetro-Puro-scramble or pSuperRetro-Puro-eNOS1819i and pBabe-Hygro vectors encoding HA-IKKα, followed by selection with zeocin (Life technologies R250-01) at 200 μg/ml, puromycin (Sigma P8833) at 2 μg/ml, or hygromycin (Life technologies 10687-010) at 100 μg/ml respectively.

2.3.3 Immunoblot analysis

Cells were serum starved overnight and treated with 10 ng/ml TNFα (Sigma 8916) or 100 ng/ml LIGHT (Enzo Life Sciences, ALX-522-018-C010) for different time points before being harvested. The indicated cells were lysed with RIPA buffer (1% NP-40, 20 mM Tris pH 8.0, 137 mM NaCl, 10% glycerol, 2mM EDTA) and protein concentrations determined by Bradford assay (Bio-Rad). Equal amounts of protein lysates (50 μg) were resolved by SDS-PAGE, transferred to a PVDF membrane, and immunoblotted with primary anti-HA antibody (Covance, diluted 1:1000), anti-β-tubulin antibody (Sigma T5201, diluted 1:2000), anti-p65 antibody (Cell signaling 4764, diluted 1:1000), anti-phospho-p65 (Ser 536) antibody (Cell signaling 3031, diluted 1:500), anti-p100/p52 antibody (Cell signaling 4882, diluted 1:1000), followed by incubation

with either goat anti-rabbit (Santa Cruz sc-2004, diluted 1:5000) or anti-mouse (Invitrogen G21040, diluted 1:10000) IgG-HRP (Horseradish peroxidase) conjugated secondary antibodies and detected by ECL (GE healthcare).

2.3.4 Immunoprecipitation and *in-vitro* kinase assay

$2X10^6$ of the HEK TtH cells expressing HA-IKKα were lysed with RIPA lysis buffer as above. Equal amount of cell lysates were mixed with pre-washed Gamma beads (GE Healthcare 17-0885-01), rotated at 4°C for two hours, followed by addition of 2 μg anti-HA antibodies (Covance MMR-101R) and rotation at 4°C overnight. The beads were then isolated by centrifuge and washed three times with RIPA lysis buffer at 4°C. IKKα-containing immunoprecipitates are added to a mixture containing kinase reaction buffer (20mM HEPES, 2mM $MgCl_2$, 2mM $MnCl_2$, 10mM β-glycerophosphate, 10mM NaF, 10mM PNPP, 300μM Na_3VO_4, 1mM benzamadine, 2mM PMSF, 1μg/ml aprotinin, 1mM DTT), substrate peptides histone H3.2 (NEB 2506), and 10μM ATP (Invitrogen) to allow for the kinase reaction at 30°C for 30-60 minutes. After termination of the kinase reaction, the samples were loaded to SDS-PAGE gel, transferred to a PVDF membrane, and immunoblotted using an anti-histone H3 antibody (Cell signaling 9715, diluted 1:500), and an anti-phospho-histone H3 (Ser-10) antibody (Cell signaling 9701, diluted 1:1000).

2.3.5 Real-time PCR

RNA was extracted from cells and reverse transcribed as described in **2.1.3**. cDNA was used as a template and mixed with SYBR Green PCR mix (Biorad 170-8882) and primer pair P28+P29 or P30+P31 (Table 8) at 900 nM each to amplify *IL-6* or *I κBα* respectively. GAPDH was also similarly amplified using primer pair P22+P23 (Table 8) as an internal control. Each sample was plated in triplicate in 96-well plates (Biorad) on a real-time PCR machine (Biorad) using standard protocol from the manufacturer. After the PCR program ended, the average number of dCT from each type of reaction was calculated, and the levels of the gene of interest (*IL-6* or *I κBα*) were analyzed base on the difference between the dCT of the gene of interest (*IL-6* or *I κBα*) and the dCT of GAPDH internal control.

2.3.6 Biotin-switch assay

In HEK TtH cells stably expressing HA-IKKα or HA-IKKα^{C178S}, or those transiently transfected with HA-IKKα (1-300) or its mutants, levels of S-nitrosylated IKKα were measured by biotin-switch assays using the following protocol:

1) Sample preparation: Cells are lysed with appropriate amount of lysis buffer (25 mM HEPES, 50 mM NaCl, 0.1 mM NaCl, 0.1 mM EDTA, 1% NP40, 0.5 mM PMSF plus protease inhibitors, pH 7.4, avoid DTT). Repeated passage (about 10 times) through a 25-gauge needle and

rotation at 4°C may be done to increase the lysis efficiency. After centrifugation at maximum speed for 10 mintures, protein concentrations were measured using Bradford assay (Bio-Rad).

2) Blocking: equal amounts of proteins (0.5-2 mg) are diluted to 1.8ml with HEN buffer (100 mM HEPES, 1 mM EDTA, 0.1 mM neocuproine, pH8.0). 0.2 ml of 25% SDS is added along with 20 μl of 10% MMTS (final 2.0 ml volume with 2.5% SDS and 0.1% MMTS). Samples are incubated at 50°C in the dark for 20 minutes with frequent vortexing.

3) Precipitation: three volumes of cold acetone (6ml) are added to each sample. Proteins are precipitated for at least 20 min at -20°C and collected by centrifugation at 2000 g for 5 minutes. The clear supernatant is aspirated and the protein pellet is gently washed with 70% acetone four times (5 ml each time).

4) Labeling: after resuspension in 0.24 ml HENS buffer (HEN buffer plus 1% SDS), the material is transferred to a fresh 1.7-ml microfuge tube containing 30 μl biotin-HPDP (Thermo Scientific 21341, 2.5 mg/ml). The labeling reaction is initiated by adding 30 μl of 200 mM sodium ascorbate (Sigma A7631). An equivalent concentration of NaCl can be used as an ascorbate-free negative control. Samples are rotated at room temperature in the dark for 1 hour (avoid any sources of sunlight).

5) Precipitation: three volumes of cold acetone (about 900 μl) are added to each sample. Proteins are precipitated for at least 20 minutes at -20°C and collected by centrifugation at 5000 g for 5 minutes. The clear supernatant is aspirated and the protein pellet is gently washed with 70% acetone four times (1 ml each).

6) Pulldown: after complete resuspension in 0.25 ml HENS/10 buffer (HEN buffer diluted 10 fold with water, with 1% SDS), 0.75 ml of neutralization buffer (25 mM HEPES, 100 mM NaCl, 1 mM EDTA, 0.5% Triton X-100, pH 7.5) is added. A small fraction of each sample (about 10 μl) is removed for analysis of protein input. The remaining material is transferred to a fresh microfuge tube containing 25-50 μl of prewashed streptavidin-affinity resin (Fluka 85881). The samples are gently rotated for 12-18 hours at 4°C.

7) Washing: streptavidin beads are collected by centrifugation at 200 g for 10 seconds and washed with wash buffer (neutralization buffer containing 600 mM NaCl) four times (1 ml each). After the final wash, the beads are fully dried via gentle aspiration with a 25-gauge needle.

8) Elution: 30-50 μl of elution buffer is added to each sample. Proteins are eluted at room temperature with frequent agitation, followed by centrifugation at 5000 g for 30 seconds. Supernatants is collected

without disturbing the pelleted resin and mixed with 6X loading buffer.

9) SDS-PAGE and immunoblot: protein input and biotin-switched samples are boiled for 10 minutes and loaded to SDS-PAGE gel, transferred to a PVDF membrane and immunoblotted for the gene of interest (an anti-HA antibody was used in this study).

2.4 Other experimental procedures in Kras^{C118S} study

2.4.1 Cell growth analysis

Primary human IMR-90 fibroblasts (from ATCC, Pd. 35-37) or MEFs (generated as described in **2.1.5**) were infected with retrovirus encoding pBabePuro with no insert or indicated wild-type or oncogenic *HRAS* or *KRAS* transgenes and selected with 2 μg/ml puromycin. Cells were then plated in 24-well plates in triplicate or quadruplicate at 4000 cells/well for IMR-90 cells and 1000 cells/well for MEFs. At different days after plating, cells were fixed with 10% formalin and stained with 0.1% crystal violet (Sigma). At the end of an experiment, pictures were taken, and crystal violet was extracted with 10% acetic acid from all the 24-well plates at indicated days. Absorbance at 600 nm was measured and normalized to the average level at Day 1. Growth curve was generated using Graphpad Prism 5 software.

2.4.2 DMBA/TPA-induced skin tumor analysis

All animal experiments were approved by an Institutional Animal Care and Use Committee at Duke University. 16 *Kras*$^{+/+}$ and 14 *Kras*$^{C118S/C118S}$ mice were enrolled in the study and treated with DMBA at 8-12 weeks old. The back of each mouse was shaved with a beard trimmer before topical application with the chemical. After shaving, a pipette was used to coat the back of the mouse with 150 μl of 125 μg/ml DMBA (in DMSO), followed by immediate even distribution of the DMBA on the shaved portion of the back using a presaturated q-tip. One week after DMBA treatment, TPA (150 μl of 10^{-4} M TPA) was applied to the mice in the exact same fashion twice weekly for 20 weeks. After tumors began to arise, the number of tumors on each mouse was counted, and the length (L) and width (W) of each tumor were measured with a caliper twice weekly. Tumor volumes were calculated by $0.5*L*W^2$. Body weight of mice was also monitored twice weekly until reaching end point (a weight loss of 15% or more). All mice were euthanized at end point, and some papillomas were taken out for analysis.

2.4.3 Oncogenic Kras^{G12D}-driven pancreatic lesions

All animal experiments were approved by an Institutional Animal Care and Use Committee at Duke University. *Kras*$^{LSL\text{-}G12D/+}$ and *Kras*$^{LSL\text{-}G12D/C118S}$ mice (described in **2.1.8**) were crossed with *Pdx1-Cre* transgenic mice (from Jackson Laboratory), generating *Kras*$^{LSL\text{-}G12D/+}$; *Pdx1-Cre* and *Kras*$^{LSL\text{-}G12D/C118S}$; *Pdx1-Cre* mice that will develop pancreatic

lesions. 18 *Kras*$^{LSL\text{-}G12D/+}$*; Pdx1-Cre* and 16 *Kras*$^{LSL\text{-}G12D/C118S}$*; Pdx1-Cre* mice were enrolled in the study, and the development of facial and vulva papillomas as well as body weight was monitored over time starting from two months old. All mice were euthanized at six months old, and the pancreatic tissues were stained with H&E as described in **2.1.9**. For H.E stained pancreatic tissues of each mouse, pictures of five random fields at 10X magnification were taken, and the normal (without lesions) as well as total pancreatic tissues in each picture were circled using the free selection tool in Photoshop software, based on which the percentage of normal pancreatic tissues in each picture were calculated.

3. Decreased tumorigenesis in mice with a *Kras* point mutation at C118

3.1 Introduction

The Ras family of small GTPases, comprised of the *KRAS*, *NRAS*, and *HRAS* genes, are mutated to encode constitutively-active, GTP-bound, oncogenic proteins in upwards of one quarter of all human cancers, which is well established to promote tumorigenesis (Pylayeva-Gupta, Grabocka et al. 2011). Despite the prominent role these genes play in human cancer, the encoded proteins have proven difficult to pharmacologically inhibit (Downward 2003, Gysin, Salt et al. 2011). As such, it is important to understand how Ras proteins are activated. In this regard, Ras proteins cycle between GDP-bound inactive and GTP-bound active states, the latter being catalyzed by guanine nucleotide exchange factors (GEFs) (Bos, Rehmann et al. 2007, Vigil, Cherfils et al. 2010). GEFs are not, however, the only means of activating Ras proteins. Free radical oxidants can lead to *S*-nitrosylation or *S*-glutathiolation and activation of Ras in a manner dependent on the thiol residue of cysteine 118 (C118) (Lander, Milbank et al. 1996, Raines, Bonini et al. 2007, Hobbs, Bonini et al. 2013). Accumulating evidence supports the possibility that such redox-dependent reactions with C118 may have cellular consequences. Specifically, an increase in *S*-nitrosylation and activation of Ras can stimulate MAPK signaling (Lander, Jacovina et al. 1996, Lander, Milbank et al. 1996, Lander, Hajjar et al. 1997, Lin, Raab-Graham et al. 2004, Raines, Cao et al. 2006, Ibiza,

Perez-Rodriguez et al. 2008, Switzer, Cheng et al. 2012), PI3K signaling (Lee and Choy 2013), and/or cell proliferation (Batista, Ogata et al. 2013). Similarly, an increase in *S*-glutathiolation and activation of Ras impacts a variety of signaling pathways in a manner apparently dependent upon C118 (Adachi, Pimentel et al. 2004, Clavreul, Adachi et al. 2006). Finally, reducing the expression of endothelial nitric oxide synthase (eNOS), which catalyzes the production of nitric oxide (Dudzinski, Igarashi et al. 2006), decreases the levels of *S*-nitrosylated and active Ras as well as xenograft tumor growth in a number of cancer cell lines (Lim, Ancrile et al. 2008).

Despite accumulating data, the effect of specifically blocking redox-dependent reactions with C118 on the function of endogenous mammalian Ras remains to be explored *in vivo.* This is especially important in terms of cancer, as tumor initiation appears to be incredibly sensitive to the level of activated Ras (Sarkisian, Keister et al. 2007). Fortunately, there is a very precise separation-of-function mutation that apportions these effects from other functions of Ras. Specifically, substitution of C118 for serine (C118S), a very minor modification in which the thiol residue of this cysteine is replaced with a hydroxyl group, renders Ras completely insensitive to activation by free radical mediated oxidants, with no measureable effect on the protein structure, GTPase activity, intrinsic and GEF-mediated guanine nucleotide dissociation rate, or the ability to bind an effector (Lander, Milbank et al. 1996, Lander, Hajjar et al. 1997, Mott, Carpenter et al. 1997, Williams, Pappu et al. 2003, Adachi, Pimentel et al. 2004, Heo and

Campbell 2004, Clavreul, Adachi et al. 2006, Raines, Cao et al. 2006, Hobbs, Bonini et al. 2013). Thus, here I assessed the consequences of introducing the C118S mutation into the endogenous murine *Kras* gene on tumorigenesis *in vivo*, and found a reduction in carcinogen-induced lung tumorigenesis in mice bearing this mutated allele.

3.2 Results

3.2.1 Generation of mice with a *Kras^{C118S}* allele.

To investigate the effect of mutating C118 on Ras function *in vivo* during tumorigenesis, a targeting vector was created to insert a single point mutation, namely a G353 transversion to C (G353>C) encoding the C118S mutation, into exon 3 of the murine *Kras* gene (Figure 1a). C118S was chosen because this precise separation-of-function mutation specifically blocks the redox-dependent reactions at this site that lead to Ras activation (Lander, Milbank et al. 1996, Lander, Hajjar et al. 1997, Mott, Carpenter et al. 1997, Williams, Pappu et al. 2003, Adachi, Pimentel et al. 2004, Heo and Campbell 2004, Clavreul, Adachi et al. 2006, Raines, Cao et al. 2006, Hobbs, Bonini et al. 2013). *Kras* was chosen, as this is the isoform most commonly mutated in human cancers (Pylayeva-Gupta, Grabocka et al. 2011). This vector was electroporated into embryo stem (ES) cells, and cells were selected for resistance to G418 and ganciclovir. Successful recombination events in resistant clones were verified by RT-PCR and sequencing to contain the G353>C transversion in *Kras* (Figure 1b). One such clone was used to generate a founder *Kras$^{+/C118S\ (Neo)}$* mouse, the genotype of which was identified by PCR amplification from genomic DNA. A 314 bp product unique to the targeted *Kras$^{C118S\ (Neo)}$* allele was amplified (Figure 2a) using primers anchored in exon 3 of the *Kras* gene and in the *Neo* gene of the targeting vector (P3 and P4, Figure 1a), while a 621 bp product

unique to the wild type *Kras* allele was amplified (Figure 2a) using primers anchored in exon 3 and in the adjacent intron (P3 and P5, Figure 1a). These mice were crossed with *CMVCre* transgenic mice to induce Cre-mediated recombination between the *loxP* sites flanking the *Neo* cassette. Successful excision of the *Neo* cassette was identified by PCR amplification of genomic DNA, yielding a 517 bp, instead of a 621 bp product, using primers P3 and P5, as well as by confirming the absence of the aforementioned 314 bp product using primers P3 and P4 (Figure 2b). The presence of *CMVCre* was identified by PCR amplification of genomic DNA using primers (P16 and P17, Table 8) designed to generate a 100 bp PCR product unique to this transgene (Figure 2b). *CMVCre; Kras*$^{+/C118S}$ mice identified in this fashion were then crossed with *Kras*$^{+/+}$ mice to generate *Kras*$^{+/C118S}$ mice without *CMVCre* for use in subsequent experiments, again with the desired genotypes confirmed by similar PCR strategies. Finally, *Kras*$^{+/C118S}$ mice were crossed, generating *Kras*$^{+/+}$, *Kras*$^{+/C118S}$, and *Kras*$^{C118S/C118S}$ offspring, the genotype of which were identified by PCR amplification of genomic DNA using the aforementioned primer pair P3 and P5 that distinguished wild type versus C118S *Kras* alleles by the amplification of a 621 bp versus a 517 bp product (Figure 1a, c).

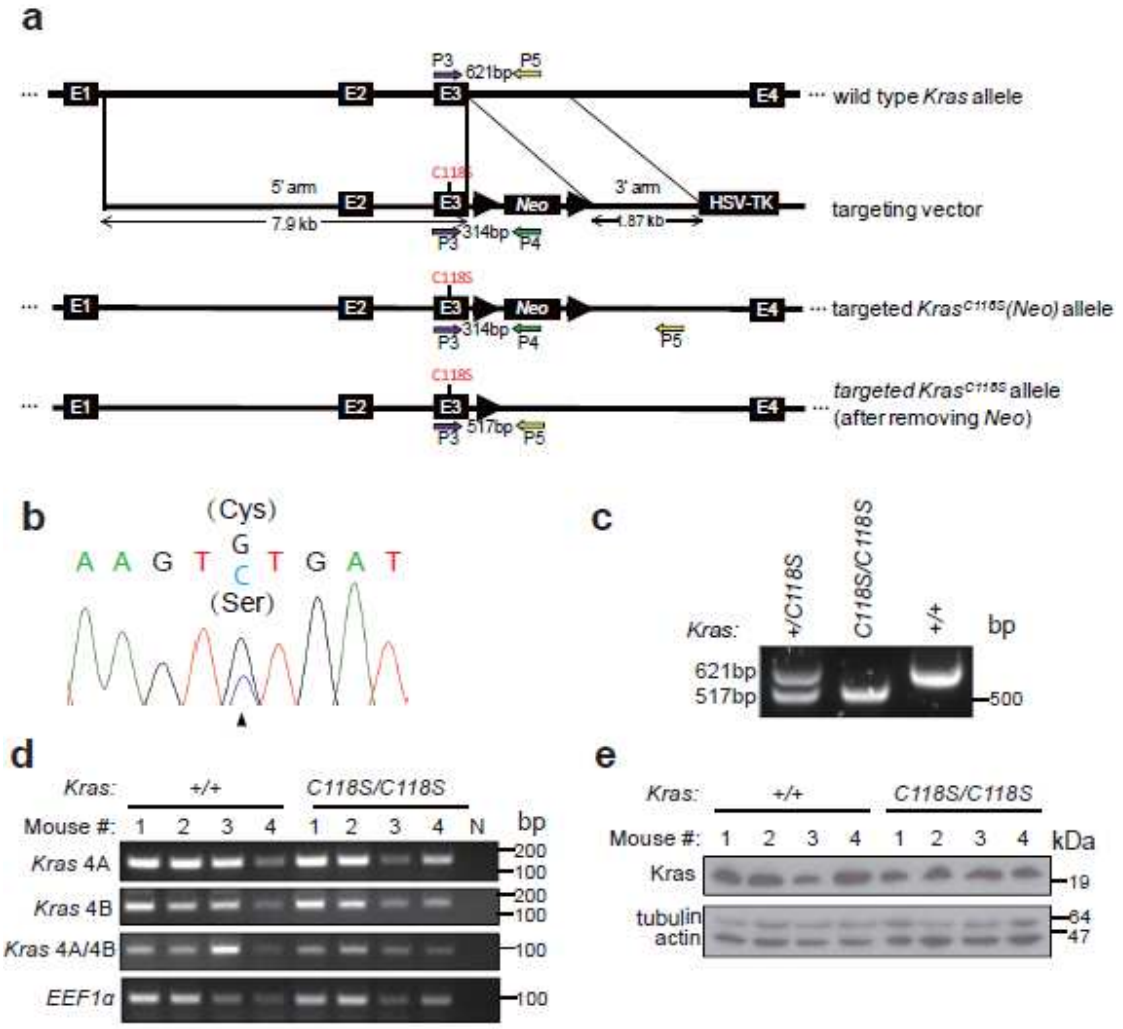

Figure 1: Generation of mice with a *Kras*^{C118S} allele.

(**a**) Schematic representation of homologous recombination (thin black lines) between the endogenous wild type *Kras* gene (E-numbered black boxes: exons, thick black lines: introns) and the *Kras*^{C118S} targeting vector (*Neo*: *Neo* selection marker; thick arrows: *loxP* recombination sites; HSV-TK: HSV promoter-driven thymidine kinase negative selection marker) as well as the resultant successfully targeted *Kras*^{C118S} knock-in allele before and after Cre-mediated recombination of the flanking *loxP* sites to excise the *Neo* selection marker. Colored arrows: PCR primers used in genotyping. (**b**) Sequencing chromatogram of RT-PCR amplified *Kras* mRNA from a successfully targeted ES cell clone identifying the wild type (G) and mutated (C) nucleotide at position 353 that changes the cysteine 118 codon to serine. (**c**) PCR amplification using the primer pair

P3+P5 of genomic DNA from offspring of the indicated genotypes from crossing *Kras*$^{+/C118S}$ mice. (**d**) RT-PCR amplification of *Kras* mRNA from the lungs of four *Kras*$^{+/+}$ mice and four *Kras*$^{C118S/C118S}$ mice (numbered 1, 2, 3 and 4) using primer pairs specific for the indicated *Kras* splice variants (*see* Table 8). N: no DNA as a negative control reaction. *EEF1α*: loading control. (**e**) Immunoblot of lysates isolated from the lungs of four *Kras*$^{+/+}$ mice and four *Kras*$^{C118S/C118S}$ mice (numbered 1, 2, 3 and 4) with an anti-Kras antibody. Tubulin and actin: loading controls.

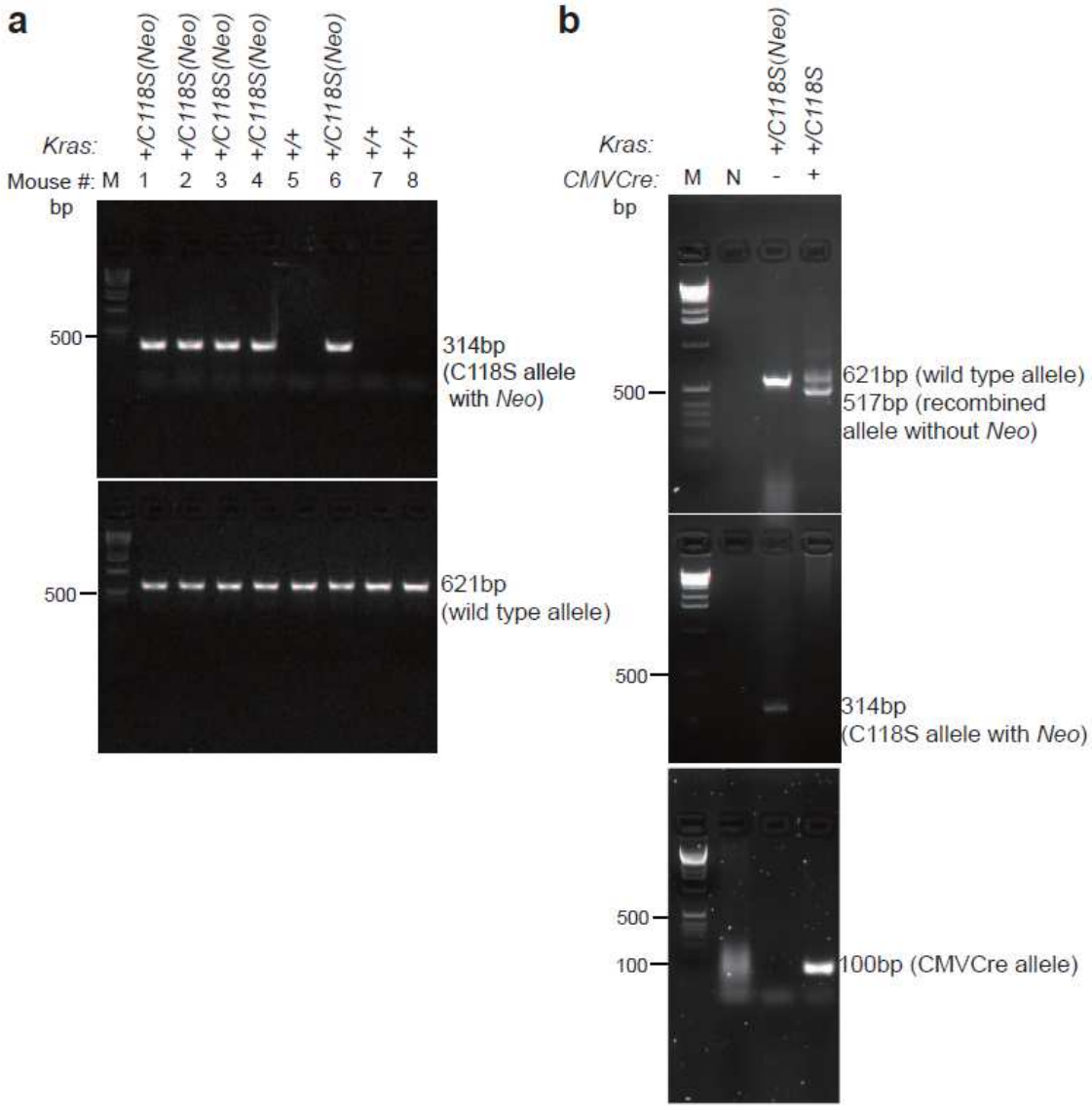

Figure 2: Identification of successful excision of the Neo cassette in the *Kras^{C118S}* allele.

(**a**) Full-length gels of PCR amplification of genomic DNA from eight mice (numbered from 1 to 8) from the breeding of a *Kras$^{+/C118S(Neo)}$* mouse and a *Kras$^{+/+}$* (BL6) mouse using the primer pair P3+P4 to amplify a 314 bp product specific to the *Kras$^{C118S(Neo)}$* allele (upper panel) or using the primer pair P3+P5 to amplify a 621 bp product specific to the wild type (+) *Kras* allele (lower panel), identifying the genotype as *Kras$^{+/C118S(Neo)}$* or *Kras$^{+/+}$* (labeled on top). (**b**) Full-length gels of PCR amplification of genomic DNA from a *Kras$^{+/C118S(Neo)}$* mouse without transgenic *CMVCre* and a *Kras$^{+/C118S}$* mouse with transgenic

CMVCre using the primer pair P3+P5 to amplify a 621 bp product specific to the wild type (+) *Kras* allele and/or a 517 bp product specific to the $Kras^{C118S}$ allele after successful excision of the *Neo* cassette (upper panel), using the primer pair P3+P4 to amplify a 314 bp product specific to the $Kras^{C118S(Neo)}$ allele with the *Neo* cassette (middle panel), or using the *CMVCre* genotyping primer pair P16+P17 to amplify a 100 bp product specific to *CMVCre* (lower panel). M: 1kb marker; N: negative (no DNA) control. All the primers are listed in Table 8.

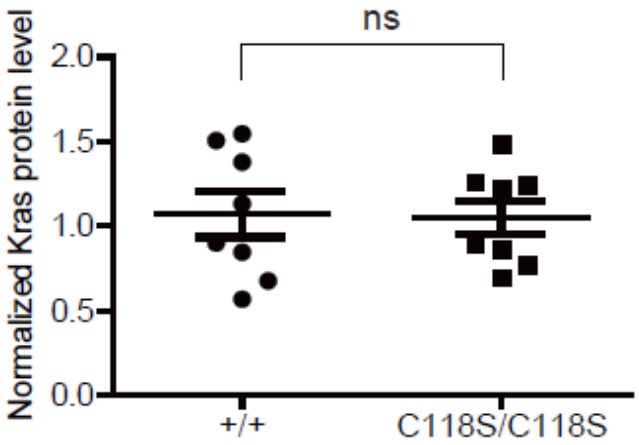

Figure 3: Similar Kras protein levels in lung tissue isolated from *Kras*$^{+/+}$ and *Kras*$^{C118S/C118S}$ mice.

Quantification of Kras protein levels (relative to tubulin and actin) from immunoblot of lysates derived from lung tissue of eight *Kras*$^{+/+}$ (+/+) and eight *Kras*$^{C118S/C118S}$ (C118S/C118S) mice. Bars: Mean ± SEM. ns: non-significant (P>0.05), as determined by two-tailed unpaired Student's t test.

3.2.2 Characterization of the *Kras*^{C118S} allele.

We confirmed that the strategy to introduce the G353>C transversion into the *Kras* gene did not overtly affect alternative splicing of terminal exons 4A and 4B, an important consideration as both splice forms are important for carcinogen-induced lung tumorigenesis (Patek, Arends et al. 2008, To, Wong et al. 2008). Specifically, RT-PCR analysis with primers designed to amplify only *Kras* 4A or only *Kras* 4B detected both versions in lung tissue isolated from *Kras*$^{+/+}$ and *Kras*$^{C118S/C118S}$ mice (Figure 1d). Similarly, we confirmed that this alteration of the *Kras* gene did not overtly affect protein expression, given that tumor initiation is sensitive to the level of Ras protein (Sarkisian, Keister et al. 2007). Specifically, immunoblot analysis revealed no detectable difference in the amount of Kras protein in lung tissue isolated from *Kras*$^{+/+}$ versus *Kras*$^{C118S/C118S}$ mice (Figure 1e and Figure 3). Finally, we demonstrate that introducing the C118S mutation into endogenous *Kras* gene can affect the ability of eNOS to stimulate the MAPK pathway. Specifically, mouse embryonic fibroblasts (MEFs) were isolated from two control *Kras*$^{+/+}$ and two experimental *Kras*$^{C118S/C118S}$ embryos and immortalized with the SV40 early region. These four cell lines were then stably infected with a retrovirus encoding no transgene or the S1177D activated mutant version of HA-tagged eNOS (Dimmeler, Fleming et al. 1999, Fulton, Gratton et al. 1999). Lysates isolated seven independent times from the resultant eight cell lines were then immunoblotted for ectopic HA-tagged eNOS, endogenous Kras, and tubulin, as well as total (T) and

phosphorylated (P) Erk1/2. While the normalized levels of P-Erk1/2 varied from experiment to experiment amongst the samples, on average there was a smaller fold increase in the normalized P-Erk1/2 levels upon expression of eNOS^{S1177D} in *Kras*$^{C118S/C118S}$ compared to *Kras*$^{+/+}$ MEFs (0.90 ± 0.14 versus 3.21±0.91, P<0.02, Figure 4). Collectively, we conclude that the single G353>C transversion encoding the desired C118S mutation was successfully knocked into the *Kra*s locus with no overt effect on the expression of the resultant gene products.

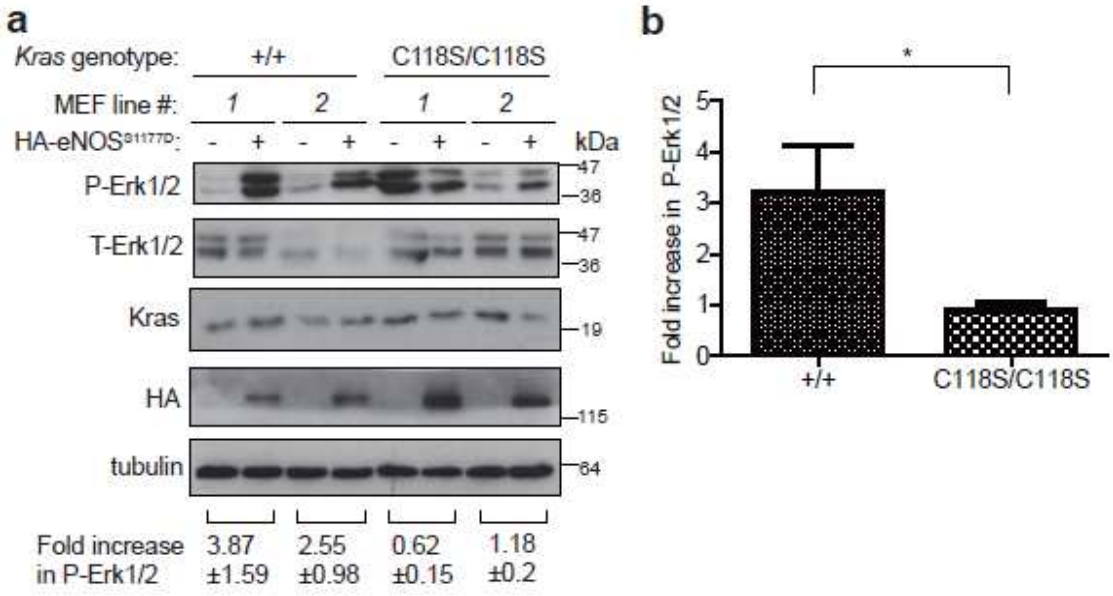

Figure 4: Reduced increase in P-Erk1/2 levels in *Kras*$^{C118S/C118S}$ MEFs upon expressing activated eNOS.

(**a**) Immunoblot of ectopic HA-tagged eNOS, endogenous Kras, and tubulin, as well as total (T) and phosphorylated (P) Erk1/2 from two *Kras*$^{+/+}$ and two *Kras*$^{C118S/C118S}$ SV40-immortalized MEF cell lines in the absence or presence of HA-eNOS^{S11777D}. Bottom: mean ± SEM of the indicated fold increase in P-Erk1/2 (normalized to T-Erk1/2) from immunoblot analysis of lysates derived seven independent times. (**b**) Mean ± SEM fold increase in P-Erk1/2 levels (normalized to T-Erk1/2) upon expression of eNOS^{S1177D} from lysates derived seven independent times from the two *Kras*$^{+/+}$ (+/+) or two *Kras*$^{C118S/C118S}$ (C118S/C118S) SV40-immortalized MEF cell lines. *: $P<0.05$, as determined by two-tailed unpaired student's *t* test.

3.2.3 *Kras*$^{C118S/C118S}$ mice appear normal.

Identification of genotypes of 580 offspring from crossing *Kras*$^{+/C118S}$ mice revealed that there was no statistical difference between the observed frequency versus the expected Mendelian ratio of the three genotypes of *Kras*$^{+/+}$, *Kras*$^{+/C118S}$, and *Kras*$^{C118S/C118S}$ (Chi-square test, P=0.545, Table 1). *Kras*$^{C118S/C118S}$ mice were also phenotypically indistinguishable from *Kras*$^{+/+}$ mice (Figure 5a). Weekly weight measurements, beginning at 8 weeks of age and continuing for another 17 weeks, revealed no statistical difference in the weight of either male or female mice between the *Kras*$^{+/+}$ versus *Kras*$^{C118S/C118S}$ genotypes (Figure 5b,c). The *Kras*$^{-/-}$ genotype is embryonic to neonatal lethal, and is characterized by defective cardiovascular function (Koera, Nakamura et al. 1997). As heart defects are a hallmark of defective Kras function (Koera, Nakamura et al. 1997), I also compared the heart-to-body weight ratio between *Kras*$^{+/+}$ versus *Kras*$^{C118S/C118S}$ mice, finding no significant difference between the two cohorts (Figure 5d). Finally, *Kras*$^{+/+}$ mice had a median lifespan of 847 days while *Kras*$^{C118S/C118S}$ mice had a median lifespan of 670 days, but the difference was not significant (Figure 5e). Collectively, these data indicate that mice with one or more *Kras*^{C118S} alleles do not have any obvious developmental or physiological defects.

To investigate the possibility that the existing wild-type *Hras* and *Nras* may compensate for the loss-of-function of *Kras*^{C118S} mutant, *Kras*$^{C118S/+}$ mice were crossed into *Hras*$^{-/-}$;*Nras*$^{-/-}$ background, generating *Hras*$^{-/-}$;*Nras*$^{-/-}$;*Kras*$^{+/C118S}$ mice that only have the *Kras*

gene but not *Hras* or *Nras* genes. Identification of genotypes of 42 offspring from crossing $Hras^{-/-};Nras^{-/-};Kras^{+/C118S}$ mice revealed that there was no statistical difference between the observed frequency versus the expected Mendelian ratio of the three genotypes of $Hras^{-/-};Nras^{-/-};Kras^{+/+}$, $Hras^{-/-};Nras^{-/-};Kras^{+/C118S}$, and $Hras^{-/-};Nras^{-/-};Kras^{C118S/C118S}$ (Chi-square test, P=0.377, Table 2). Taken together, these results suggest that $Kras^{C118S}$ mutant allele does not seem to affect the role of *Kras* in development.

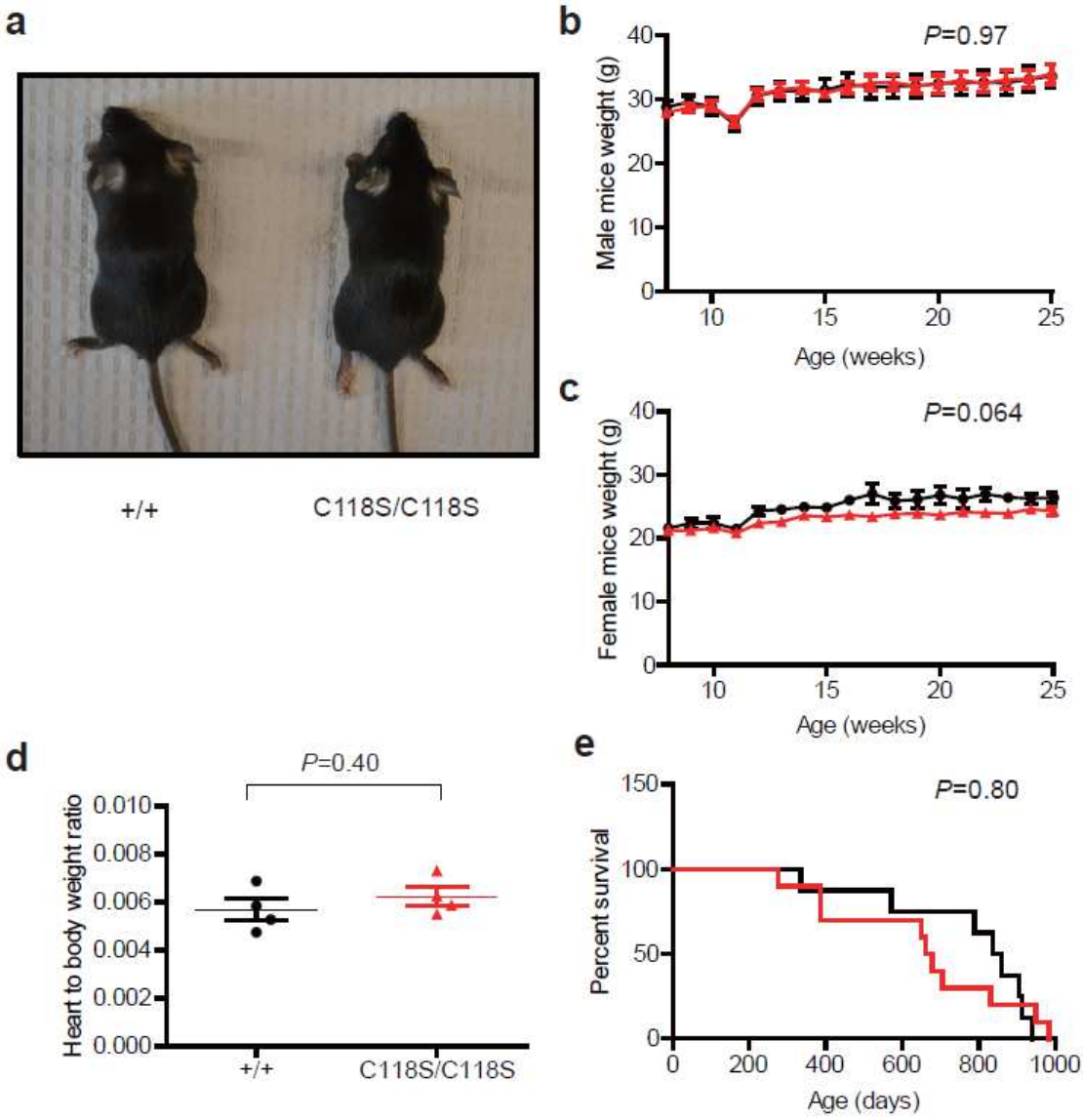

Figure 5: *Kras*$^{C118S/C118S}$ mice have no overt phenotypes.

(**a**) Photograph of a *Kras*$^{+/+}$ (+/+) and *Kras*$^{C118S/C118S}$ (C118S/C118S) adult mouse at three weeks of age. (**b, c**) Mean body weight ± SEM of (●) *Kras*$^{+/+}$ versus (▲) *Kras*$^{C118S/C118S}$ (**b**) male (n=6 versus 5) and (**c**) female mice (n= 4 versus 5) from 8 to 25 weeks of age. (**d**) Mean heart to body weight ratio ± SEM of four week old *Kras*$^{+/+}$ (+/+) versus *Kras*$^{C118S/C118S}$ (C118S/C118S) mice (n=4). (**e**) Kaplan-Meier survival curves of *Kras*$^{+/+}$ (black line, n=8) versus *Kras*$^{C118S/C118S}$ (red line, n=10) mice. *P* value was determined by MANOVA test (**b, c**), two-tailed unpaired student's *t* test (**d**) and long-rank test (**e**).

Table 1: Expected and observed frequencies of offspring from crossing *Kras*$^{+/C118S}$ mice.

Kras Genotype	Expected Frequency	Observed Frequency
+/+	25% (145/580)	26.72% (155/580)
+/C118S	50% (290/580)	47.93% (278/580)
C118S/C118S	25% (145/580)	25.34% (147/580)

Table 2: Expected and observed frequencies of offspring from crossing *Nras*$^{-/-}$;*Hras*$^{-/-}$;*Kras*$^{+/C118S}$ mice.

Kras Genotype	Expected Frequency	Observed Frequency
+/+	25% (10.5/42)	26.19% (11/42)
+/C118S	50% (21/42)	40.48% (17/42)
C118S/C118S	25% (10.5/42)	33.33% (14/42)

3.2.4 Reduced carcinogenesis in mice with a *Kras^{C118S}* allele.

To determine the impact of the *Kras^{C118S}* mutation on carcinogenesis, I assessed the effect of treating *Kras$^{+/+}$*, *Kras$^{+/C118S}$*, and *Kras$^{C118S/C118S}$* mice with the carcinogen urethane (ethyl carbamate), which induces lung tumors characterized by oncogenic Q61R/L mutations in *Kras* (You, Candrian et al. 1989). We chose this approach to model a *Kras* mutation-positive cancer spontaneously arising from an environmental insult (You, Candrian et al. 1989) in the lung, especially given the prevalence of *KRAS* mutations in human lung cancer (Ding, Getz et al. 2008). As an important note, the *Pas1* locus responsible for the different susceptibilities to urethane-induced tumorigenesis observed amongst inbred strains of mice maps to a region containing six genes, one being *Kras* (Manenti, Galbiati et al. 2004). Therefore, *Kras$^{+/C118S}$* mice, which possess the *Kras^{C118S}* allele from the 129S6/SvEvTac background, but the other native *Kras* allele from the C57/BL6 background (introduced during the excision of the *Neo* cassette), were crossed with *Kras$^{+/+}$* mice from the 129S6/SvEvTac background. Resultant *Kras$^{+/C118S}$* mice were then crossed to generate *Kras$^{+/+}$*, *Kras$^{+/C118S}$*, and *Kras$^{C118S/C118S}$* mice in which both *Kras* alleles originated from a 129S6/SvEvTac background. Cohorts of 27 *Kras$^{+/+}$*, 25 *Kras$^{+/C118S}$*, and 25 *Kras$^{C118S/C118S}$* littermates from multiple breeding pairs were then intraperitoneally injected with urethane at eight weeks of age. Eight months later, mice from all three cohorts were euthanized and lungs removed for analysis.

Comparison of the number and size of visible surface lung lesions revealed that *Kras*$^{+/C118S}$ or *Kras*$^{C118S/C118S}$ mice developed fewer tumors with a smaller average tumor size, resulting in an overall reduction in tumor burden, as defined by the sum of the diameters of all visible surface tumors per mouse, compared to control *Kras*$^{+/+}$ mice (Figure 6a-d). There was no statistical difference in tumor number or size between the *Kras*$^{+/C118S}$ and *Kras*$^{C118S/C118S}$ cohorts (Figure 6a-d and Table 3). Binning tumors based on size, namely small (≤1mm), medium (1-3 mm), or large (≥3mm), revealed a significant shift (Chi-square test, P=0.0014) from larger tumors in *Kras*$^{+/+}$ mice to smaller tumors in *Kras*$^{C118S/C118S}$ mice (Table 3). To independently validate these results, one lung from each of the mice in the three cohorts was formalin fixed, paraffin embedded, sectioned, H&E stained, and the type and size of tumors analyzed. Focusing on the most common type of lesion, adenomas were microscopically counted and binned as above as being small, medium, or large. Again, there was a shift to smaller tumors in mice having one or more *Kras*^{C118S} alleles. Specifically, large adenomas were only detected in *Kras*$^{+/+}$ mice, and these mice also had a higher incidence of adenomas of medium size, while *Kras*$^{+/C118S}$ and *Kras*$^{C118S/C118S}$ mice had a statistically higher incidence of small-sized adenomas (Chi-square test, P≤0.01, Table 4). Collectively, these data demonstrate that the presence of the *Kras*^{C118S} allele impairs urethane carcinogenesis.

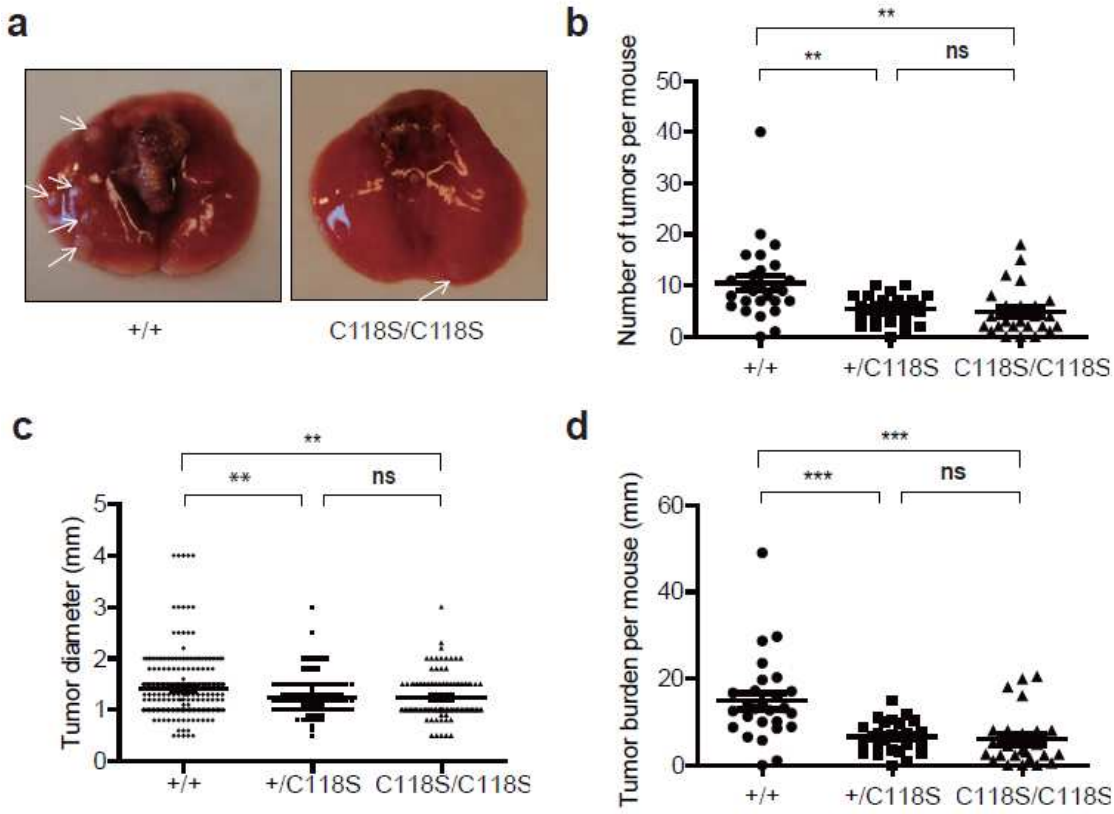

Figure 6: Decreased urethane-induced lung tumorigenesis in mice with a *Kras*^{C118S} allele.

(**a**) Visible lesions (arrows) of lungs from one *Kras*$^{+/+}$ (+/+) and one *Kras*$^{C118S/C118S}$ (C118S/C118S) mouse eight months after treatment with urethane. (**b**) Number of visible surface tumor lesions per mouse, (**c**) diameter of each visible surface tumor lesion and, (**d**) tumor burden, as defined by the sum of the diameters of all visible surface tumor lesions per mouse, from *Kras*$^{+/+}$ (+/+, 27 mice, 285 visible surface tumors), *Kras*$^{+/C118S}$ (+/C118S, 25 mice, 132 visible surface tumors), and *Kras*$^{C118S/C118S}$ (C118S/C118S, 25 mice, 121 visible surface tumors) mice eight months after treatment with urethane. Bars: mean ± SEM. ns: non-significant ($P>0.05$), **$P<0.01$ and ***$P<0.001$, as determined using one-way ANOVA plus post-hoc Bonferroni's multiple comparison test.

Table 3: Quantification of surface lung tumors from urethane-treated mice.

Kras genotype	Number of mice	Tumor incidence	Mean ± SEM tumors per lung	Total number of tumors	Tumor incidence by size (mm)		
					≤1	1 – 3	≥3
+/+	27	96.3%	10.52 ± 1.46	285	37.5%	58.9%	3.5%
+/C118S	25	96.0%	5.36 ± 0.56	132	41.7%	57.6%	0.76%
C118S/C118S	25	88.0%	4.84 ± 0.95	121	56.2%	43.0%	0.83%

Table 4: Histological quantification of lung adenomas from urethane-treated mice.

Kras genotype	Number of lung sections	Adenoma incidence	Mean ± SEM adenomas per section	Total number of adenomas	Adenoma incidence by size (mm)		
					≤1	1 – 3	≥3
+/+	27	85.2%	2.52 ± 0.35	68	52.9%	41.2%	5.9%
+/C118S	25	80.0%	1.92 ± 0.26	48	87.5%	12.5%	0 %
C118S/C118S	25	80.0%	1.64 ± 0.38	41	80.5%	19.5%	0%

To assess whether there was also an impact on tumor progression, lesions were graded (Stathopoulos, Sherrill et al. 2007) as being atypical adenomatous hyperplasia (AAH), adenoma (AD), or adenocarcinoma (AC) by histology (Figure 7). This analysis revealed a similar tumor spectrum amongst the three genotypes. Specifically, regardless of the genotype, the majority of the tumors were AD, with only a few AAHs and an infrequent number of AC in each group (Table 5). AD lesions were further classified (Avanzo, Mesnil et al. 2004) into papillary, solid, or mixed solid/papillary subtypes (Figure 7). There was no significant difference in the incidence of solid AD among the three groups, although the *Kras*$^{+/C118S}$ mice appeared to have fewer papillary AD and more mixed solid/papillary AD (Table 6). Finally, immunohistochemical analysis of lung lesions in four to six random microscope fields from five mice each having the genotypes *Kras*$^{+/+}$, *Kras*$^{+/C118S}$, or *Kras*$^{C118S/C118S}$ after treatment with urethane did not show any overt difference in the level of Ras signaling, as assessed by P-Erk1/2 or P-Akt immunostaining, or in proliferation, as assessed by Ki67 immunostaining, with the exception of reduced P-Akt in the *Kras*$^{+/C118S}$ cohort (Figure 8). Collectively, these data point towards a negative effect of the *Kras*^{C118S} allele, particularly at the stage of tumor initiation.

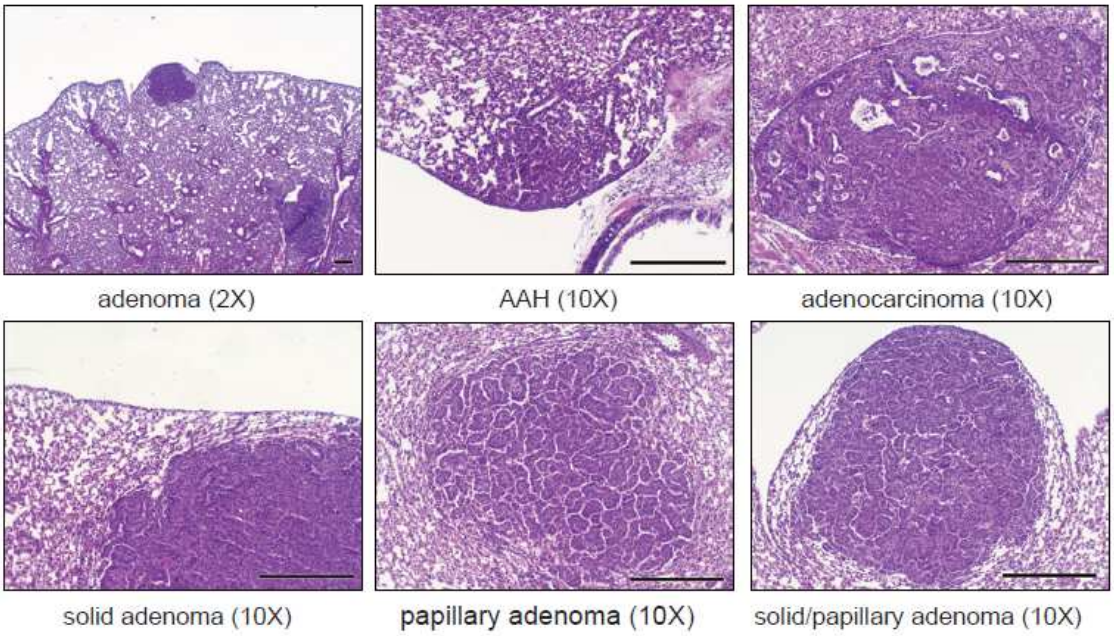

Figure 7: Representative images of different types of tumors detected in H&E-stained lung sections from urethane-treated mice.

Scale bar: 300 μm. 2X or 10 X: magnification.

Table 5: Histological characterization of lung tumors from urethane-treated mice.

Kras genotype	Number of lung sections	Tumor incidence	Mean ± SEM tumors per section	Total number of tumors	Tumor incidence by classification		
					AAH	AD	AC
+/+	27	85.2%	2.96 ± 0.44	80	11.3%	85.0%	3.8%
+/C118S	25	80.0%	2.28 ± 0.326	57	14.0%	84.2%	1.8%
C118S/C118S	25	80.0%	2.00 ± 0.44	50	16.0%	82.0%	2.0%

Table 6: Subtypes of lung adenomas from urethane-treated mice.

Kras genotype	Total number of adenomas	Adenoma incidence by classification		
		Solid	Papillary	Solid/ Papillary
+/+	68	39.7%	16.2%	44.1%
+/C118S	48	37.5%	4.2%	58.3%
C118S/C118S	41	43.9%	22.0%	34.2%

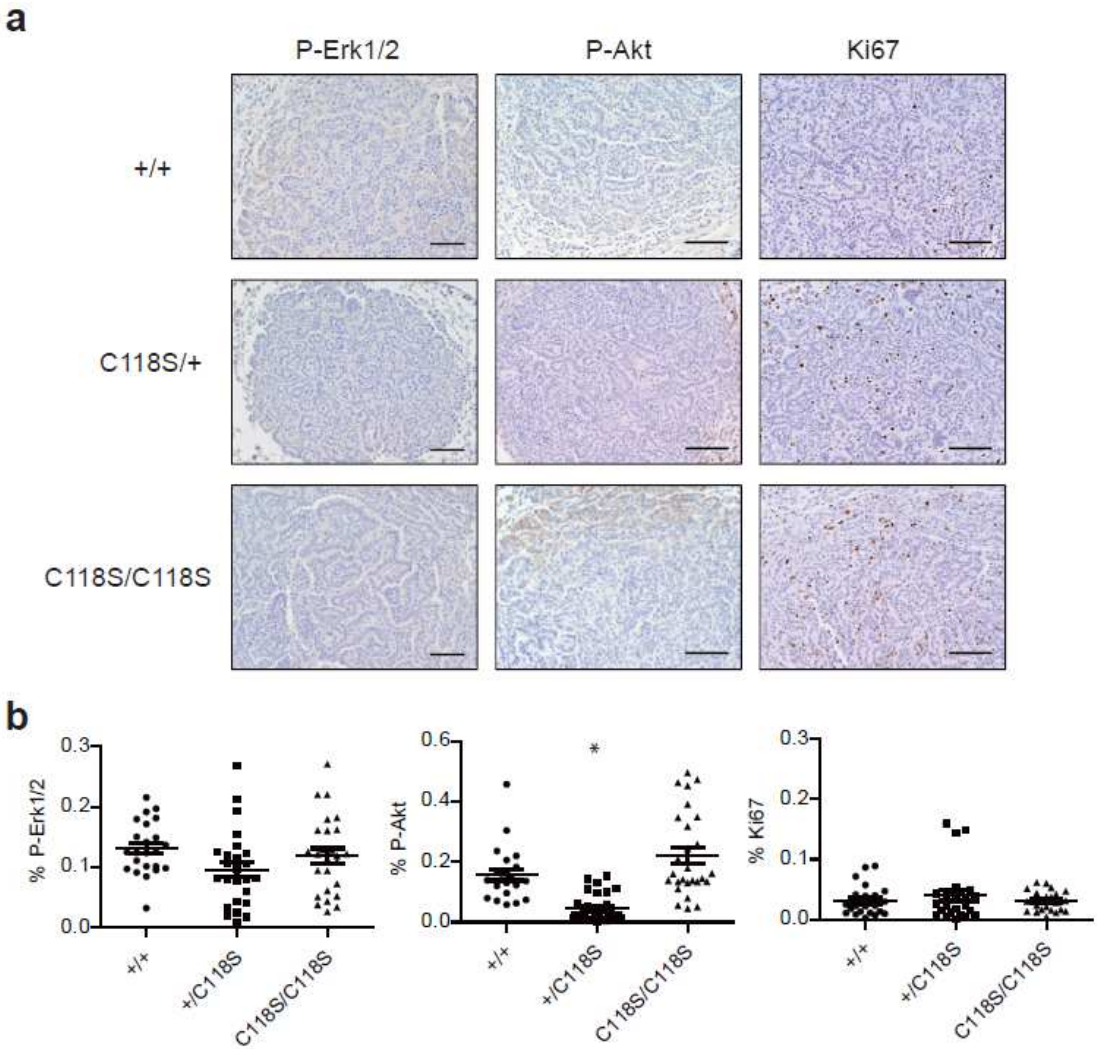

Figure 8: P-Erk1/2, P-Akt, and Ki67 immunohistochemical analysis of lung tumors.

(**a**) Representative photograph (scale bar: 100 μm) and (**b**) quantification of the percent positive staining for P-Erk1/2, P-Akt, or Ki67 per tumor area (bars: mean ± SEM) from four to six high-power (20X) random fields of lung sections from five mice from each of the $Kras^{+/+}$ (+/+), $Kras^{+/C118S}$ (+/C118S), and $Kras^{C118S/C118S}$ (C118S/C118S) cohorts. No significant difference was noted except in one case (*: P<0.001 between C118S/+ versus +/+ or C118S/C118S).

3.2.5 Similar tumorigenesis between *Kras*$^{LSL\text{-}G12D/+}$ and *Kras*$^{LSL\text{-}G12D/C118S}$ mice.

In the urethane-induced lung tumor model, typically only one *Kra*s allele acquires an oncogenic mutation. While the oncogenic *Kras* allele is well established to promote tumorigenesis, the remaining non-oncogenic allele has actually been found to be tumor suppressive (Zhang, Wang et al. 2001). As such, the observed negative effect of the *Kras*^{C118S} allele on lung tumorigenesis is ostensibly due to the C118S mutation either suppressing the tumorigenic activity of oncogenic *Kras* allele and/or enhancing tumor suppressive effect of the remaining non-oncogenic *Kras* allele. To test the latter possibility, we took advantage of mice with a conditionally oncogenic *LSL-Kras*^{G12D} allele to compare the effect of the remaining *Kras* allele with or without a C118S mutation on lung tumorigenesis. In more detail, infection of lung tissue upon intranasal administration of adenovirus encoding Cre (AdCre) induces recombination of *loxP* sites flanking a transcriptional/translational STOP sequence (*LSL*) upstream of *Kras* harboring a G12D oncogenic mutation, thereby permitting expression of the *Kras*^{G12D} allele, which promotes lung tumorigenesis (Jackson, Willis et al. 2001). Thus, *LSL-Kras*$^{G12D/+}$ mice were crossed with *Kras*$^{+/C118S}$ mice in which both *Kras* alleles were of the 129S6/SvEvTac background. Cohorts of 21 resultant *Kras*$^{LSL\text{-}G12D/+}$ and 17 *Kras*$^{LSL\text{-}G12D/C118S}$ littermates from multiple breeding pairs were treated intranasally with AdCre at eight weeks of age. Four months later, mice from both cohorts were euthanized and lungs removed for analysis. Quantification of the number, size, and total burden of visible surface lesions

revealed no statistical difference between the two cohorts (Figure 9a-c). The sizes of these cohorts were powered to detect differences in the number, burden, and size of 1.52, 1.78 mm, and 0.52 mm, respectively. Similarly, microscopic quantification of the number of lesions in H&E stained lung sections from these mice (Figure 10) revealed no significant difference between these two cohorts (Figure 9d). Thus, the C118S mutation does not appear to confer any overt change to the tumor suppressive activity to the non-oncogenic allele in a lung tumor model driven by $Kras^{G12D}$.

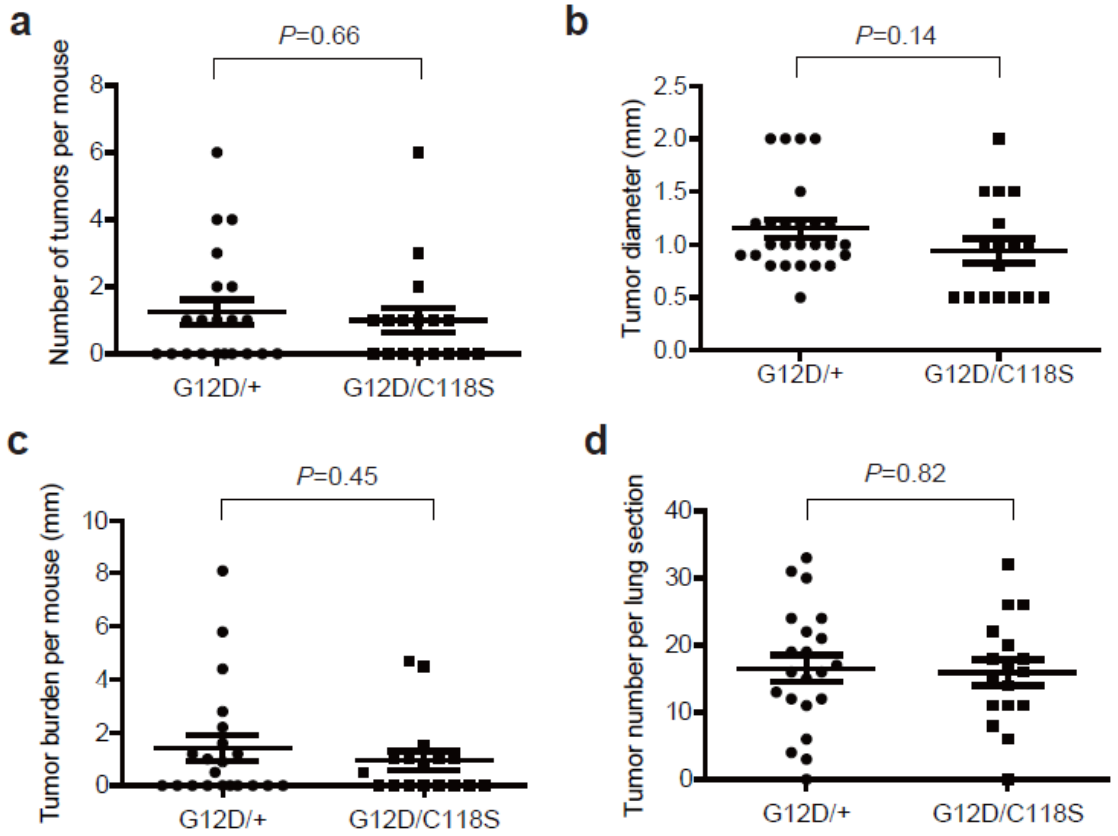

Figure 9: *Kras*^{G12D}-driven lung tumorigenesis is similar when the remaining *Kras* allele is wild-type or C118S.

(**a**) Number of visible surface tumor lesions per mouse, (**b**) diameter of each visible surface tumor lesion, (**c**) tumor burden, as defined by the sum of the diameters of all visible surface tumor lesions per mouse, and (**d**) number of lesions detected in each H&E stained section from *Kras*$^{LSL\text{-}G12D/+}$ (G12D/+, 21 mice, 26 visible surface tumors) versus *Kras*$^{LSL\text{-}G12D/C118S}$ (G12D/C118S, 17 mice, 17 visible surface tumors) mice four months after intranasal administration of AdCre. Bars: mean ± SEM. *P* values were determined using two-tailed unpaired student's *t*-test.

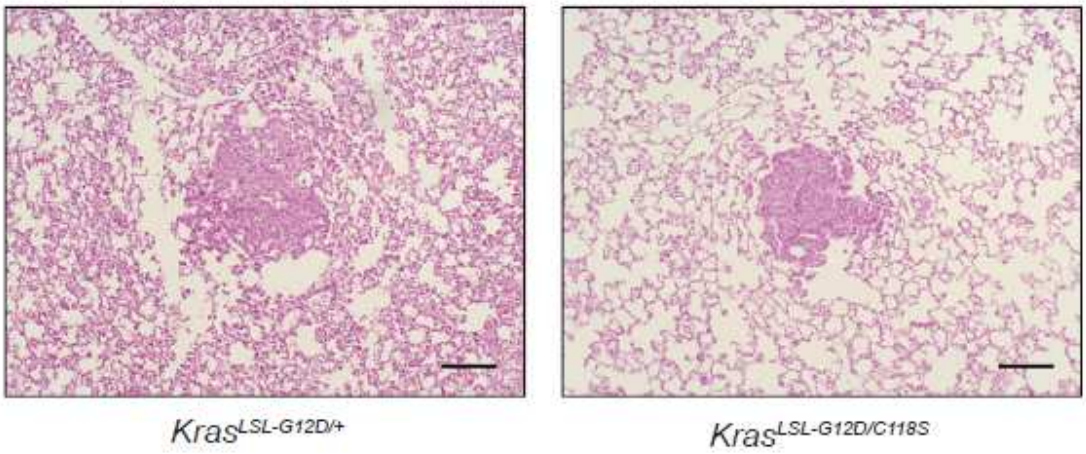

Figure 10: A representative image of an H&E stained lung section from an AdCre-treated *Kras*$^{LSL\text{-}G12D/+}$ or *Kras*$^{LSL\text{-}G12D/C118S}$ mouse at 4X magnification.

Scale bar: 300 μm.

3.2.6 Mutational bias against the *Kras*^{C118S} allele.

We next tested whether there was a bias of oncogenic mutations induced by urethane in either the native or C118S *Kras* allele in *Kras*$^{+/C118S}$ mice. To this end, RNA was extracted from 65 lung tumors from 20 *Kras*$^{+/C118S}$ mice treated with urethane. *Kras* mRNA was then RT-PCR amplified, cloned, and sequenced to identify the allelic origin (native or C118S) and mutation status (wild type or oncogenic). No oncogenic mutation was detected in either *Kras* allele in 21 tumors, only one allele was recovered in another nine tumors, and a mutation was detected in both alleles in three tumors. As such, these samples were excluded from the analysis (Table 7). Of the remaining 32 tumors (derived from 15 *Kras*$^{C118S/+}$ mice) in which both *Kras* alleles were recovered and there was an oncogenic mutation in only one of the *Kras* alleles, 20 tumors had an oncogenic Q61R/L mutation in the native *Kras* allele, while 12 had the mutation in the *Kras*^{C118S} allele (Figure 11 and Table 7). This almost two-fold enrichment in mutations recovered in the native *Kras* allele was significantly different from the expected frequency, assuming the incidence of oncogenic Q61R/L mutations occurring on the native *Kras* and the *Kras*^{C118S} allele was both 50% (Chi-square test, P=0.0455).

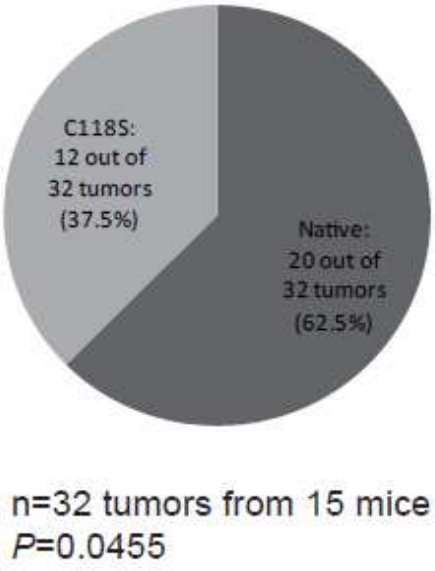

Figure 11: Oncogenic Q61 mutations occur preferentially on the native *Kras* allele.

Pie chart of the number and percent of Q61R/L oncogenic mutations found in the native versus the C118S *Kras* allele, as determined by RT-PCR amplification and sequencing of *Kras* mRNA isolated from 32 lung lesions from 15 $Kras^{+/C118S}$ mice eight months after treatment with urethane. *P* value was determined using the Chi-square test to compare the difference between the observed and the expected frequency.

Table 7: *Kras* sequencing analysis from lung tumors of urethane-treated *Kras*$^{+/C118S}$ mice.

Q61 mutation	Total	Q61L	Q61R
Present on native *Kras* allele	20	8	12
Present on C118S *Kras* allele	12	0	12
Present on both *Kras* alleles	3	1	2
Absent from both *Kras* alleles	21		
Only one *Kras* alleles recovered	9		
Total tumors analyzed	65	9	26

3.2.7 Introducing a C118S mutation reduces the oncogenic activity of $Kras^{G13D}$

The above results suggest a bias against oncogenic mutations in the $Kras^{C118S}$ allele. Therefore, I tested whether oncogenic $Kras^{Q61L,C118S}$ had reduced activity compared with $Kras^{Q61L}$ by measuring RAS downstream signaling in cells expressing $Kras^{Q61L,C118S}$ or $Kras^{Q61L}$. Specifically, $Kras^{C118S/C118S}$ MEFs immortalized with the SV40 early region and transformed with either $Kras^{Q61L,C118S}$ or $Kras^{Q61L}$ were treated with epidermal growth factor (EGF) to stimulate GEF activity, given the potential involvement of GEFs in activating oncogenic Ras proteins (Hocker, Cho et al. 2013, Huang, Daniluk et al. 2014). Lysates derived four independent times from these two cell lines were then immunoblotted to detect ectopic Kras, endogenous tubulin, as well as total (T) and phosphorylated (P) Erk1/2. On average, normalized P-Erk1/2 level upon EGF treatment were found to be similar between $Kras^{C118S/C118S}$ MEFs transformed with $Kras^{Q61L,C118S}$ and those transformed with $Kras^{Q61L}$ (Figure 12a,b). To exclude an involvement of wild type *Hras* and *Nras* isoforms (Lim, Ancrile et al. 2008, Jeng, Taylor et al. 2012), the $Kras^{C118S/C118S}$ genotype was crossed into an $Hras^{-/-};Nras^{-/-}$ background to generate $Kras^{C118S/C118S};Hras^{-/-};Nras^{-/-}$ MEFs, which were then immortalized with the SV40 early region and transformed with either $Kras^{Q61L,C118S}$ or $Kras^{Q61L}$. Based on one experiment, normalized P-Erk1/2 level upon EGF treatment was slightly decreased in $Kras^{C118S/C118S};Hras^{-/-};Nras^{-/-}$ MEFs transformed with $Kras^{Q61L,C118S}$ (Figure 12c,d). These

results suggest that the $Kras^{C118S}$ mutation may have little or a slight inhibitory effect on $Kras^{61L}$ downstream signaling.

While preliminary experiments revealed that ectopic $Kras^{Q61L,C118S}$ and $Kras^{Q61L}$ behaved rather similarly with regards to downstream signaling, there did appear to be a potential consequence of mutating C118 to serine in the G13D oncogenic mutant background. Specifically, $Kras^{C118S/C118S}$ MEFs immortalized with the SV40 early region and transformed with either $Kras^{G13D,C118S}$ or $Kras^{G13D}$ were treated with EGF to stimulate GEF activity. Lysates derived three independent times from these two cell lines were then immunoblotted to detect ectopic Kras, endogenous tubulin, as well as total (T) and phosphorylated (P) Erk1/2. On average, this analysis revealed a trend towards a lower normalized P-Erk1/2 level upon EGF treatment in the $Kras^{G13D,C118S}$ compared to $Kras^{G13D}$ transformed MEFs (Figure 13a,b). To exclude an involvement of wild type *Hras* and *Nras* isoforms (Lim, Ancrile et al. 2008, Jeng, Taylor et al. 2012), $Kras^{C118S/C118S};Hras^{-/-};Nras^{-/-}$ MEFs were immortalized with the SV40 early region and transformed with either $Kras^{G13D,C118S}$ or $Kras^{G13D}$. Based on three independent experiments, on average there was a decrease in the normalized P-Erk1/2 levels upon EGF treatment in the $Kras^{G13D,C118S}$ compared to the $Kras^{G13D}$ transformed $Kras^{C118S/C118S};Hras^{-/-};Nras^{-/-}$ MEFs (Figure 13 c,d). These results suggest that a C118S mutation in the oncogenic $Kras^{G13D}$ affects oncogenic Kras downstream Erk1/2 signaling.

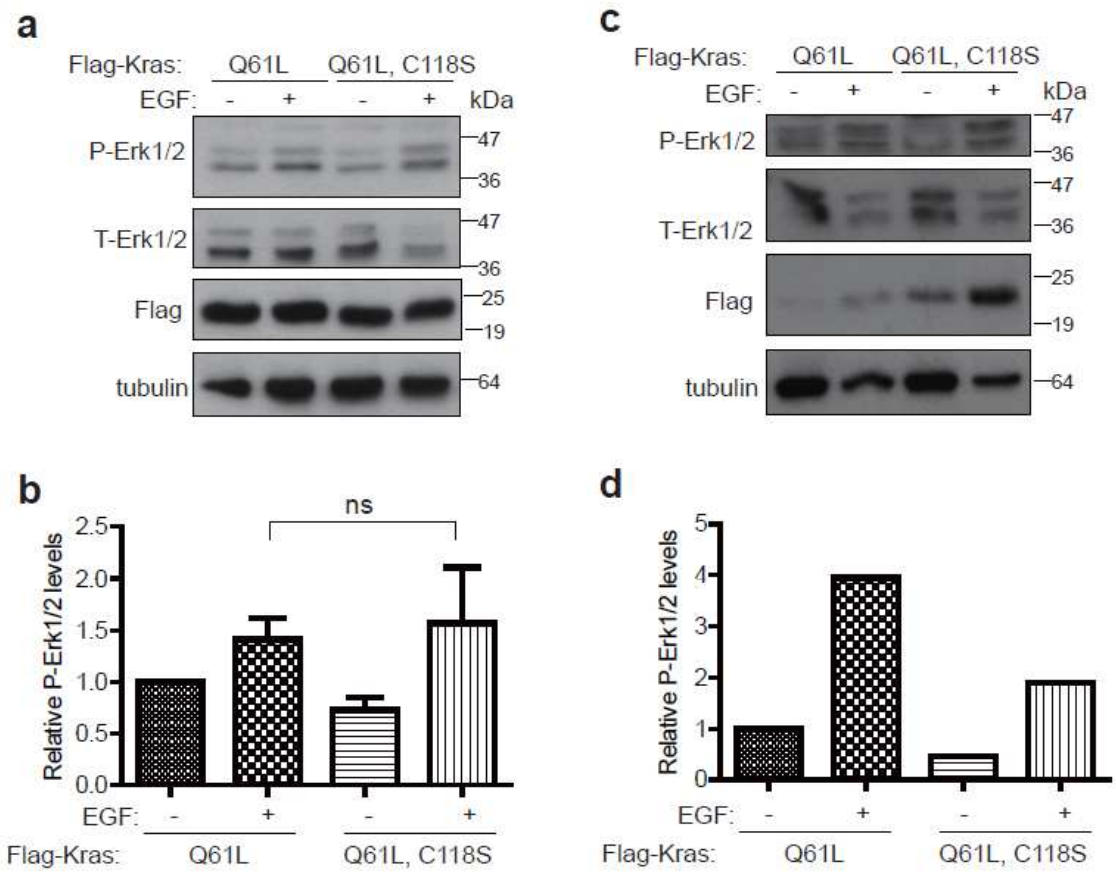

Figure 12: Similar levels of Erk1/2 levels of MEFs transformed with Kras^{Q61L} and Kras^{Q61L,C118S} upon EGF treatment.

Immunoblot of Flag-tagged ectopic Kras, tubulin, as well as total (T) and phosphorylated (P) Erk1/2 from (**a**) *Kras$^{C118S/C118S}$* or (**c**) *Nras$^{-/-}$;Hras$^{-/-}$;Kras$^{C118S/C118S}$* MEFs immortalized with the SV40 early region and transformed with either Flag-Kras^{Q61L} or Flag-Kras^{Q61L,C118S} in the absence or presence of EGF stimulation. (**b**) Mean ± SEM of P-Erk1/2 levels (normalized to T-Erk1/2) from four independent experiments and (**d**) P-Erk1/2 levels (normalized to T-Erk1/2) from one experiment using lysates from (**b**) *Kras$^{C118S/C118S}$* and (**d**) *Nras$^{-/-}$;Hras$^{-/-}$;Kras$^{C118S/C118S}$* MEFs immortalized with the SV40 early region and transformed with either Flag-Kras^{Q61L} or Flag-Kras^{Q61L,C118S} in the absence or presence of EGF stimulation. ns: non-significant (P>0.05), as determined using one-way ANOVA plus post-hoc Bonferroni's multiple comparison test.

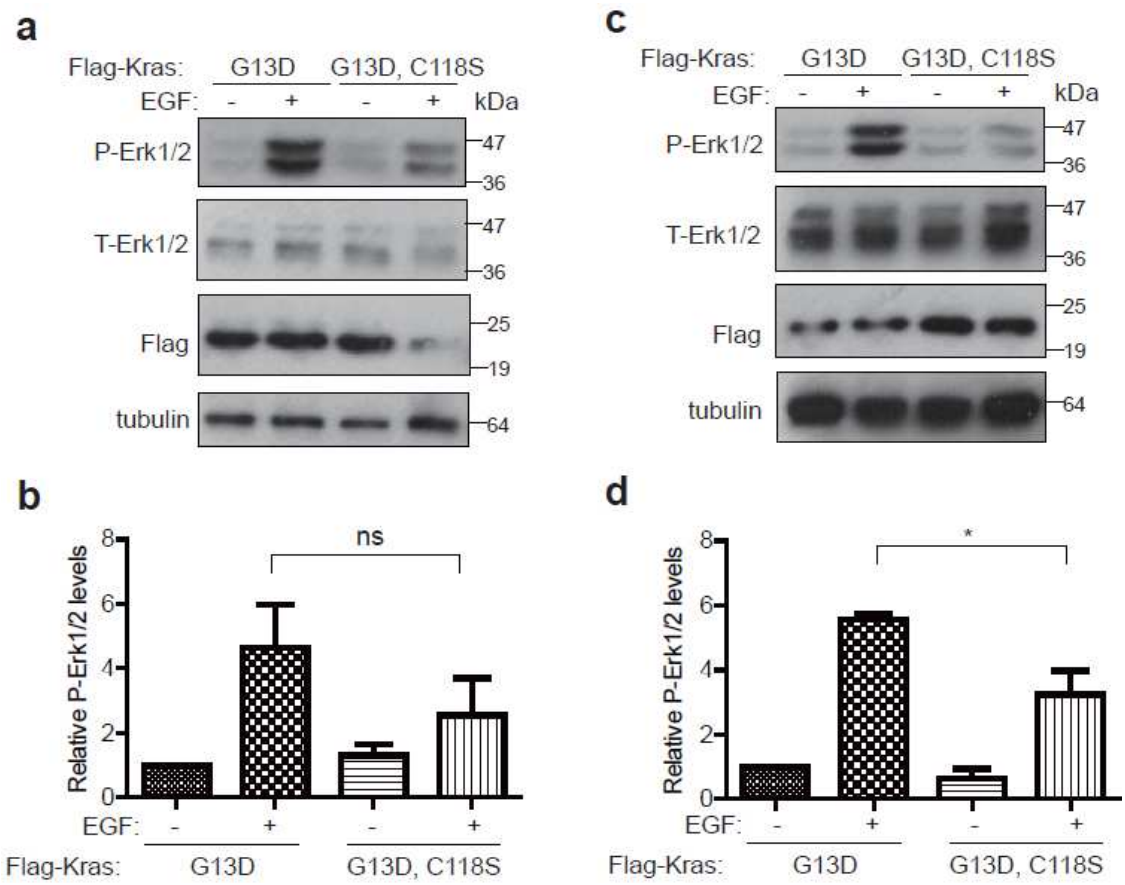

Figure 13: Reduced increase in P-Erk1/2 levels in MEFs transformed with Kras^{G13D,C118S} upon EGF treatment.

Immunoblot of Flag-tagged ectopic Kras, tubulin, as well as total (T) and phosphorylated (P) Erk1/2 from (**a**) *Kras$^{C118S/C118S}$* or (**c**) *Nras$^{-/-}$;Hras$^{-/-}$;Kras$^{C118S/C118S}$* MEFs immortalized with the SV40 early region and transformed with either Flag-Kras^{G13D} or Flag-Kras^{G13D,C118S} in the absence or presence of EGF stimulation. (**b**, **d**) Mean ± SEM of P-Erk1/2 levels (normalized to T-Erk1/2) from three independent experiments using lysates from (**b**) *Kras$^{C118S/C118S}$* or (**d**) *Nras$^{-/-}$;Hras$^{-/-}$;Kras$^{C118S/C118S}$* MEFs immortalized with the SV40 early region and transformed with either Flag-Kras^{G13D} or Flag-Kras^{G13D,C118S} in the absence or presence of EGF stimulation. ns: non-significant (P>0.05). *: P<0.05, as determined using one-way ANOVA plus post-hoc Bonferroni's multiple comparison test.

3.3 Discussion

I have found that mutating C118 of endogenous Kras to serine suppressed urethane-induced lung tumorigenesis. It is formally possible that the recombined *loxP* sites introduced into the intron during the generation of the $Kras^{C118S}$ allele could underlie this effect rather than the C118S mutation. However, such a possibility seems less likely given that the $Kras^{C118S}$ allele yielded both *Kras* 4A and *Kras* 4B transcripts, produced similar levels of protein compared to the native *Kras* allele, and had no observable phenotype in a homozygous setting. The C118S mutation also inhibits the ability of Ras proteins to be activated in the presence of reactive nitrogen or oxygen species (Lander, Milbank et al. 1996, Lander, Hajjar et al. 1997, Mott, Carpenter et al. 1997, Williams, Pappu et al. 2003, Adachi, Pimentel et al. 2004, Heo and Campbell 2004, Clavreul, Adachi et al. 2006, Raines, Cao et al. 2006, Hobbs, Bonini et al. 2013). Thus, prior research additionally supports a plausible correlation between the mutation of the redox-reactive moiety at the C118 site and the observed reduction in tumorigenicity in mice with one or two $Kras^{C118S}$ alleles.

Introducing a C118S mutation into the remaining *Kras* allele in the *LSL-*$Kras^{G12D}$ model of lung cancer had no obvious effect on the number or size of resultant tumors, suggesting that the C118S mutation does not confer any overt change to the tumor suppressive activity of the non-oncogenic allele. This does not, however, exclude a role for the C118 in the wild type Kras protein in other settings. Indeed, the C118S mutation

in wild type Hras and Nras inhibits the xenograft tumor growth of some cancer cell lines (Lim, Ancrile et al. 2008). As such, the effect of mutating this residue may be temporal or context-dependent in cancer, consistent with the highly variable effects of, for example, nitric oxide on tumorigenesis (Fukumura, Kashiwagi et al. 2006). Nevertheless, extrapolating the results from this experiment, I suggest that the reduction of lung tumors in urethane-treated $Kras^{C118S/+}$ or $Kras^{C118S/C118S}$ mice may be more related to the oncogenic, rather than remaining non-oncogenic *Kras* allele.

Sequencing analysis suggests a preference of oncogenic mutations in the native compared to the C118S allele in tumors from $Kras^{+/C118S}$ mice treated with urethane. It is formally possible that carcinogens cause fewer mutations in the $Kras^{C118S}$ allele by some unknown mechanism. However, the C118S is only a point mutation, lies more than 2 kb away and in a completely different exon from where the Q61 oncogenic mutations occur, and is well established to block redox-dependent activation of Ras (Lander, Milbank et al. 1996, Lander, Hajjar et al. 1997, Mott, Carpenter et al. 1997, Williams, Pappu et al. 2003, Adachi, Pimentel et al. 2004, Heo and Campbell 2004, Clavreul, Adachi et al. 2006, Raines, Cao et al. 2006, Hobbs, Bonini et al. 2013). Thus, we favor a model whereby an oncogenic mutation in the $Kras^{C118S}$ allele is less likely to lead to productive tumorigenesis. Accumulating evidence suggests a potential role of GEFs in activating oncogenic Ras proteins (Hocker, Cho et al. 2013, Huang, Daniluk et al. 2014), and in this regard, there was a difference in the ability of EGF to stimulate the MAPK

pathway in cells transformed by $Kras^{G13D,C118S}$ versus $Kras^{G13D}$. However the relationship of NO and urethane tumorigenesis is undoubtedly more complex. NO can be generated from urethane derivatives in the appropriate conditions *in vitro* (Sakano, Oikawa et al. 2002) and *iNOS* knockout mice are resistant to this carcinogen (Kisley, Barrett et al. 2002). As such, the apparent preference of oncogenic mutations in the native compared to the C118S allele of *Kras* awaits a biochemical or cellular explanation. In summary, these results indicate that urethane carcinogenesis is reduced in mice with the $Kras^{C118S}$ allele, an effect that may be linked to the oncogenic rather than the native *Kras* version of the gene.

4. Reduced HRAS^{G12V}-driven tumor growth of cells expressing KRAS^{C118S}

4.1 Introduction

The *RAS* family of small GTPases is comprised of three genes in humans, *HRAS*, *NRAS*, and *KRAS* that encode the proteins HRAS, NRAS, KRAS4A, and KRAS4B. Activation of growth factor receptors as well as other receptors recruits Guanine nucleotide Exchange Factors (GEFs), which then stimulate the exchange of GDP on RAS for GTP, rendering the protein active. In this active state, RAS recruits and activates RAF kinases, PI3 kinases, RalGEFs, and other proteins that are well known to mediate a host of cellular phenotypes, including cell proliferation and survival. RAS is, in turn, returned to the inactive GDP-bound state through association with GTPase Activating Proteins (GAPs) (Bos, Rehmann et al. 2007, Vigil, Cherfils et al. 2010).

In up to a third of all human cancers, one of the three *RAS* genes harbor a mutation, usually at G12, G13, or Q61, that leads to chronic GTP binding and, correspondingly, oncogenic activation of the protein (Prior, Lewis et al. 2012). A wealth of studies demonstrate that expression of any of the RAS proteins containing an oncogenic mutation can impart transformed and tumorigenic phenotypes to cells, and when oncogenic mutations are engineered into endogenous *Ras* genes in mice, such changes can initiate cancer (Pylayeva-Gupta, Grabocka et al. 2011).

Accumulating evidence supports both tumor-suppressive and tumor-promoting roles for wild-type RAS proteins in cancer. In terms of a tumor-suppressive role, loss of one or both of any of the wild-type *Ras* alleles increases the sensitivity of mice to the carcinogen urethane, which induces lung adenomas with an oncogenic mutation in *Kras* (Zhang, Wang et al. 2001, To, Rosario et al. 2013). In terms of a tumor-promoting role, loss of *Hras* or *Nras* renders mice more resistant to DMBA and TPA treatment, which induces skin papillomas with an oncogenic mutation in *Hras* (To, Rosario et al. 2013). Wild-type HRAS, NRAS, or KRAS have also been shown to promote proliferation of oncogenic RAS-driven cancer cell lines by mediating EGF signaling (Young, Lou et al. 2013). Knocking down Hras sensitized oncogenic Kras-transformed murine cells to DNA damaging chemotherapeutics (Grabocka, Pylayeva-Gupta et al. 2014). Finally, wild-type KRAS has been shown to inhibit apoptosis induced by oncogenic KRAS (Matallanas, Romano et al. 2011).

Oncogenic KRAS has been shown to activate PI3K-AKT pathway (Pylayeva-Gupta, Grabocka et al. 2011), and activated AKT can phosphorylate S1177 of endothelial nitric oxide synthase (eNOS), activating the enzyme to produce nitric oxide (NO) (Dimmeler, Fleming et al. 1999, Fulton, Gratton et al. 1999, Michell, Griffiths et al. 1999). NO as well as other free radical oxidants has been shown to facilitate *S*-nitrosylation or *S*-glutathiolation of wild-type HRAS in a manner dependent upon the thiol residue of C118, and further, that such alterations activate HRAS (Lander, Milbank et al. 1996,

Raines, Bonini et al. 2007, Hobbs, Bonini et al. 2013). Substitution of C118 for serine (C118S), a very minor modification in which the thiol residue of this cysteine is replaced with a hydroxyl group, renders HRAS completely insensitive to activation by free radical oxidants, with no measureable effect on the protein structure, GTPase activity, intrinsic and GEF-mediated guanine nucleotide dissociation rate, or the ability to bind an effector (Lander, Milbank et al. 1996, Lander, Hajjar et al. 1997, Mott, Carpenter et al. 1997, Williams, Pappu et al. 2003, Adachi, Pimentel et al. 2004, Heo and Campbell 2004, Clavreul, Adachi et al. 2006, Raines, Cao et al. 2006, Hobbs, Bonini et al. 2013). Reducing the expression of wild-type HRAS or NRAS by shRNA reduces oncogenic KRAS-driven tumorigenesis in some cell lines, which can be rescued by re-expressing wild-type HRAS or NRAS, but not the C118S mutant variants (Lim, Ancrile et al. 2008). These results support a role for redox-dependent reactions with C118 of wild-type HRAS and NRAS in oncogenic KRAS-driven tumorigenesis. However, it remains unclear whether C118 of wild-type KRAS is similarly required to promote tumorigenesis. Thus, I explored the effect of mutating C118 to serine in KRAS on oncogenic HRAS-driven tumorigenesis.

4.2 Results

4.2.1 A C118S mutation introduced into wild-type KRAS reduces oncogenic HRAS-driven tumorigenesis

To evaluate the effect of blocking redox-dependent reactions with C118 in wild-type KRAS on RAS tumorigenesis, oncogenic $HRAS^{12V}$-transformed human HEK TtH cells (Lim, Ancrile et al. 2008) were first stably infected with a retrovirus encoding p110-CAAX, a constitutive active PI3K to activate AKT and promote S1177 phosphorylation and activation of eNOS (Dimmeler, Fleming et al. 1999, Fulton, Gratton et al. 1999, Michell, Griffiths et al. 1999). Appropriate expression of p110-CAAX was validated by RT-PCR (Figure 14a). To then parse out the contribution of wild-type KRAS in the tumorigenic growth of these cells, this cell line was stably infected with a retrovirus encoding a scramble or *KRAS*-specific shRNA. Appropriate knockdown of endogenous KRAS was validated by immunoblot (Figure 14b). Resultant cells in which the expression of KRAS was knocked down were stably infected with a retrovirus encoding N-terminal, Flag epitope-tagged wild-type or C118S-mutant KRAS engineered to be resistant to the *KRAS* shRNA. Re-expression of wild-type and C118S Flag-KRAS was confirmed by RT-PCR (Figure 14a).

To evaluate the effect of replacing endogenous KRAS with the C118S mutant form on tumorigenesis, all four of the above cell lines were injected into the flanks of five immuno-compromised mice each, after which tumor growth was monitored over time.

Consistent with the finding that knocking down wild-type HRAS or NRAS can reduce tumor growth of some *KRAS* mutation-positive cancer cells (Lim, Ancrile et al. 2008), knocking down KRAS also reduced tumor growth over time (Figure 14c), resulting in a statistically significant 91% reduction in tumor weight at endpoint compared to scramble shRNA control cells (Figure 14d, e). This effect was fully reversible by re-expressing shRNA-resistant wild-type Flag-KRAS, as evident from the similar tumor growth and tumor weight at endpoint between the KRAS-knockdown cells re-expressing wild-type Flag-KRAS and the scramble shRNA control cells (Figure 14c-e). However, the ability of Flag-KRAS to rescue the poor tumor growth of KRAS-knockdown cells was lost if the C118S mutation was introduced into KRAS. Specifically, there was no statistical difference between KRAS-knockdown cells re-expressing Flag-KRAS^{C118S} and KRAS-knockdown cells with regards to tumor growth or tumor weight at endpoint (Figure 14c-e). Thus, wild-type KRAS promotes xenograft tumor growth of oncogenic HRAS-transformed cells expressing constitutively active PI3K in a manner dependent upon C118.

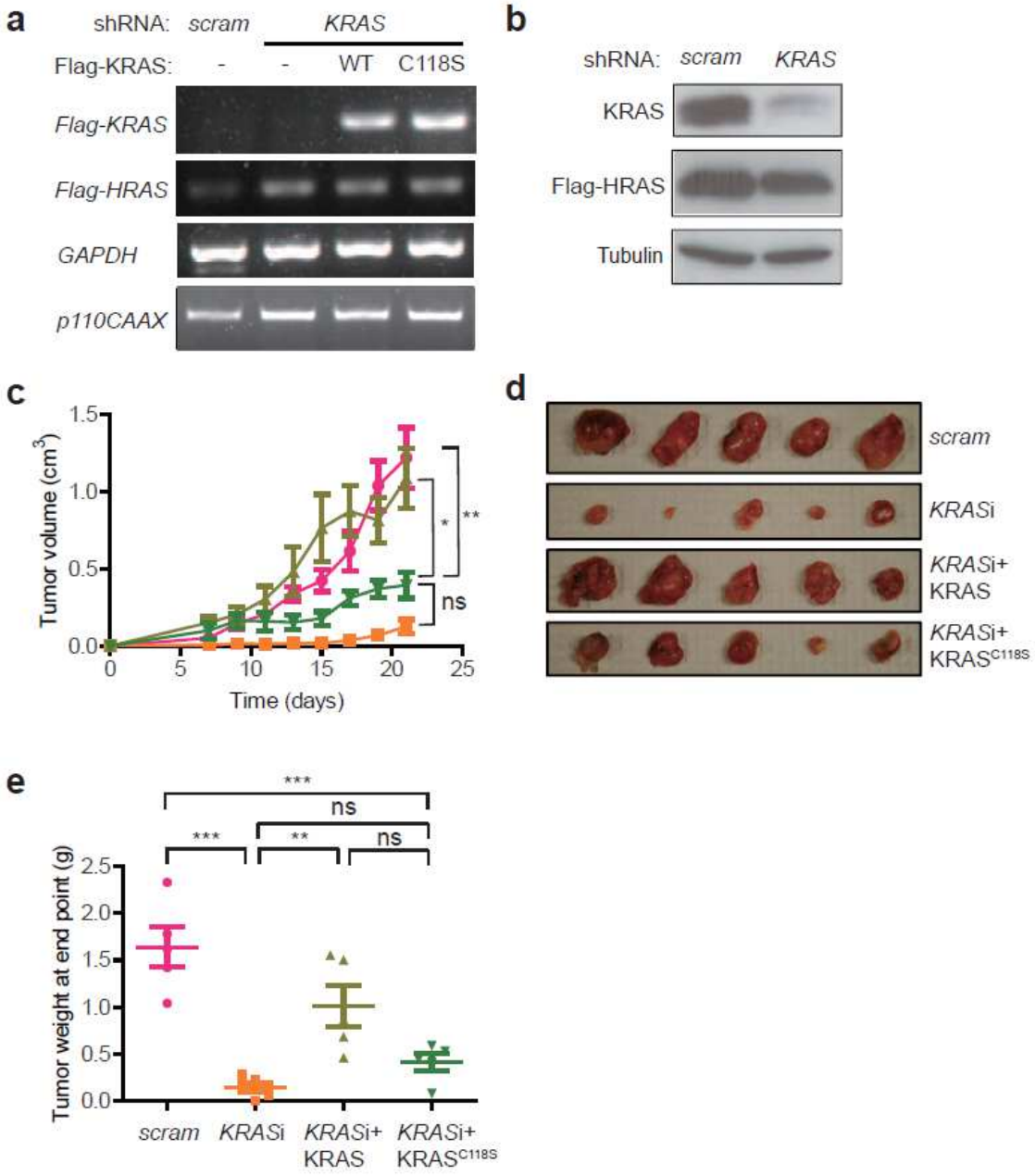

Figure 14: Introducing a C118S mutation into wild-type KRAS inhibits $HRAS^{G12V}$-driven tumor growth.

(**a**) RT-PCR amplification of *Flag-KRAS*, *Flag-HRAS*, *p110CAAX* and *GAPDH* mRNA (one of two replicate experiments), (**c**) mean ± SEM tumor volume over time, (**d**) photographs of excised tumors at end point, and (**e**) mean ± SEM tumor weight at end

point of tumors developing in immunocompromised mice (n=5) injected with Flag-HRAS^{G12V}-transformed HEK-TtH cells infected with retroviruses encoding p110CAAX and either scramble (scram) control shRNA (pink circles) or *KRAS* shRNA without (orange squares) or in conjunction with shRNA-resistant wild-type (WT, light green triangles) or C118S mutant (dark green reverse triangles) Flag-tagged KRAS. ns: non-significant, *: $P<0.05$, **: $P<0.01$ and ***: $P<0.001$, as determined by one-way ANOVA plus post-hoc Bonferroni's multiple comparison test using GraphPad Prism 5 Software. (**b**) Immunoblot detection of endogenous KRAS, Flag-tagged HRAS^{G12V}, and tubulin in Flag-HRAS^{G12V}-transformed HEK-TtH cells infected with retroviruses encoding p110-CAAX and either KRAS shRNA or a scramble control (scram) shRNA. One of three replicate experiments.

4.2.2 The C118S mutation impairs activation of wild-type KRAS

To determine whether the C118S mutation could block the ability of KRAS to be activated downstream of activated eNOS, HEK-TtH cells were stably infected with retroviruses encoding either the C-terminal, HA epitope-tagged S1177D constitutively-active (Fulton, Gratton et al. 1999) or S1177A inactive (Fulton, Gratton et al. 1999) mutant forms of eNOS and either the wild-type or C118S mutant form of Flag-KRAS*, a N-terminal, Flag epitope-tagged version of KRAS optimized for expression (Lampson, Pershing et al. 2013). Ectopic expression of HA-eNOS and Flag-KRAS was validated by immunoblot analysis (Figure 15a). To assess whether Flag-KRAS* was activated in the presence of HA-eNOS^{S1177D}, GTP-bound RAS proteins were captured from all four cell lines using the RAS-binding domain of RAF1 (de Rooij and Bos 1997) followed by immunoblot with an anti-Flag antibody to specifically detect ectopic Flag-KRAS*. Consistent with the findings that HRAS and NRAS are activated downstream of eNOS (Lim, Ancrile et al. 2008), the level of GTP-bound Flag-KRAS* was higher in cells expressing HA-eNOS^{S1177D} compared to those expressing HA-eNOS^{S1177A}. This activation could be ascribed to C118S, as the level of GTP-bound Flag-KRAS*^{C118S} remained low, regardless of whether cells express HA-eNOS^{S1177D} or HA-eNOS^{S1177A} (Figure 15a).

The same effect was also observed in a different cell type. Specifically, SV40-immortalized mouse embryonic fibroblasts (MEFs) were stably infected with retroviruses encoding either Flag-KRAS* or Flag-KRAS*^{C118S} in conjunction with either

HA-eNOS^{S1177D} or HA-eNOS^{S1177A}. Appropriate expression of these transgenes was verified by immunoblot (Figure 15b). As above, cells expressing Flag-KRAS* and HA-eNOS^{S1177D} exhibited higher levels of GTP-bound ectopic Flag-KRAS than cells expressing Flag-KRAS* and HA-eNOS^{S1177A} or cells expressing Flag-KRAS*^{C118S} and HA-eNOS^{S1177D} or HA-eNOS^{S1177A} (Figure 15b). Thus, the C118S mutation impairs eNOS-dependent activation of wild-type KRAS in two independent types of cells.

4.2.3 The C118S mutation impairs signaling by wild-type KRAS

To determine whether the C118S mutation could block the ability of KRAS to properly signal, the aforementioned HRAS^{G12V}-transformed HEK-TtH cells expressing p110-CAAX and either scramble control or *KRAS* shRNA in the absence or presence of shRNA-resistant Flag-KRAS or Flag-KRAS^{C118S} were serum starved over night. Lysates were then collected and immunoblotted for total (T-) and phosphorylated (P-) AKT and ERK1/2, markers of activation of the PI3K and MAPK RAS effector pathways (Karnoub and Weinberg 2008). While knocking down KRAS did not have a marked effect on the basal levels of P-AKT and P-ERK1/2 compared to scramble control cells, there was a more obvious reduction in basal P-ERK1/2 levels in the cells reconstituted with Flag-KRAS^{C118S} compared to Flag-KRAS. Wild-type RAS proteins have been reported to be activated by *E*pidermal *G*rowth *F*actor (EGF) in the presence of oncogenic RAS (Young, Lou et al. 2013). Thus, we also measured the levels of P-AKT and P-ERK1/2 upon EGF

stimulation. In this case, knocking down endogenous KRAS did reduce the level of P-AKT and P-ERK1/2 induced by EGF compared to scramble control cells. Moreover, stimulation of AKT and ERK1/2 phosphorylation by EGF in KRAS-knockdown cells was restored by re-expressing Flag-KRAS, but not Flag-KRAS^{C118S} (Figure 15c). Thus, the C118S mutation impairs signaling by wild-type KRAS in HRAS^{G12V}-transformed cells, primarily in the setting of EGF stimulation.

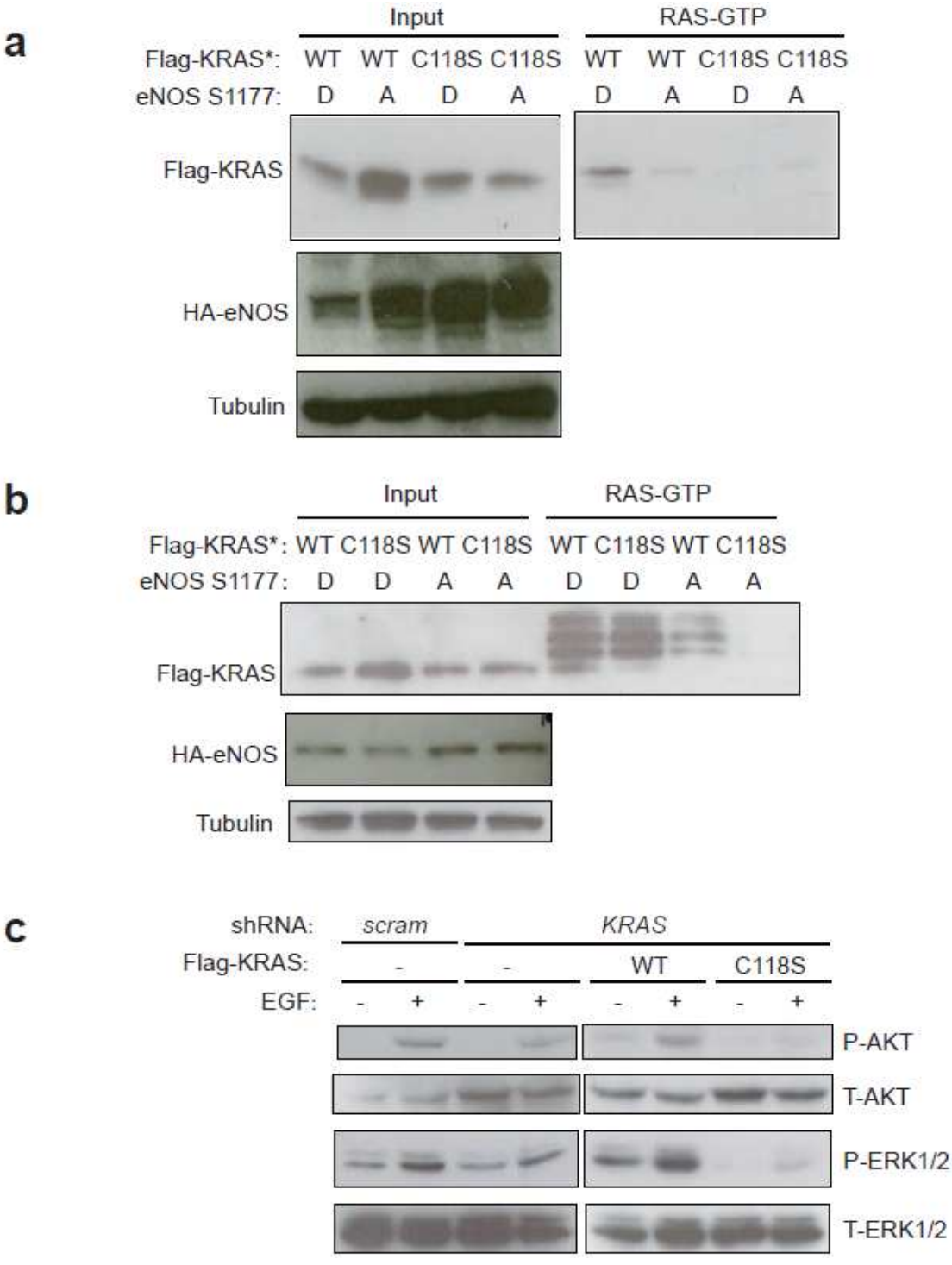

Figure 15: Introducing a C118S mutation into wild-type KRAS inhibits RAS activation and EGF stimulation of AKT and ERK1/2 signaling.

Immunoblot detection of input and GTP-bound Flag-KRAS captured by the Ras-binding domain of Raf1, as well as HA-eNOS and tubulin, in (**a**) HEK-TtH cells or (**b**) SV40-immortalized MEFs stably infected with retroviruses encoding either wild-type (WT) or C118S-mutant Flag-tagged KRAS* in conjunction with either the HA-tagged S1177D constitutively-active or the S1177A inactive mutant versions of eNOS. One of three replicate experiments. (**c**) Immunoblot detection of total (T) and phosphorylated (P) Akt and ERK1/2 in HEK-TtH cells stably infected with retroviruses encoding a scramble control (scram) shRNA, a *KRAS* shRNA, or *KRAS* shRNA and wild-type (WT) or C118S-mutant Flag-tagged shRNA-resistant KRAS and serum starved overnight and treated without (-) or with (+) EGF for five minutes. One of three replicate experiments.

4.2.4 An activating mutation in wild-type KRAS overcomes the reduction of tumor growth imparted by the C118S mutation

The findings that the C118S mutation inhibits the activation and signaling as well as tumorigenesis mediated by wild-type KRAS argue that these two effects are related. To genetically test whether the defect inflicted by the C118S mutation could be overcome by activating $KRAS^{C118S}$, the above $HRAS^{G12V}$-transformed HEK-TtH cells expressing p110-CAAX and KRAS shRNA were engineered to express no other transgene or shRNA-resistant Flag-tagged KRAS, $KRAS^{C118S}$, or $KRAS^{C118S}$ with an activating (G12V) mutation. Re-expression of the three versions of Flag-KRAS was confirmed by RT-PCR (Figure 16a). The four resultant cell lines were then injected into the flanks of five immunocompromised mice each, after which tumor growth was monitored over time. As already observed (Figure 14), the reduced tumor growth of the KRAS-knockdown cells was reversible by re-expressing shRNA-resistant wild-type Flag-KRAS, as these cells formed tumors significantly larger (7.3 fold) than the KRAS-knockdown cells. Again, re-expressing the C118S mutant version was incapable of rescuing this phenotype, as evidenced by similar tumor growth and tumor size and weight at endpoint in tumors derived from the KRAS-knockdown cells and the KRAS-knockdown cells expressing Flag-$KRAS^{C118S}$ (Figure 16b-d). Importantly, the inability of Flag-$KRAS^{C118S}$ to restore the reduced tumor growth upon knocking down endogenous KRAS was rescued if Flag-$KRAS^{C118S}$ was engineered to contain an activating (G12V) mutation, as evident from the similar growth kinetics (Figure 16b) and tumor size and

weight at endpoint between the KRAS-knockdown cells expressing wild-type Flag-KRAS versus Flag-KRAS^{C118S,G12V} (Figure 16b-d). These results support the contention that the C118S mutation blocks activation of wild-type KRAS and the ability of this protein to support tumor growth.

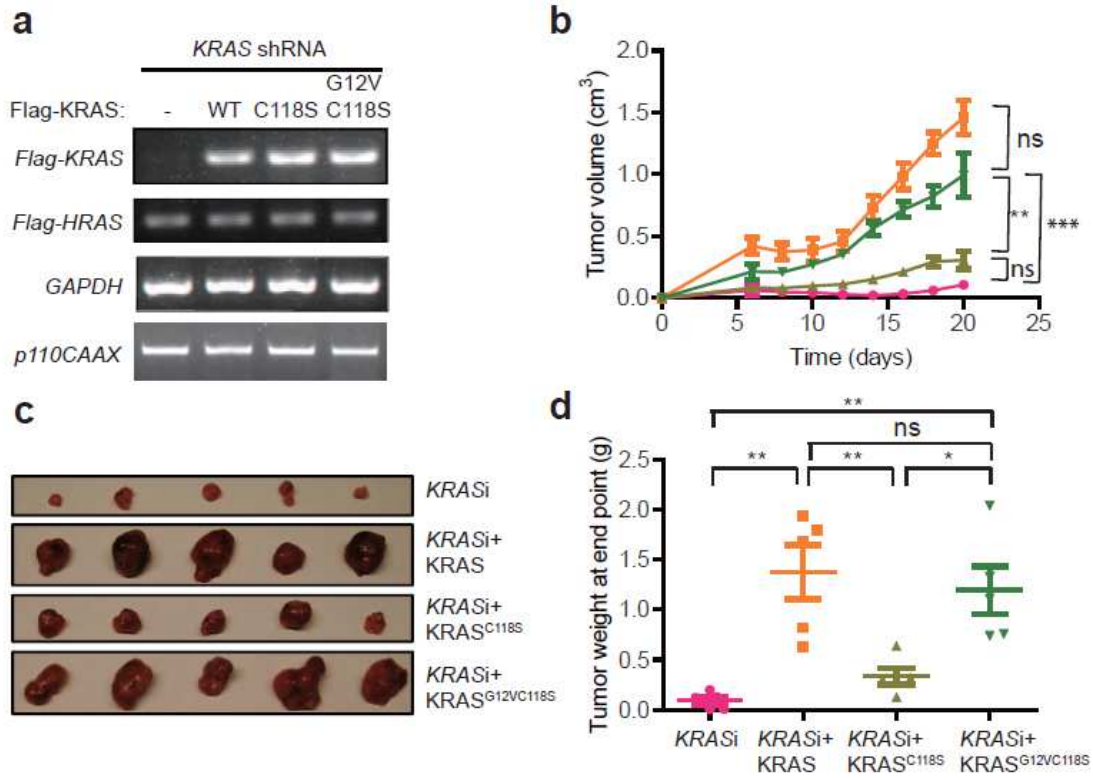

Figure 16: Introducing a G12V activating mutation overcomes the inability of KRAS^{C118S} to promote HRAS^{G12V}-driven tumor growth.

(**a**) RT-PCR amplification of *Flag-KRAS*, *Flag-HRAS*, *p110CAAX* and *GAPDH* mRNA (note that this is the same gel as in Fig 14a, except with the addition of analysis for Flag-KRAS^{G12V,C118S}, one of two replicate experiments), (**b**) mean ± SEM tumor volume over time, (**c**) photographs of excised tumors at end point, and (**d**) mean ± SEM tumor weight at end point of tumors developing in immunocompromised mice (n=5) injected with Flag-HRAS^{G12V}-transformed HEK TtH cells infected with retroviruses encoding p110CAAX and *KRAS* shRNA alone (pink circles) or with wild-type (WT, orange squares), C118S-mutant (light green triangles) or G12V,C118S-mutant (dark green reverse triangles) Flag-tagged and shRNA-resistant KRAS. ns: non-significant, *: P<0.05, **: P<0.01 and ***: P<0.001, as determined by one-way ANOVA plus post-hoc Bonferroni's multiple comparison test using GraphPad Prism 5 Software.

4.2.5 The C118S mutation introduced into the endogenous murine wild-type *Kras* gene reduces oncogenic HRAS-driven transformation

Admittedly, one caveat to the above experiments was that KRAS was restored in KRAS-knockdown cells by ectopic expression of the various KRAS proteins. Thus, we determined the effect on tumorigenesis when the C118S mutation was introduced into the endogenous *Kras* gene. Specifically, MEFs were isolated from three $Kras^{+/+}$ mouse embryos and three $Kras^{C118S/C118S}$ mouse embryos in which the C118S mutation was knocked into both alleles of the endogenous *Kras* gene (Huang, Carney et al. 2014). The resultant six cultures were immortalized by stable infection with a retrovirus encoding the early region of SV40, and the *Kras* genotype confirmed by PCR in the resultant immortalized MEF cell lines (Figure 17a). Immunoblot analysis revealed varying levels of Kras protein regardless of the genotype (Figure 17b). Given this, we focused on comparing $Kras^{+/+}$ cell line 3 with $Kras^{C118S/C118S}$ cell line 5, which have similar levels of Kras protein expression. These two cell lines were stably infected with a retrovirus encoding no transgene (vector) or oncogenic $HRAS^{G12V}$. Appropriate expression of $HRAS^{G12V}$ was validated by immunoblot (Fig 17b). The four cell lines were then assayed in triplicate for the transformed phenotype of growth in soft agar. As expected, vector control cells did not grow in soft agar, but introduction of oncogenic $HRAS^{G12V}$ permitted this growth. However, there was a statistically significant, 70% reduction in the mean number of colonies that grew in plates seeded with $HRAS^{G12V}$-transformed

Kras$^{C118S/C118S}$ versus *Kras*$^{+/+}$ MEFs (Figure 17c,d). Thus, introduction of the C118S mutation into the endogenous *Kras* gene inhibits oncogenic HRAS^{G12V}-mediated transformation.

4.2.6 The C118S mutation introduced into the endogenous murine wild-type *Kras* gene reduces oncogenic HRAS-driven tumorigenesis

To assess whether the reduction in growth in soft agar observed with the HRAS^{G12V}-transformed *Kras*$^{C118S/C118S}$ MEFs reflected a defect in the more relevant *in vivo* phenotype of tumor growth, these cells and the control HRAS^{G12V}-transformed *Kras*$^{+/+}$ MEFs were injected into the flanks of five immuno-compromised mice each, after which tumor growth was monitored over time. This analysis revealed that tumors derived from HRAS^{G12V}-transfromed *Kras*$^{C118S/C118S}$ MEFs grew more slowly than the control *Kras*$^{+/+}$counterparts (Figure 17e), which was manifested at endpoint as much smaller tumors (Figure 17f) that weighed 78% significantly less (Figure 17g). As a control, we demonstrate that re-expression of ectopic wild-type KRAS* was more effective than KRAS*^{C118S} at restoring tumor growth to HRAS^{12V}-transformed *Kras*$^{C118S/C118S}$ MEFs (Figure 17h). Finally, to assess the impact of the C118S mutation on the clinically relevant endpoint of survival, the above three *Kras*$^{+/+}$ and three *Kras*$^{C118S/C118S}$ immortalized MEFs were also transformed with HRAS^{G12V} and the resultant six cell lines were each injected into the flank of five immunocompromised mice. Each mouse was then euthanized when reaching a tumor mass of 1.5 cm^3 or losing >15% of body weight. A plot of the percent of mice surviving over time revealed that mice injected with HRAS^{G12V}-

transformed *Kras*$^{C118S/C118S}$ MEFs exhibited a 62% greater, significant survival advantage over mice injected with the positive-control HRAS^{G12V}-transformed *Kras*$^{+/+}$ MEFs (Figure 17i). Thus, introducing the C118S mutation into the endogenous *Kras* gene inhibits oncogenic HRAS^{G12V}-mediated xenograft tumor growth.

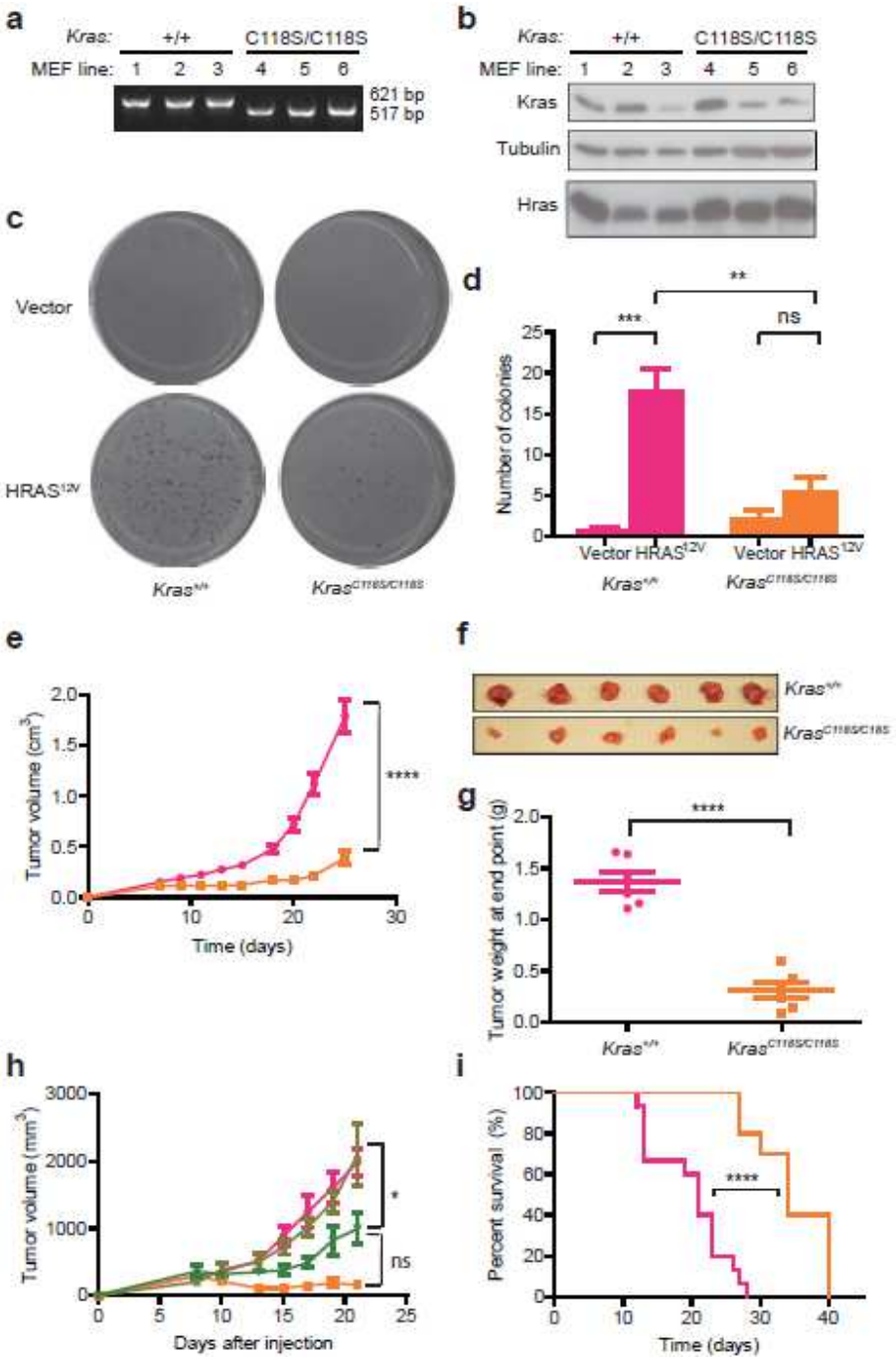

Figure 17: Introducing a C118S mutation into the endogenous wild-type *Kras* gene inhibits HRAS^{G12V}-driven xenograft tumor growth.

(**a**) PCR amplification of genomic DNA yielding a 621 bp or 517bp fragment indicative of the wild-type or C118S *Kras* alleles in three SV40-immortalized $Kras^{+/+}$ or $Kras^{C118S/C118S}$ MEF cell lines, respectively. One of three replicate experiments. (**b**) Immunoblot detection of endogenous Kras, HRAS, and tubulin in the indicated SV40-immortalized $Kras^{+/+}$ or $Kras^{C118S/C118S}$ MEF cell lines transformed with $HRAS^{G12V}$. One of three replicate experiments. (**c**) Representative images and (**d**) the mean ± SEM number of colonies growing in soft agar by SV40-immortalized $Kras^{+/+}$ versus $Kras^{C118S/C118S}$ MEF cell lines stably infected with a retrovirus encoding no transgene (vector) or Flag-$HRAS^{G12V}$. Each cell line was seeded in triplicate. (**e**) Mean ± SEM tumor volume over time, (**f**) photographs of excised tumors at end point, and (**g**) mean ± SEM tumor weight at end point of tumors developing in immunocompromised mice (n=5) injected with SV40-immortalized $Kras^{+/+}$ (pink circles) versus $Kras^{C118S/C118S}$ (orange squares) MEF cell lines transformed with $HRAS^{G12V}$. (**h**) Mean ± SEM tumor volume over time of tumors developing in immunocompromised mice (n=5) injected with SV40-immortalized and $HRAS^{G12V}$-transformed $Kras^{+/+}$ MEFs (pink circles), $Kras^{C118S/C118S}$ MEFs (orange squares) or $Kras^{C118S/C118S}$ MEFs stably infected with a retrovirus encoding KRAS* (light green triangles) or $KRAS^{*C118S}$ (dark green reverse triangles). (**i**) Kaplan-Meier survival curves based on the time to reach end point of immunocompromised mice (n=5) each injected with one of the three SV40-immortalized $Kras^{+/+}$ (pink line) versus $Kras^{C118S/C118S}$ (orange line) MEF cell lines transformed with $HRAS^{G12V}$. ns: non-significant, **: $P<0.01$, ***: $P<0.001$ and ****: $P<0.0001$ as determined by one-way ANOVA plus post-hoc Bonferroni's multiple comparison test (d, h), two-tailed unpaired student's *t* test (e, g) or long-rank test (i) using GraphPad Prism 5 Software.

4.3 Discussion

I have shown that xenograft tumor growth of an oncogenic $HRAS^{G12V}$-transformed human cell line engineered to express activated PI3K was diminished upon knockdown of endogenous KRAS, and that this effect was rescued by re-expressing the wild-type, but not the C118S-mutant KRAS. Oncogenic $HRAS^{G12V}$-transformed $Kras^{C118S/C118S}$ MEFs also exhibited reduced anchorage-independent and tumorigenic growth compared to similarly transformed $Kras^{+/+}$ MEFs. Again, there was a trend in these cells towards the re-expression of the wild-type KRAS being more effective in rescuing this phenotype than the C118S-mutant KRAS. Thus, introducing the C118S mutation into wild-type KRAS inhibits oncogenic $HRAS^{G12V}$-mediated tumorigenesis in two different experimental settings. The same C118S mutation engineered into HRAS and NRAS was previously shown to reduce the tumor growth of the *KRAS* mutation-positive human pancreatic cancer cell line CFPac-1 (Lim, Ancrile et al. 2008). As such, mutating C118 in the different wild-type RAS proteins may reduce tumorigenesis driven by different oncogenic RAS isoforms.

I also demonstrate that the level of GTP-bound wild-type KRAS in the presence of mutationally-active eNOS was reduced when the C118S mutation was introduced into the *KRAS* transgene. EGF stimulation of $HRAS^{G12V}$-transformed human cells was blunted when endogenous KRAS was replaced with the C118S mutant version, as evidenced by reduced P-AKT and P-ERK1/2 levels in these cells. It was previously

demonstrated that knocking down endogenous eNOS reduced the level of *S*-nitrosylated and GTP-bound HRAS and NRAS in cells expressing p110-CAAX to activate eNOS (Lim, Ancrile et al. 2008). There is also accumulating evidence that wild-type RAS proteins are activated in cells harboring an oncogenic RAS mutation (Lim, Ancrile et al. 2008, Jeng, Taylor et al. 2012, Young, Lou et al. 2013). In this regard, I genetically demonstrated that the inability of $KRAS^{C118S}$ to restore tumor growth of $HRAS^{G12V}$-transformed human cells upon knocking down endogenous KRAS could be restored, in large part, by introducing an activating (G12V) mutation into the $KRAS^{C118S}$ transgene. As the C118S mutation does not alter other known activities of RAS aside from activation by NO, these results collectively support the contention that activation of eNOS through the PI3K/AKT signaling arm of oncogenic RAS leads to *S*-nitrosylation or other redox-dependent reactions with C118 in the remaining wild-type RAS proteins, leading to their activation and promotion of tumorigenesis.

The effect of the C118S mutation on the ability of wild-type KRAS to promote HRAS oncogenesis may nevertheless be dependent upon the stage of tumorigenesis or types of cancer. Specifically, although initiation of lung tumorigenesis in $Kras^{C118S/C118S}$ mice treated with the carcinogen urethane was reduced compared to $Kras^{+/+}$ mice, this effect was linked the oncogenic rather than the remaining non-mutated $Kras^{C118S}$ allele (Huang, Carney et al. 2014). These results suggest that either later stages of tumorigenesis, such as those modeled in cancer cell lines, or specific types of cancer are

sensitive to loss of redox-dependent reactions with C118 of wild-type KRAS. In agreement, knocking out wild-type *Ras* genes in mice can be either tumor promoting or suppressing depending upon the carcinogen, cancer type, or the *Ras* isoform acquiring the oncogenic mutation (To, Rosario et al. 2013). Nevertheless, in the settings studied, I propose that redox-dependent reactions with C118 of wild-type KRAS activate the protein to stimulate xenograft tumor growth of oncogenic $HRAS^{G12V}$-driven cell lines. These results, coupled with previous findings of a similar role for wild-type HRAS and NRAS in oncogenic KRAS-driven tumorigenesis (Lim, Ancrile et al. 2008, Jeng, Taylor et al. 2012, Grabocka, Pylayeva-Gupta et al. 2014), suggest that activation of wild-type RAS isoforms can promote oncogenic RAS-driven tumorigenesis in some settings.

.

5. eNOS inhibits NF-κB signaling through *S*-nitrosylation of IKKα

5.1 Introduction

Protein *S*-nitrosylation, a posttranslational modification of cysteine residues through nitric oxide (NO), has been found to affect protein functions and cell signaling, thereby playing important roles in normal physiology and human diseases, including cancer (Stamler, Lamas et al. 2001, Mannick and Schonhoff 2002, Foster, Hess et al. 2009). NO is generated by nitric oxide synthases (NOS), which include neuronal NOS (nNOS), inducible NOS (iNOS) and endothelial NOS (eNOS) (Foster, Hess et al. 2009). Among these, eNOS has been found to mediate tumor maintenance by enhancing the *S*-nitrosylation and activation of wild-type RASs proteins (Lim, Ancrile et al. 2008). Since NO is diffusible, it is likely that eNOS promotes tumorigenesis by producing NO that could also *S*-nitrosylate other downstream proteins and affect their functions in cell signaling.

Kinases and phosphatases are important mediators of cell signaling pathways, and their activity may be regulated by *S*-nitrosylation. In order to search for potential signaling pathways that eNOS may affect and potential kinase/phosphotase targets of *S*-nitrosylation downstream of eNOS, an array for phosphorylated proteins was done in cells expressing p110-CAAX, a constitutively active subunit of PI3K (to activate the

PI3K-Akt-eNOS cascade), and either scramble control shRNA or *eNOS*-specific shRNA. Lysates from each type of cells were added to a chip with a variety of antibodies against specific phosphorylated proteins, and the changes in the level of these phosphorylated proteins upon eNOS knockdown can be determined in this way.

The phosphorylation of several proteins were found to be affected by eNOS, including NF-κB p65 (Ser-536) and histone H3 (Ser-10), whose levels of phosphorylation were higher in cells with eNOS shRNA (eNOS1819i) than in cells with scramble shRNA (Figure 18, Ancrile et al., unpublished data). The upregulation of levels of NF-κB p65 (Ser-536) phosphorylation upon eNOS knockdown suggests that eNOS may affect the activity of some kinases in the NF-κB pathway that can phosphorylate p65 at Ser-536. IKKα and IKKβ, two catalytic subunits of the IKK (IκB kinase) complex, can both phosphorylate p65 at Ser-536 (Hoberg, Popko et al. 2006). However, only IKKα, not IKKβ, has been reported to phosphorylate histone H3 at Ser-10, both globally and at specific genes (Yumi Yamamoto and Gaynor 2003, Anest, Cogswell et al. 2004). Taken together, it is likely that IKKα kinase activity could be negatively affected by eNOS.

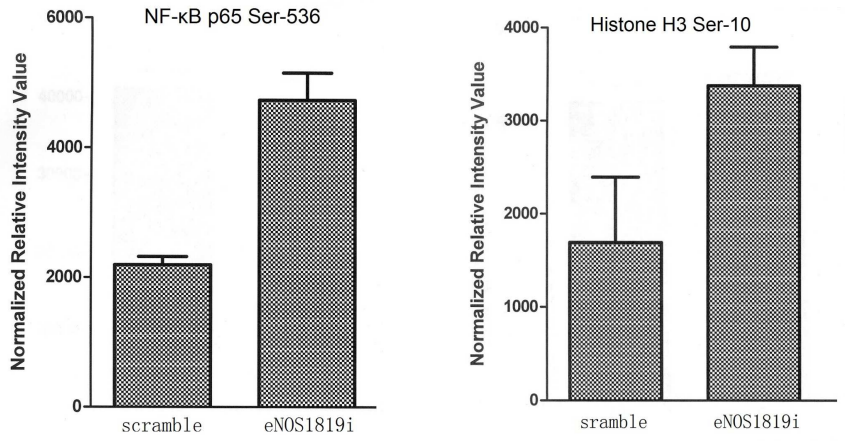

Figure 18: eNOS knockdown enhances the phosphorylation of NF-κB p65 Ser-536 and Histone H3 Ser-10.

An array for phosphorylated proteins was done in HEK TtH cells expressing p110CAAX, the constitutively active subunit of PI3K (to activate PI3K-Akt-eNOS cascade), and either scramble control shRNA or eNOS-specific shRNA (eNOS1819i). Lysates from each type of cells were added to a chip with a variety of antibodies against specific phosphorylated proteins, and the normalized relative intensity of different protein phosphorylation was measured. Two targets of upregulated phosphorylation upon eNOS knockdown are shown. (Ancrile et al., unpublished data)

IKKα is highly homologous with IKKβ. Alignment of IKKα and IKKβ shows a 52% identity in their overall sequences and 65% identity in their kinase domains (Zandi, Rothwarf et al. 1997). Despite structural similarity, IKKα and IKKβ have distinct functions. IKKβ is the predominant kinase within the IKK complex that is required for IκB phosphorylation and degradation, resulting in NF-κB p65/p50 translocation into the nucleus and activating the canonical NF-κB pathway. In contrast, as a component of IKK complex, IKKα also contributes to but is not essential for canonical NF-κB activation. Instead, IKKα plays an important role in the non-canonical pathway, leading to NF-κB2 p100 precursor protein processing to the p52 form, which then results in the formation of the p52-RelB heterodimer that enters the nucleus and regulates NF-κB responsive gene expression (Dejardin 2006, Gilmore 2006, Xiao, Rabson et al. 2006). Furthermore, IKKα is critical in normal physiology (Yumi Yamamoto and Gaynor 2003). Many studies have demonstrated the anti-proliferative function of IKKα in keratinocytes and have identified IKKα as a critical regulator of epidermal differentiation as well as a suppressor of skin cancer (Descargues, Sil et al. 2008).

Besides its cytoplasmic role in the NF-κB canonical and noncanonical pathways, IKKα also has important functions in the nucleus. IKKα activates NF-κB responsive gene expression in the nucleus usually through some modifications of proteins around promoters, including the phosphorylation and acetylation of histone H3 on the chromatin and NF-κB p65 around the gene promoters. For example, activated IKKα

interacts with CREB-binding protein and in conjunction with Rel A/p65 is recruited to the promoters of NF-κB responsive genes and mediates the phosphorylation of histone H3 Ser-10 and subsequent acetylation of Lys-14 in histone H3, leading to sustained transcription of these genes (Yumi Yamamoto and Gaynor 2003). IKKα has also been found to induce the phosphorylation of Rel A/p65 at Ser-536, which displaces SMRT-HDAC3 corepressor activity and allows p300-mediated acetylation of RelA/p65 and subsequent activation of NF-κB responsive genes (Hoberg, Popko et al. 2006). These findings demonstrate a novel nuclear role of IKKα, which involves inducible chromatin modification leading to the activation of NF-κB responsive genes.

IKKβ has been found to be *S*-nitrosylated at Cys-179. This *S*-nitrosylation inhibits IKKβ kinase activity and thus IκB phosphorylation, and activation of IKKβ by TNF-α is coordinated with denitrosylation (Marshall, Hess et al. 2004, Reynaert, Ckless et al. 2004). It is not yet known whether IKKα is also a target of *S*-nitrosylation and whether its activity can be similarly regulated. Since IKKα is highly homologous with IKKβ, it is likely that IKKα could also be *S*-nitrosylated and its activity negatively regulated by this modification. Here I have shown for the first time that IKKα is a target of *S*-nitrosylation, and eNOS may repress IKKα activity through *S*-nitrosylation.

5.2 Results

5.2.1 eNOS inhibits TNFα-induced p65 Ser-536 phosphorylation

To confirm the results from the phospho-protein array, I first examined whether eNOS affects NF-κB p65 Ser-536 phosphorylation upon cytokine stimulation. HEK TtH cells expressing p110CAAX and either scramble control shRNA or *eNOS*-specific shRNA (eNOS1819i) were treated with TNF-α for indicated times to stimulate NF-κB pathway. Lysates from these cells were then immunoblotted with an anti-p65 antibody or an antibody directed against p65 phosphorylated at Ser-536. As shown in Figure 19, while the total p65 levels were similar between samples at different time points, p65 Ser-536 phosphorylation was induced more dramatically in cells transduced with eNOS shRNA compared with those transduced with scramble shRNA. This result suggests that eNOS may suppress the activity of a kinase in the NF-κB pathway by inhibiting one or both of IKKα or IKKβ.

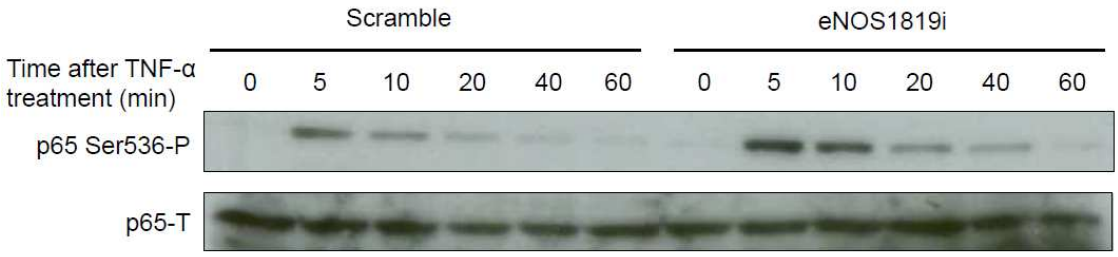

Figure 19: TNFα-induced p65 phosphorylation is upregulated in eNOS knockdown cells.

Immunoblot of p65 phosphorylated at Ser536 (p65 Ser536-P) and total p65 (p65-T) in HEK TtH cells expressing p110CAAX and either scramble control shRNA or eNOS-specific shRNA (eNOS1819i) serum starved overnight and treated without or with TNFα for the indicated minutes (min) before being harvested. One representative picture of three independent experiments is shown.

5.2.2 eNOS inhibits IKKα kinase activity to phosphorylate histone H3

IKKα has been reported to phosphorylate histone H3 at Ser-10 both globally and at specific genes (Yumi Yamamoto and Gaynor 2003, Anest, Cogswell et al. 2004). To test whether eNOS specifically inhibits IKKα kinase activity to phosphorylate histone H3, HA-tagged IKKα was immunoprecipitated from HEK TtH cells expressing p110CAAX, HA-IKKα, and either scramble control shRNA or eNOS-specific shRNA. The immunoprecipitate was then added to an *in vitro* kinase reaction employing histone H3 peptide as a substrate. The reaction products were then detected by immunoblot with a specific antibody against the histone H3 phosphorylated at Ser-10, and as a loading control, an anti-histone H3 antibody. As shown in Figure 20a, histone H3 Ser10 phosphorylation mediated by IKKα was upregulated when IKKα was immunoprecipitated from cells expressing eNOS shRNA compared with those expressing scramble control shRNA. Quantification revealed this to be a 2.2-fold increase in the level of histone H3 Ser10 phosphorylation relative to total histone H3 (Figure 20b). This result is consistent with the previously mentioned phosphoproteome array identifying histone H3 Ser10 phosphorylation to be elevated in cells expressing *eNOS* shRNA (Figure 18). Taken together, these results support the notion that eNOS inhibits the ability of IKKα to phosphorylate histone H3 at Ser-10.

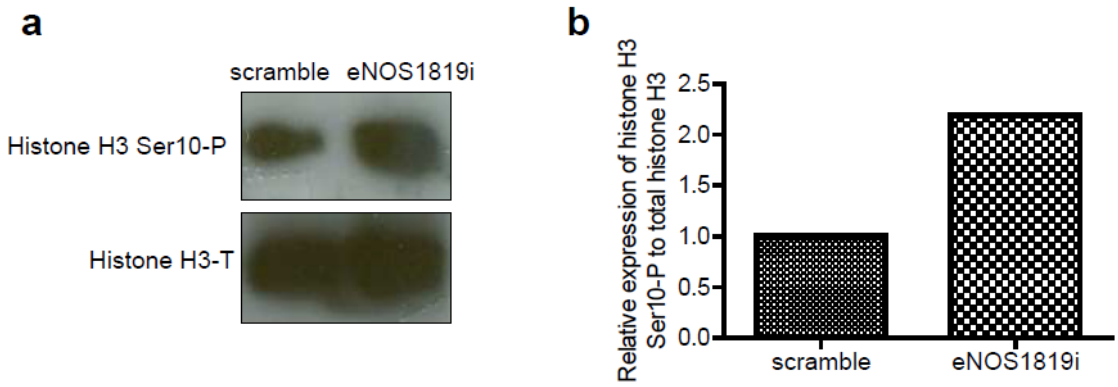

Figure 20: IKKα *in-vitro* kinase activity increases in eNOS knockdown cells.

(**a**) HA-tagged IKKα was immunoprecipitated using an anti-HA antibody from HEK TtH cells expressing p110CAAX, HA-IKKα and either scramble control shRNA or eNOS-specific shRNA (eNOS1819i), which was then added to *in vitro* kinase assay reactions containing kinase buffer, ATP and histone H3 peptide as a substrate. The kinase reactions were then boiled, loaded to a SDS-PAGE gel, and immunoblotted with an anti-histone H3 antibody (histone H3-T) or a specific antibody against the histone H3 phosphorylated at Ser-10 (hisotne H3 Ser10-P). (**b**) The bands in (**a**) were quantified using Image J software, and the level of histone H3 Ser10-P expression relative to total histone H3 was calculated. The relative expression level of histone H3 Ser10-P in cells expressing scramble control shRNA was set to 1, and the relative expression level of histone H3 Ser10-P in cells expressing eNOS-specific shRNA was calculated accordingly.

5.2.3 eNOS is more likely to affect IKKα-dependent than IKKβ-dependent gene transcription

The above results suggest that eNOS may inhibit IKKα kinase activity, but cannot rule out an effect of eNOS on IKKβ activity. To study whether eNOS specifically affects IKKα versus IKKβ, the expression of both NF-κB downstream genes specifically dependent on IKKα and those primarily dependent on IKKβ were examined. In this regard, *IL-6* is an NF-κB-regulated gene that requires prior chromatin modifications to ensure accessibility to NF-κB (Anest, Hanson et al. 2003), and only IKKα, and not IKKβ, has been shown to phosphorylate histone H3 and to affect chromatin modification at this locus (Yumi Yamamoto and Gaynor 2003). Therefore, *IL-6* gene transcription is dependent on IKKα rather than IKKβ. In contrast, *IκBα* is a gene regulated by the canonical NF-κB pathway, in which IKKβ plays a predominant role (Hayden and Ghosh 2008). *IκBα* gene transcription does not require prior chromation modifications and thus primarily depends on IKKβ. Thus, to study whether eNOS affects cytokine-stimulated expression of these downstream genes, HEK TtH cells expressing p110CAAX and either scramble control shRNA or *eNOS*-specific shRNA were treated with TNF-α for 2 hours or 4 hours followed by real-time RT-PCR to amplify *IL-6* and *IκBα* genes. As shown in Figure 21, *IL-6* mRNA was induced more in cells with eNOS shRNA than in those with scramble shRNA (Figure 21a), while induction of *IκBα* mRNA was similar between the two types of cells (Figure 21b). This result suggests that eNOS is likely to inhibit the

ability of IKKα to phosphorylate histone H3 and induce *IL-6* gene expression upon cytokine treatment, but is less likely to affect IKKβ activity.

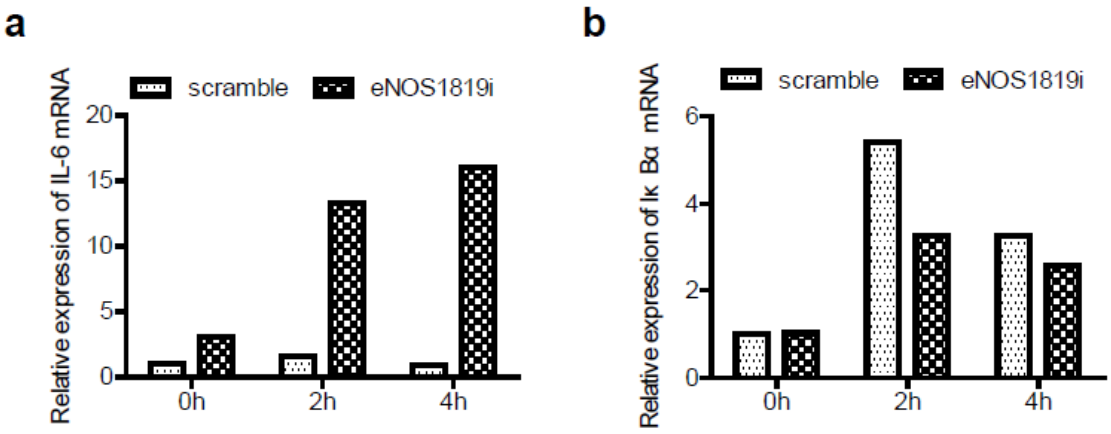

Figure 21: Transcription of *IL-6*, but not *IκBα*, is induced more dramatically in eNOS knockdown cells.

HEK TtH cells expressing p110CAAX and either scramble control shRNA or eNOS-specific shRNA (eNOS1819i) were treated with TNF-α for 0, 2 or 4 hours(h) followed by extraction of RNA from cells and real-time RT-PCR to amplify (a) *IL-6* and (b) *IκBα* respectively. The expression of (**a**) *IL-6* or (**b**) *IκBα* in untreated cells (0h) expressing scramble control shNRA was set to 1, and the relative expression in scramble control or eNOS knockdown cells treated with TNF-α for different time points were calculated accordingly.

5.2.4 eNOS inhibits IKKα-mediated p100 processing to p52

I next examined whether eNOS affects IKKα-specific cellular activities. IKKα, not IKKβ, plays an important role in the non-canonical NF-κB pathway, in which IKKα targets cytoplasmic p100-RelB dimers, phosphorylates the inhibitory C terminus of p100 and process p100 to generate p52, resulting in the translocation of the p52-RelB heterodimer into the nucleus and the subsequent regulation of a small panel of genes such as lymphoid and homeostatic chemokines (Dejardin 2006, Gilmore 2006, Xiao, Rabson et al. 2006, Madge and May 2010). This non-canonical pathway can be activated by a subset of stimuli including ligation of the lymphotoxin-β receptor (LTβR) by LTα1β2 (lymphotoxin α1β2) and LIGHT (*l*ymphotoxin-related *i*nducible ligand that competes for *g*lycoprotein D binding to *h*erpes virus entry mediator on *T* cells (TNFSF14)) (Madge and May 2010).

To investigate whether eNOS affects IKKα-mediated p100 processing to p52, HEK TtH cells expressing p110CAAX and either scramble control shRNA or *eNOS*-specific shRNA were treated with LIGHT for different number of hours followed by immunoblot to examine the levels of p100, p52 and tubulin. As shown in Figure 22, p100 processing to p52 started at 2 hours after stimulation in eNOS knockdown cells, but did not start until 6 hours after stimulation in control cells. The accelerated p100 to p52 processing in eNOS knockdown cells suggests that eNOS inhibits IKKα-mediated processing of p100 to p52.

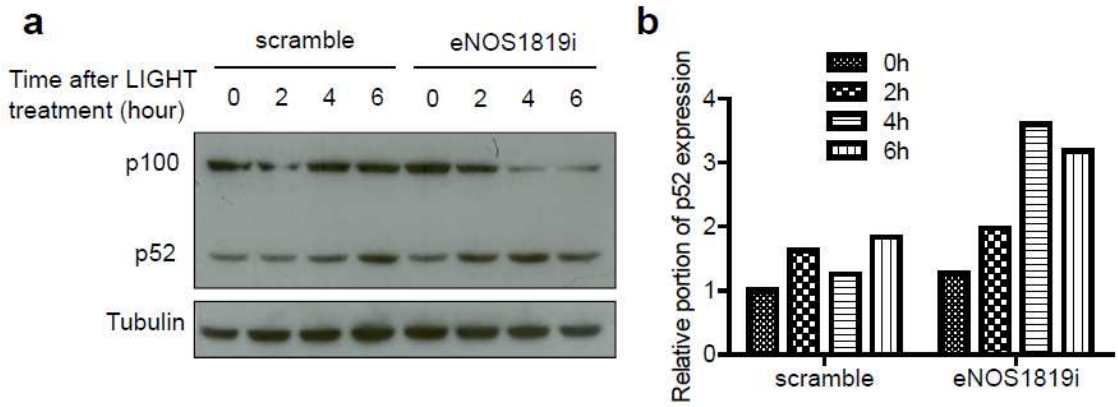

Figure 22: eNOS inhibits p100 processing to p52.

(**a**) HEK TtH cells expressing p110CAAX and either scramble control shRNA or eNOS-specific shRNA (eNOS1819i) were treated with LIGHT for indicated number of hours followed by immunoblot using an anti-p100/p52 antibody and an anti-β-tubulin antibody as a loading control. One representative picture of three independent experiments is shown. (**b**) The bands in (**a**) were quantified using Image J software, and the percentage of p52 expression out of the total of p100 and p52 expression was calculated. The percentage of p52 in untreated cells (0h) expressing scramble control shRNA was set to 1, and the relative percentage of p52 in scramble control or eNOS knockdown cells treated with LIGHT for different time points were calculated accordingly.

5.2.5 IKKα is a target of *S*-nitrosylation downstream of eNOS

The above data demonstrate that histone H3 Ser-10 phosphorylation, p65 ser-536 phosphorylation, *IL-6* gene induction upon TNF-α treatment, and processing of NF-κB2 p100 to p52, which are all dependent on IKKα, are all upregulated in HEK TtH p110CAAX cells upon knockdown of eNOS, suggesting that eNOS may negatively regulate IKKα activity in these cells. Whether this effect is direct, through production of NO and *S*-nitrosylation of IKKα, or indirectly affecting IKKα is not known. To determine whether IKKα is a target of *S*-nitrosylation, HEK TtH p110CAAX cells expressing HA-tagged IKKα were treated with or without the NO donor *S*-nitrosoglutathinone (GSNO), and *S*-nitrosylated HA-IKKα levels were measured by biotin-switch assays, an established technique to detect *S*-nitrosylated proteins (protein-SNOs) in cells (Jaffrey and Snyder 2001, Zhang, Keszler et al. 2005, Forrester, Foster et al. 2007, Forrester, Foster et al. 2009). As shown in Figure 23a, *S*-nitrosylated HA-IKKα was detected without GSNO treatment, although at a low level (Lane 1), suggesting that IKKα is *S*-nitrosylated by endogenous NO, which is likely to be generated by endogenous eNOS activated by PI3K-Akt-eNOS cascade in HEK TtH p110CAAX cells. Moreover, the addition of GSNO dramatically increased the *S*-nitrosylated HA-IKKα levels (Lane 2 compared to Lane 1), suggesting that IKKα is *S*-nitrosylated by exogenous NO donors. For both samples (with or without GSNO treatment), the assay was also

performed without ascorbate as negative controls (Lane 3 and Lane 4). These results suggest that IKKα is a target of *S*-nitrosylation.

To further demonstrate whether IKKα is *S*-nitrosylated downstream of eNOS, biotin-switch assays were performed in HEK TtH cells expressing p110CAAX, HA-tagged IKKα and either scramble control shRNA or *eNOS*-specific shRNA (eNOS1819i) to examine levels of S-nitrosylated HA-IKKα. As shown in Figure 23b, in the presence of p110CAAX to activate PI3K-AKT-eNOS cascade, the high levels of *S*-nitrosylated HA-IKKα in scramble control cells (Lane 1) is dramatically decreased when *eNOS*-specific shRNA is expressed instead (Lane 2). Therefore, knockdown of eNOS diminishes IKKα *S*-nitrosylation, suggesting that IKKα is *S*-nitrosylated downstream of eNOS.

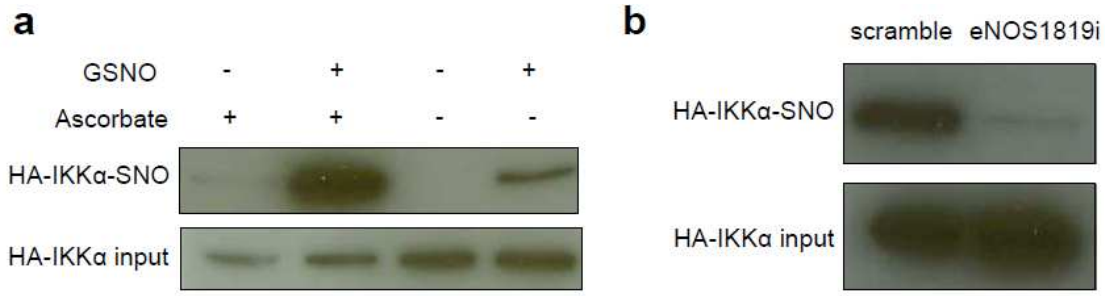

Figure 23: IKKα is a target of *S*-nitrosylation downstream of eNOS.

(**a**) HEK TtH cells expressing p110CAAX and HA-tagged IKKα were treated with (+) or without (-) the NO donor *S*-nitrosoglutathinone (GSNO), followed by biotin-switch assays to examine levels of *S*-nitrosylated HA-IKKα (HA-IKKα-SNO) as well as total HA-IKKα protein (HA-IKKα input) using an anti-HA antibody. The assay was also performed without (-) ascorbate to serve as negative controls. (**b**) Biotin-switch assays were performed in HEK TtH cells expressing p110CAAX, HA-tagged IKKα and either scramble control shRNA or eNOS-specific shRNA (eNOS1819i) to examine levels of *S*-nitrosylated HA-IKKα (HA-IKKα-SNO) as well as total HA-IKKα protein (HA-IKKα input) using an anti-HA antibody.

5.2.6 Identification of sites of *S*-nitrosylation on IKKα

I found that IKKα is *S*-nitrosylated downstream of eNOS. Since IKKβ is already known to be *S*-nitrosylated at a specific site Cys-179 (Reynaert, Ckless et al. 2004), I aligned the sequence of IKKα and IKKβ to help identify the potential site(s) of *S*-nitrosylation on IKKα. Alignment of IKKα and IKKβ shows a 52% identity in their overall sequences and 65% identity in their kinase domains (Zandi, Rothwarf et al. 1997). Furthermore, the two proteins exhibit 100% identity in the region 174-193 (of IKKβ), which contains the *S*-nitrosylation site Cys-179 of IKKβ (Marshall, Hess et al. 2004, Reynaert, Ckless et al. 2004). Since this site is conserved in IKKα, I explored whether Cys-178 is also *S*-nitrosylated in IKKα.

To determine whether IKKα is *S*-nitrosylated at this site, site-directed mutagenesis was performed to replace Cys-178 of IKKα with serine, generating the mutant IKKα^{C178S}. HEK TtH p110CAAX cells were stably infected with retroviral vectors expressing HA-tagged wild-type IKKα (IKKα^{WT}) or IKKα^{C178S} mutant. *S*-nitrosylated proteins were isolated by the biotin switch assay from these cells and immunoblotted with anti-HA antibody to specifically measure *S*-nitrosylation of HA-IKKα. As shown in Figure 24a, the level of *S*-nitrosylated IKKα was slightly decreased in IKKα^{C178S}-expressing cells compared with IKKα^{WT}-expressing cells, suggesting that Cys-178 is a site of *S*-nitrosylation on IKKα. However, the fact that IKKα^{C178S}-expressing cells also

have high levels of *S*-nitrosylated IKKα indicates the existence of some other sites of *S*-nitrosylation in addition to Cys-178.

To search for additional sites of *S*-nitrosylation on IKKα, I focused on the cysteines around C178 and within the N-terminal 300 amino acids of IKKα, which contain the catalytic domain of IKKα and are most critical for its kinase function. There are 12 cysteines within IKKα (1-300) fragment: cysteine 30, 46, 59, 77, 98, 113, 114, 178, 214, 241, 245, and 265. I did site-directed mutagenesis to mutate each individual cysteine to serine one by one, generating an IKKα (1-300) construct with all cysteines mutated to serine (Figure 24b, None). This construct was further mutated individually to contain only one cysteine at a specific site (or two cysteines at 113,114) and all the other cysteines mutated to serine (Figure 24b). All these mutant constructs, together with wild-type IKKα (1-300), were each introduced into HEK TtH cells expressing p110CAAX, followed by examination of *S*-nitrosylated IKKα levels by biotin-switch assay. As shown in Figure 23c, the IKKα (1-300) with only cysteine 46, only cysteine 59, or only cysteine 178 had upregulated *S*-nitrosylation compared with the no-cysteine mutant (NONE), suggesting that cysteine 46, 59 and 178 of IKKα are sites of *S*-nitrosylation.

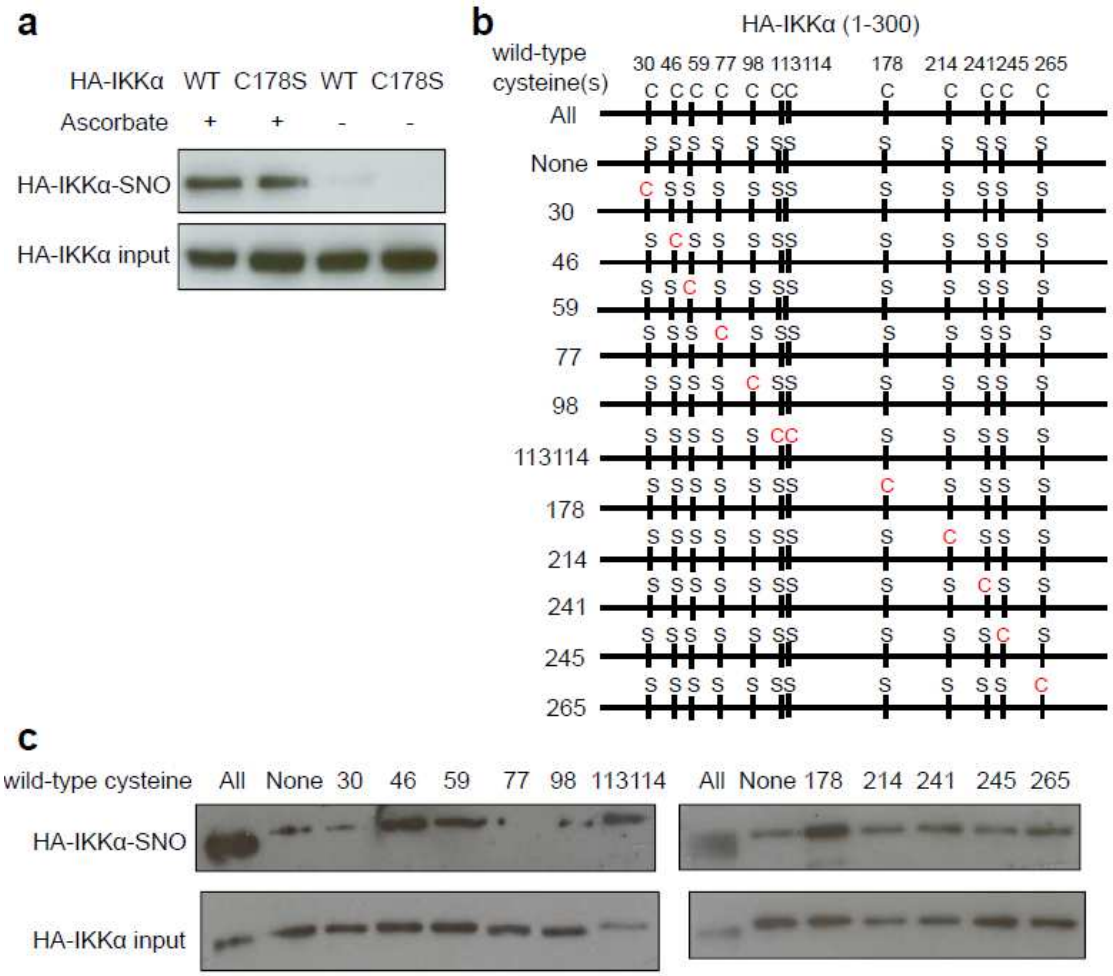

Figure 24: Identification of sites of *S*-nitrosylation on IKK*α* kinase domain.

Biotin-switch assays were performed in (**a**) HEK TtH cells expressing p110CAAX and HA-tagged wild-type IKK*α* (WT) or IKKα^{C178S} mutant (C178S) and (**c**) HEK TtH cells expressing p110CAAX and transfected individually with 13 differentially mutated HA-tagged IKK*α* (1-300) constructs to examine levels of S-nitrosylated HA-IKK*α* (HA-IKK*α*-SNO) as well as total HA-IKK*α* protein (HA-IKK*α* input) using an anti-HA antibody. (**b**) Schematic demonstration of 13 different IKK*α* (1-300) constructs with all cysteines wild-type (All), all cysteines mutated to serine (None), or those containing only one wild-type cysteine at a specific site (or two cysteines at 113,114) and all the other cysteines mutated to serine (30, 46, 59, 77, 98, 113114, 178, 214, 241, 245, and 265). C: cysteine; S: serine.

5.3 Discussion

As an important component of NF-κB pathway, IKKα not only contributes to canonical and non-canonical NF-κB pathways, but also plays important physiological roles, such as mediating epidermal development and suppressing skin tumorigenesis (Descargues, Sil et al. 2008). It is important to study the regulation of IKKα activity by post-translational modifications and how these modifications affect normal physiology and tumorigenesis. Here, I demonstrated for the first time that IKKα is *S*-nitrosylated downstream of eNOS, and eNOS inhibits IKKα kinase activity.

Several pieces of evidence support the hypothesis that eNOS inhibits IKKα kinase activity. Compared with control cells, HEK TtH cells expressing p110CAAX and *eNOS*-specific shRNA show an increase in: 1) NF-κB p65 Ser536 phosphorylation and histone H3 Ser10 phosphorylation in phospho-protein array, 2) NF-κB p65 Ser536 phosphorylation when stimulated fby TNFα, 3) histone H3 Ser10 phosphorylation in *in-vitro* kinase assay of IKKα, 4) transcription of *IL-6* gene, which is dependent on IKKα, and 5) p100 to p52 processing mediated by IKKα. All these results points towards a suppressive effect of eNOS on IKKα kinase activity.

IKKβ has been reported to be *S*-nitrosylated and its kinase activity inhibited by *S*-nitrosylation (Reynaert, Ckless et al. 2004). Despite high homology between IKKα and IKKβ, whether IKKα can also be *S*-nitrosylated and similary regulated has never been reported. My findings that IKKα is *S*-nitrosylated indicate that eNOS may suppress

IKKα kinase activity by generating NO that could *S*-nitrosylate IKKα. Consistent with this hypothesis, *S*-nitrosylated IKKα levels were decreased upon eNOS knockdown. However, it remains unclear how eNOS-mediated IKKα *S*-nitrosylation affects IKKα kinase activity and IKKα-mediated cellular signaling.

To further investigate on the mechanism that eNOS-mediated *S*-nitrosylation of IKKα inhibits its activity, I mapped putitive sites of S-nitrosylation on IKKα. Initially I focused on IKKα Cys-178, which is conserved with Cys-179 in IKKβ that has been reported to be *S*-nitrosylated (Reynaert, Ckless et al. 2004). Mutation of this Cys-178 to serine, however, did not lead to a large increase in the level of *S*-nitrosylated IKKα. This result suggests that IKKα may be *S*-nitrosylated at additional cysteines. To identify other potential sites of *S*-nitrosylation, I attempted to use mass spectrometric analysis on purified recombinant GST-IKKα protein treated with or without NO donors or on IKKα immunoprecipitated from cells overexpressing HA-IKKα treated with or without NO donors. However, this was not successful. Therefore, I switched to another method. Specifically, I generated a construct with the N-terminal 1-300 amino acids of IKKα, which contains the catalytic domain of this kinase. To identify which one(s) of the 12 cysteines on this fragment can be *S*-nitrosylated, I generated different mutant constructs of IKKα (1-300) with only one cysteine wild-type and all the other cysteines mutated to serine. The examination of levels of *S*-nitrosylated IKKα in cells expressing these different mutants could suggest which cysteine is likely to be a site of *S*-nitrosylation.

Using this method, I have successfully identified cysteine 46, 59, and 178 as sites that can be *S*-nitrosylated. Mutating these *S*-nitrosylation sites to serine would generate *S*-nitrosylation-resistant mutants of IKKα, which will be useful to evaluate the role of *S*-nitrosylation of IKKα in normal physiology and tumorigenesis.

Table 8: Primer sequences.

Primer	Sequence
P1 (*Kras* RT-PCR F)	atgactgaatataaacttgtgg
P2 (*Kras* RT-PCR R)	ttacataattacacactttgtc
P3 ($Kras^{C118S}$ genotyping F)	agaacaaattaaaagagtaaaggac
P4 ($Kras^{C118S}$ genotyping R-targeting vector)	ccaagctagcttggctggacgtaaa
P5 ($Kras^{C118S}$ genotyping R-*Kras* genomic)	atgtaaaatgtactctagacggaac
P6 (343F *Kras* RT-PCR)	tatagggcgaattggagctcatgactgagtataaacttgtg
P7 (343R *Kras* RT-PCR)	cggtatcgataagctttcacataactgtacaccttgtc
P8 (*Kras* 4A RT-PCR F)	gggctttctttgtgtatttgc
P9 (*Kras* 4A RT-PCR R)	caatgtataaaaagcatcctcca
P10 (*Kras* 4B RT-PCR F)	tgcaatgagggaccagtaca
P11 (*Kras* 4B RT-PCR R)	tagaaggcatcgtcaacacc
P12 (*Kras* 4A/4B RT-PCR F)	acttgtggtggttggagctg
P13 (*Kras* 4A/4B RT-PCR R)	ccctccccagttctcatgta
P14 (*EEF1α* RT-PCR F)	ggattgccacacggctcacatt
P15 (*EEF1α* RT-PCR R)	ggtggatagtctgagaagctctc
P16 (CMV-Cre genotyping F)	gcggtctggcagtaaaaactatc
P17 (CMV-Cre genotyping R)	gtgaaacagcattgctgtcactt
P18 (*Flag-Kras* RT-PCR F)	aaagatgacgacgataagactgaa
P19 (*Flag-Kras* RT-PCR R)	gctgtgtcgagaatatccaagaga
P20 (*Flag-Hras* RT-PCR F)	agatgacgacgataagacggaata
P21 (*Flag-Hras* RT-PCR R)	ggaatcctctatagtggggtcgta
P22 (*GAPDH* RT-PCR F)	gaaggtgaaggtcggagtcaa
P23 (*GAPDH* RT-PCR R)	gcagaggggggcagagatgat
P24 (HA-IKKα F)	ggaattcatgtacccatacgatgttccagattacgctgagcggcccccgggg
P25 (HA-IKKα R)	acgcgtcgactcattctgttaaccaact
P26 (HA-IKKα 1-300 F)	ccgccggaattcgccgccaccatgtacccatacgatgttccagat
P27 (HA-IKKα 1-300 R)	ccgccgctcgagctaacatcttggctgcttcaaagta
P28 (IL-6 RT-PCR F)	tgcgtccgtagtttccttct
P29 (IL-6 RT-PCR R)	gcctcagacatctccagtcc
P30 (I κBα RT-PCR F)	aagtgatccgccaggtgaag
P31 (I κBα RT-PCR R)	gcaatttctggctggttggt

6. Discussion and Future directions

6.1 The effect of C118S mutation on oncogenic Kras

6.1.1 Oncogenic Kras^{Q61R} and Kras^{Q61R,C118S} have similar transforming and tumorigenic potential

In Chapter 3, sequencing analysis of lung tumors from urethane-treated *Kras$^{C118S/+}$* mice revealed a bias towards oncogenic mutations occurring on the native *Kras* allele rather than the *Kras^{C118S}* allele (**3.2.6** and Figure 11), suggesting that oncogenic Kras with C118S mutation may have reduced oncogenic poetential. To test this hypothesis, I assayed the transforming potential of oncogenic Kras^{Q61R} versus Kras^{Q61R,C118S}. Specifically, a vector encoding Kras^{Q61R} or Kras^{Q61R,C118S} was stably transduced into SV40 early region immortalized MEFs, and the cells were plated in triplicate in soft agar. Three weeks later the number of colonies was assessed, revealing that MEFs expressing Kras^{Q61R} or Kras^{Q61R,C118S} formed a similar number and size of colonies in soft agar, although there was a slight trend towards fewer colonies in Kras^{Q61R,C118S}-transfomed MEFs (Figure 25a-d). This result suggests that Kras^{Q61R} and Kras^{Q61R,C118S} have very similar transforming potential.

To assess whether Kras^{Q61R} and Kras^{Q61R,C118S} behave similarly in the more relevant *in vivo* phenotype of tumor growth, these two MEF cell lines were injected into the flanks of five immuno-compromised mice each, after which tumor growth was

monitored over time. This analysis revealed that tumors derived from $Kras^{Q61R}$-transfromed MEFs grew at a similar rate as their $Kras^{Q61R,C118S}$–transformed counterparts (Figure 25e), which was manifested at endpoint as tumors of similar weight and size (Figure 25f, g). This result is consistent with a previous finding that cancer cells driven by $Kras^{G12V}$ and $Kras^{G12V,C118S}$ grew as xenograft tumors similaly (Lim, Ancrile et al. 2008), suggesting that oncogenic Kras with and without C118S mutation may have similar ability to transform SV40-immortalized cells.

Since oncogenic $Kras^{Q61R}$ and $Kras^{Q61R,C118S}$ did not show any significant difference in their transforming and tumorigenic potential, I next examined whether there are any difference in their ability to induce growth arrest of primary cells. In this regard, human primary fibroblast IMR-90 cells were infected with retrovirus expressing pBabePuro empty vector, pBabePuro-$Kras^{Q61R}$ or pBabePuro-$Kras^{Q61R,C118S}$ followed by selection with puromycin for three days. Equal amounts of the infected cells were each plated in quadruplicate in multiple 24-well plates, followed by examination of viable cells by crystal violet staining at different days after initial plating. This analysis revealed similar growth curve and number of viable cells at end point among cells expressing vector, $Kras^{Q61R}$ and $Kras^{Q61R,C118S}$ (Figure 26a, b). Similar results were also observed in primary wild-type MEFs (Figure 26c) and $Kras^{C118S/C118S}$ MEFs (Figure 26d).

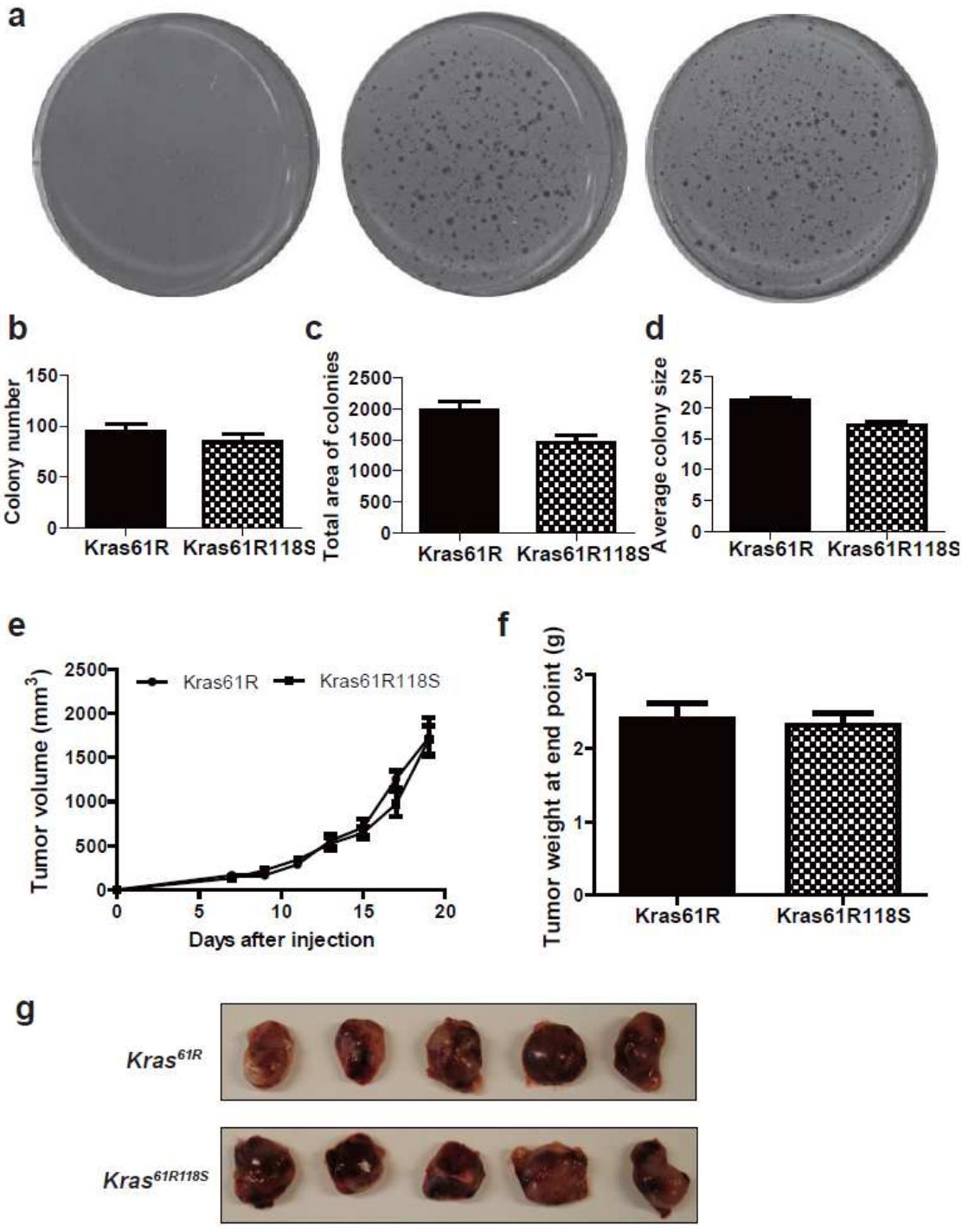

Figure 25: Kras^{Q61R} and Kras^{Q1R,C118S} have similar transforming and tumorigenic potential.

(**a**) Representative images, and the mean ± SEM of (**b**) number of colonies, (**c**) total areas of colonies, (**d**) average siza of colonies growing in soft agar by SV40-immortalized MEF lines stably infected with a retrovirus encoding no transgene (vector), Flag-$Kras^{Q61R}$ ($Kras^{61R}$) or Flag-$Kras^{Q61R,C118S}$ ($Kras^{61R118S}$). Each cell line was seeded in triplicate. (**e**) Mean ± SEM tumor volume over time, (**f**) mean ± SEM tumor weight at end point of tumors, and (**g**) photographs of excised tumors at end point developing in immunocompromised mice (n=5) injected with SV40-immortalized MEF cell lines transformed with Flag-$Kras^{Q61R}$ ($Kras^{61R}$) or Flag-$Kras^{Q61R,C118S}$ ($Kras^{61R118S}$).

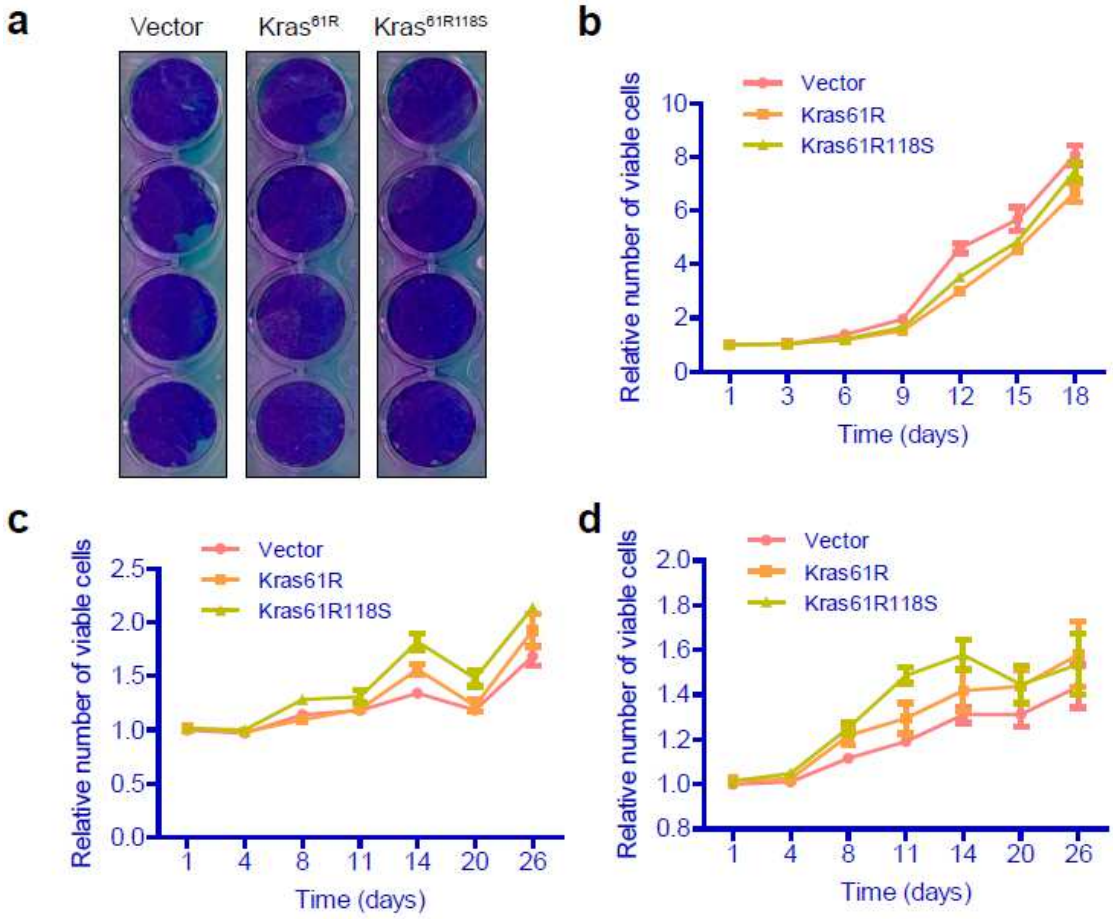

Figure 26: Kras^{Q61R} and Kras^{Q61R,C118S} have similar effect on primary cell growth.

(**a**) Images of crystal violet staining of IMR-90 cells infected with a retrovirus encoding no transgene (vector), Flag-Kras^{Q61R} (Kras^{61R}) or Flag-Kras^{Q61R,C118S} (Kras^{61R118S}) 18 days after plating. (**b**)-(**d**) Growth curve of (**b**) IMR-90 cells, (**c**) wild-type MEFs, and (**d**) *Kras$^{C118S/C118S}$* MEFs infected with a retrovirus encoding no transgene (vector), Flag-Kras^{Q61R} (Kras^{61R}) or Flag-Kras^{Q61R,C118S} (Kras^{61R118S}) based on crystal violet staining of cells at different days after plating. IMR-90 cells were plated in quadruplicate at 4000 cells/well, while MEFs were plated in quadruplicate at 1000 cells/well.

6.1.2 C118S mutation may affect oncogenic Kras downstream signaling depending on the strength of the oncogene

RAS proteins with an oncogenic mutation have traditionally been considered contitutively active. However, recent studies have indicated that the activity of oncogenic RAS could be regulated by GEFs (Hocker, Cho et al. 2013, Huang, Daniluk et al. 2014). Therefore, the C118S mutation could also potentially impair the activity of oncogenic Kras in a manner related to activation by GEFs. Since oncogenic $Kras^{Q61R}$ and $Kras^{Q61R,C118S}$ did not show significant differences in transformation, tumorigenesis, or growth arrest assays, further *in-vitro* biochemical studies are required to examine whether the C118S mutation alters the acitivity of oncogenic Kras and affects its downstream signaling.

To this end, I compared the RAS-GTP levels of SV40 immortalized MEFs expressing $Kras^{Q61R}$ or $Kras^{Q61R,C118S}$, finding that in general the levels were similar between the two cell lines, although there was much variability from experiment to experiment. The stable expression of a constitutively active $eNOS^{S1177D}$ (Michell, Griffiths et al. 1999) in the cells did not seem to significantly alter the RAS-GTP levels, nor is further treatment of the cells with the drug L-NAME (Alderton, Cooper et al. 2001) to inhibit eNOS activity. The same was true for cells expressing $Kras^{Q61L}$ or $Kras^{Q61L,C118S}$. Additionally, I also performed microarray analysis (Affymetrix GeneChip Mouse 430 2.0 array) on RNA samples from three SV40-immortalized MEF lines expressing $Kras^{Q61R}$ and three corresponding cell lines expressing $Kras^{Q61R,C118S}$, which revealed no significant

difference in the expression of any of the 39,000 transcripts included in the array. Finally, I assayed for differences in two of the most well-characterized signaling pathways downstream of RAS, the RAF-MEK-ERK and PI3K-AKT pathways, between the SV40- immortalized MEFs expressing oncogenic Kras with or without the C118S mutation. Specifically, cells were treated with EGF to stimulate GEF activity, given the potential involvement of GEFs in activating oncogenic Ras proteins (Hocker, Cho et al. 2013, Huang, Daniluk et al. 2014). For these experiments I used *Kras*$^{C118S/C118S}$ MEFs, to exclude the involvement of wild-type Kras stimulation by EGF, and *Nras*$^{-/-}$; *Hras*$^{-/-}$;*Kras*$^{C118S/C118S}$ MEFs, to exclude stimulation by wild-type Nras and Hras by EGF. Regardless of the Kras oncogene and the cell line used, levels of phosphorylated AKT were similar in cells expressing oncogenic Kras with or without the C118S mutation. However, levels of phosphorylated Erk1/2 were differentially altered by the C118S mutation depending on the Kras oncogene (Figure 12 and 13). More specifically, levels of phosphorylated Erk1/2 upon EGF stimulation were similar between Kras^{Q61L}-expressing and Kras^{Q61L,C118S}-expressing cells, but were significantly reduced in Kras^{G13D,C118S}-expressing cells compared with Kras^{G13D}-expressing cells (Figure 12 and 13). Since Kras^{G13D} is a weaker oncogene than Kras^{Q61L}, it is possible that the ability of the C118S mutation to alter oncogenic Kras activity depends on the strength of the oncogene. The weaker the oncogenic Kras is, the more likely the C118S mutation may affect its activity. In this regard, it is worth noting that of the Kras^{Q61R}, Kras^{Q61L} and

Kras^{G13D} mutants tested, the intrinsic exchange rate was the highest with the Kras^{G13D} mutant (Stites 2014) and *S*-nitrosylation of RAS is known to promote the exchange of GDP for GTP (Williams, Pappu et al. 2003). Further studies using other oncogenic Kras of different strength will be necessary to demonstrate this hypothesis. Furthermore, I have so far only tested the difference in the downstream signaling of Kras^{G13D}-expressing and Kras^{G13D,C118S}-expressing cells. It will be helpful to examine whether Kras^{G13D,C118S} have decreased transforming and tumorigenic potential compared with Kras^{G13D} in the future. Since similar transforming and tumorigenic potential of Kras^{Q61R} and Kras^{Q61R,C118S} have already been demonstrated, these results would help understand whether the C118S mutation affects the transforming and tumorigenic potential of an oncogenic Kras is dependent on the strength of that oncogene. Admittedly however, these experiments do not provide direct mechanistic insight into why there was a bias against Q61 mutations recovered in the *Kras^{C118S}* allele.

6.2 The effect of C118S mutation on wild-type Kras

6.2.1 An effect of C118S mutation on the role of wild-type Kras in cell signaling, proliferation, transformation and tumorigenesis

The findings in Chapter 4 have suggested an effect of C118S mutation on wild-type Kras, especially on its role in $HRAS^{12V}$-driven xenograft tumor growth. More specifically, I have demonstrated that C118S mutation of KRAS can: 1) reduce wild-type KRAS activation upon expression of a constitutively active eNOS, 2) almost abolish downstream P-ERK1/2 and P-AKT signaling upon stimulation with EGF, and 3) decrease tumor growth of cells transformed by $HRAS^{12V}$. Furthermore, using $Kras^{C118S/C118S}$ MEFs as a tool, I have demonstrated that C118S mutation of wild-type Kras impairs the $HRAS^{12V}$-driven transformation and tumorigenesis at the endogenous level.

To explore whether introduction of a C118S mutation of wild-type Kras has a universal effect in tumorigenesis, the same $Kras^{+/+}$ and $Kras^{C118S/C118S}$ cell lines used in Chapter 4 (**4.2.6**) was stably infected with a retrovirus encoding oncogenic $KRAS^{G12V}$, followed by injection into the flanks of five immuno-compromised mice each, after which tumor growth was monitored over time. Analysis on tumorigenesis at fixed end point of one $Kras^{+/+}$ line and one $Kras^{C118S/C118S}$ line transformed with $KRAS^{G12V}$ revealed that tumors derived from $KRAS^{G12V}$-transformed $Kras^{C118S/C118S}$ MEFs grew more slowly than the control $Kras^{+/+}$counterparts (Figure 27a), which was manifested as endpoint as much smaller tumors (Figure 27c) that weighed 98% significantly less (Figure 27b).

Furthermore, to assess the impact of the C118S mutation on the clinically relevant endpoint of survival, three *Kras*$^{+/+}$ lines and three *Kras*$^{C118S/C118S}$ lines transformed with KRAS^{G12V} were each injected into the flank of five immunocompromised mice. Each mouse was then euthanized when reaching a tumor mass of 1.5 cm^3 or losing >15% of body weight. A plot of the percent of mice surviving over time revealed that mice injected with KRAS^{G12V}-transformed *Kras*$^{C118S/C118S}$ MEFs exhibited a 52% greater, significant survival advantage over mice injected with the control KRAS^{G12V}-transformed *Kras*$^{+/+}$ MEFs (Figure 27d). Therefore, introducing the C118S mutation into the endogenous *Kras* gene also inhibits oncogenic KRAS-mediated xenograft tumor growth.

The decreased xenograft tumor growth of HRAS^{G12V}-transformed or KRAS^{G12V}-transformed *Kras*$^{C118S/C118S}$ MEFs may be due to an internal defect of *Kras*$^{C118S/C118S}$ MEFs in cell proliferation regardless of the driver oncogene. To test this possibility, two *Kras*$^{+/+}$ lines and two *Kras*$^{C118S/C118S}$ lines SV40-immortalized MEF cell lines were plated in triplicate in 24-well plates, followed by staining of the cells with crystal violet every day after plating, which is an indication of the number of viable cells. Both of the two *Kras*$^{C118S/C118S}$ lines grew more slowly than the two *Kras*$^{+/+}$ lines (Figure 28b), which was manifested at endpoint (Day 5) as fewer number of viable cells stained with crystal violet (Figure 28a). This defect of *Kras*$^{C118S/C118S}$ MEFs in cell proliferation suggests that C118S mutation of wild-type Kras could impair cell proliferation, which may partially account for the decreased tumorigenesis driven by oncogenic HRAS^{G12V} or KRAS^{G12V}.

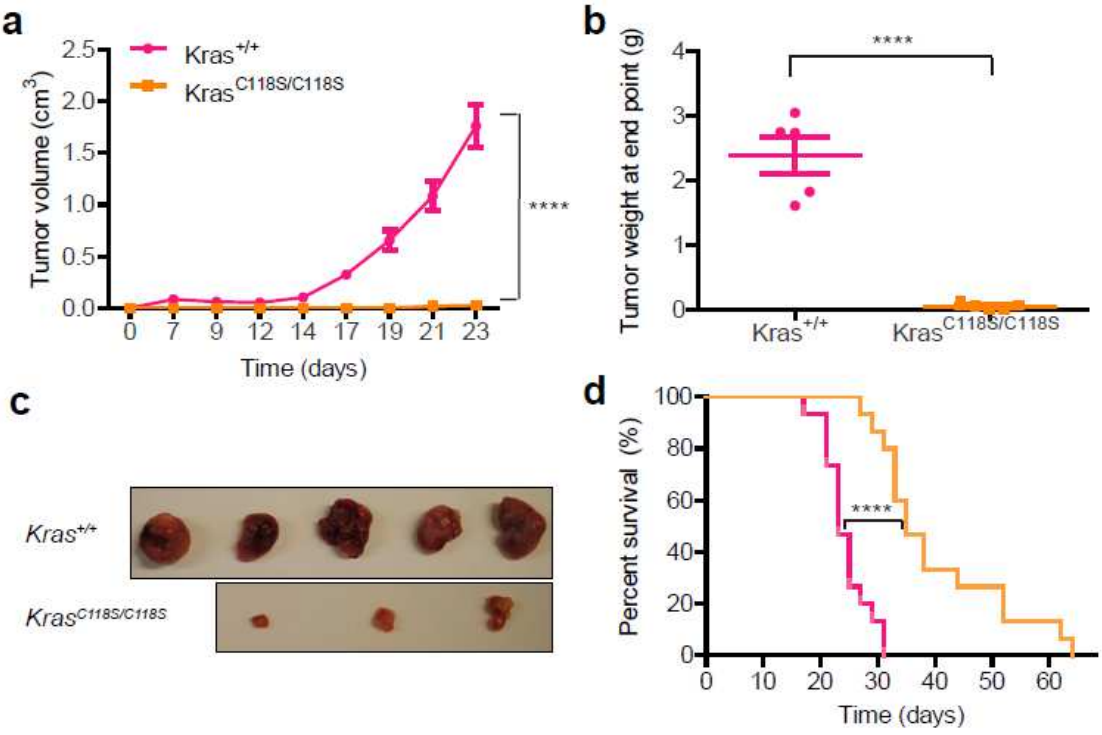

Figure 27: Introducing a C118S mutation into the endogenous wild-type Kras gene inhibits KRAS^{G12V}-driven tumor growth.

(**a**) Mean ± SEM tumor volume over time, (**b**) mean ± SEM tumor weight at end point, and (**c**) photographs of excised tumors at end point of tumors developing in immunocompromised mice (n=5) injected with SV40-immortalized *Kras*$^{+/+}$ (pink cirlces) versus *Kras*$^{C118S/C118S}$ (orange squares) MEF cell lines transformed with KRAS^{G12V}. (**d**) Kaplan-Meier survival curves based on the time to reach end point of immunocompromised mice (n=5) each injected with one of the three SV40-immortalized *Kras*$^{+/+}$ (pink line) versus *Kras*$^{C118S/C118S}$ (orange line) MEF cell lines transformed with HRAS^{G12V}. ****: P<0.0001, as determined by two-tailed unpaired student's t test (a, b) or long-rank test (d) using GraphPad Prism 5 Software.

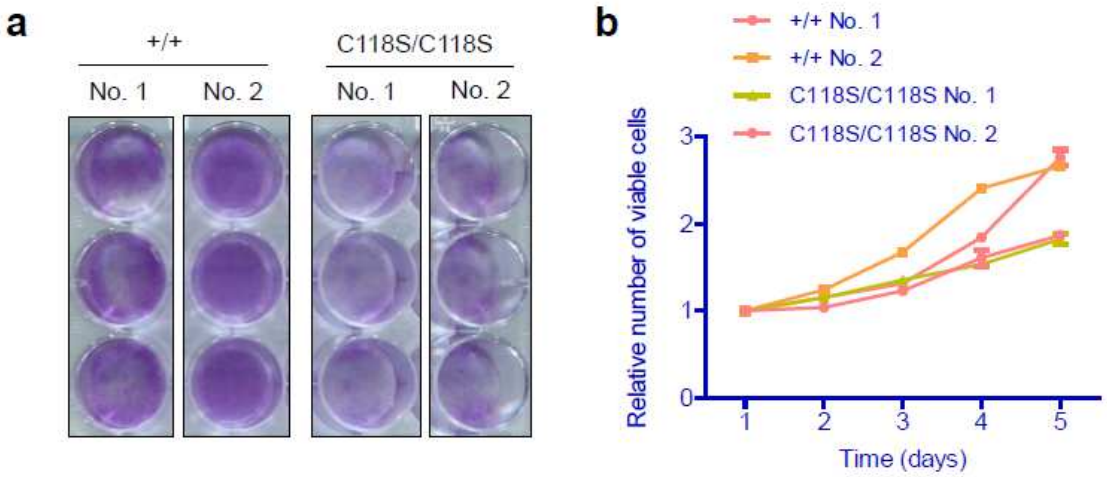

Figure 28: Immortalized *Kras*$^{C118S/C118S}$ MEFs show decreased proliferation.

Two SV40-immortalized *Kras*$^{+/+}$ *(+/+)* and two SV40-immortalized *Kras*$^{C118S/C118S}$ (C118S/C118S) MEFs were plated in triplicate at 1000 cells/well in five 24-well plates. (**a**) Images of crystal violet staining at day 5 after plating. (**b**) Growth curve of the four cell lines based on crystal violet staining of cells at different days after plating.

6.2.2 C118S mutation inhibits wild-type KRAS-induced growth arrest

To better understand the effect of introducing a C118S mutation in KRAS on tumorigenesis, it will be necessary to assess whether this mutation could affect some important steps during tumor development. At an early stage of tumor initiation, an oncogenic mutation in RAS can induce cell permanent G1 growth arrest known as oncogene-induced premature senescence, which serves as an initial tumor–suppressing mechanism and can be overcome by later events including cooperating oncogenic mutations of other genes as well as inactivating mutations or loss of tumor suppressors such as p53 and p16 (Serrano, Lin et al. 1997, Braig and Schmitt 2006, Mooi and Peeper 2006). It is possible that the C118S mutation in KRAS may affect oncogene-induced senescence. To test this possibility, primary human fibroblasts IMR-90 cells were transduced with KRAS or $KRAS^{C118S}$, followed by infection with retrovirus encoding no transgene, oncogeinc $HRAS^{G12V}$, or oncogenic $KRAS^{G12V}$. The infected cells were then plated in quadruplicate in multiple 24-well plates and stained with crystal violet at different days to track the relative number of adherant viable cells over time. Growth curves derived from this analysis revealed that IMR-90 cells transduced with either KRAS or $KRAS^{C118S}$ both grew poorly in the presence of oncogenic $HRAS^{G12V}$ (Figure 29a). Similar results were observed when the cells were transduced with oncogenic $KRAS^{G12V}$ (Figure 29b). These results suggest a minimal effect of ectopically expreesing a $KRAS^{C118S}$ mutation on oncogenic RAS^{G12V}-induced senescence. Interestingly however, in

the absence of RAS^{G12V}, IMR-90 cells expressing $KRAS^{C118S}$ consistently showed an increase in cell growth compared with cells transduced with KRAS (Figure 29a, b). Moreover, IMR-90 cells transduced with KRAS grew as poorly as those with oncogenic $HRAS^{G12V}$ or $KRAS^{G12V}$ (Figure 29a, b), suggesting that wild-type KRAS alone may induce the growth arrest of IMR-90 cells, and further, that this effect is negated by the C118S mutation.

To test this hypothesis, IMR-90 cells were infected with retrovirus enoding no transgene, KRAS, or $KRAS^{C118S}$, then plated in 24-well plates and stained with crystal violet at different days. Growth curve revealed that IMR-90 cells transduced with KRAS hardly grew, while those transduced with $KRAS^{C118S}$ or an empty vector grew at a similar rate (Figure 29c). Images of crystal violet staining at end point (day 18) show decreased staining in IMR-90 cells with KRAS but not in those with $KRAS^{C118S}$ (Figure 29d). These results indicate that ectopic expression of wild-type KRAS induces growth arrest, while $KRAS^{C118S}$ does not. Further studies are required to differentiate whether this growth arrest is senescence, apoptosis, or other events. Additionally, it remains to be determined if this effect is observed in other types of cells, and how this may influence tumorigenesis *in vivo*.

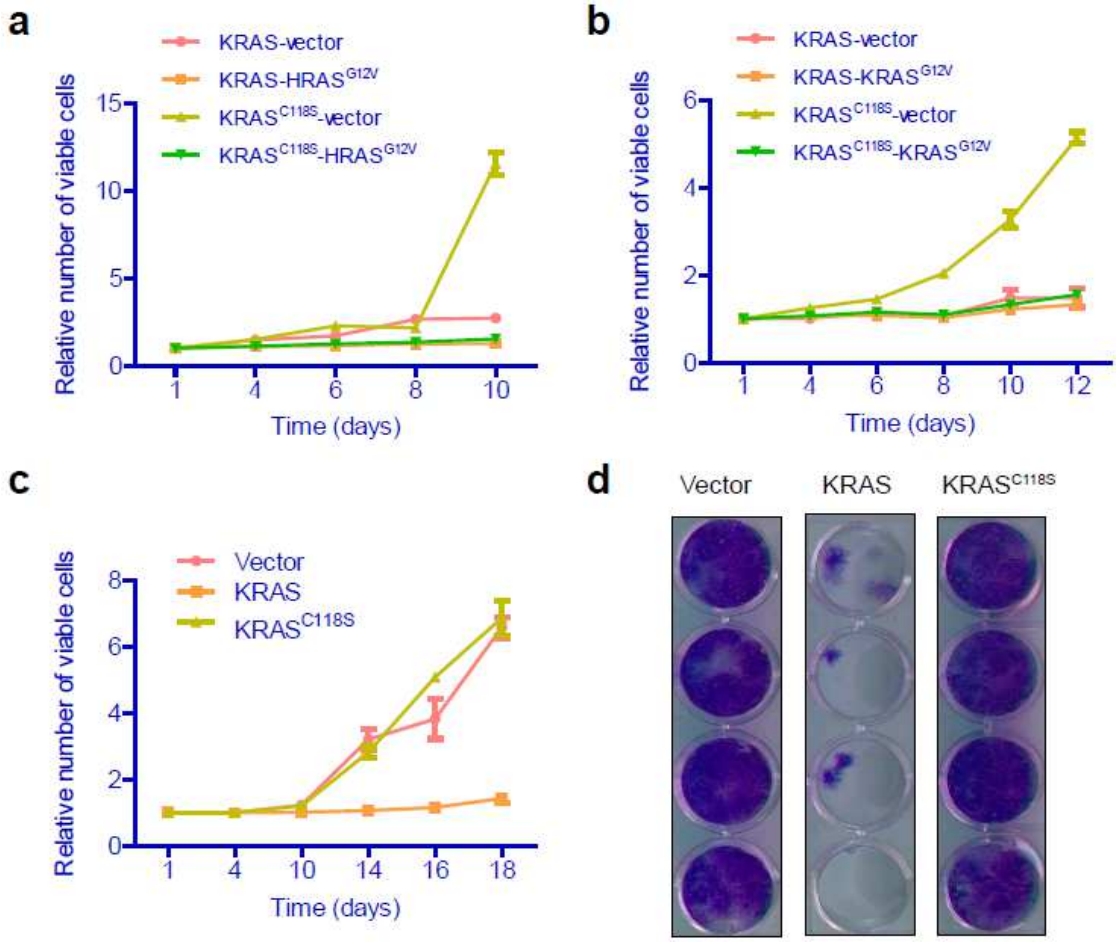

Figure 29: KRAS^{C118S} mutation blocks wild-type KRAS-induced growth arrest.

(**a, b**) Growth curve of IMR-90 cells transduced with KRAS or KRAS^{C118S} and infected with a retrovirus encoding no transgene (vector), HRAS^{G12V} (**a**) or KRAS^{G12V} (**b**). (**c**) Growth curve and (**d**) images of crystal violet staining (at day 18 after plating) of IMR-90 cells infected with a retrovirus encoding no transgene (vector), KRAS or KRAS^{C118S}. Each type of infected IMR-90 cells were plated in quadruplicate at 4000 cells/well in multiple 24-well plates, and crystal violet staining was performed at different days after plating.

6.2.3 C118S mutation in murine Kras results in a minor defect in mice

In Chapter 3 (**3.2.3**), I studied the effect of C118S mutation in endogenous murine Kras during development by comparing the phenotypes of *Kras*$^{+/+}$ and *Kras*$^{C118S/C118S}$ mice. I demonstrated that *Kras*$^{+/+}$ and *Kras*$^{C118S/C118S}$ mice were born with the expected Mendelian ratio and were phenotypically indistinguishable from each other, with no statistical difference in the weight of either male or female mice, their heart-to-body weight ratio and their life span (Table 1 and Figure 5). However, there is a trend towards *Kras*$^{C118S/C118S}$ mice having a lower body weight in females, a higher heart-to-body weight, and a shorter life span (Figure 5c-e). Furthermore, 3 out of 10 *Kras*$^{C118S/C118S}$ mice, compared to 1 out of 8 *Kras*$^{+/+}$ mice developed neurological disorders at late age. Also, 1 of the 10 *Kras*$^{C118S/C118S}$ mice was around two-fold heavier than the remaining littermates. These results suggest that C118S mutation in murine *Kras* may yet have minor effect on mouse development, although this is rather speculative at this juncture.

C118S mutation in murine *Kras* may also affect Ras signaling in mice. To test this hypothesis, equal amounts of lysates derived from the lungs of *Kras*$^{+/+}$ and *Kras*$^{C118S/C118S}$ mice were immunoblotted for Kras and its downstream signaling proteins. This analysis revealted that lysates from *Kras*$^{C118S/C118S}$ mice had similar levels of Kras protein but reduced levels of phosphorylated (P-) AKT compared with lystates derived from *Kras*$^{+/+}$ mice (Figure 30). It remains to be determined what role this plays in the observed decrease in lung tumorigenesis induced by urethane.

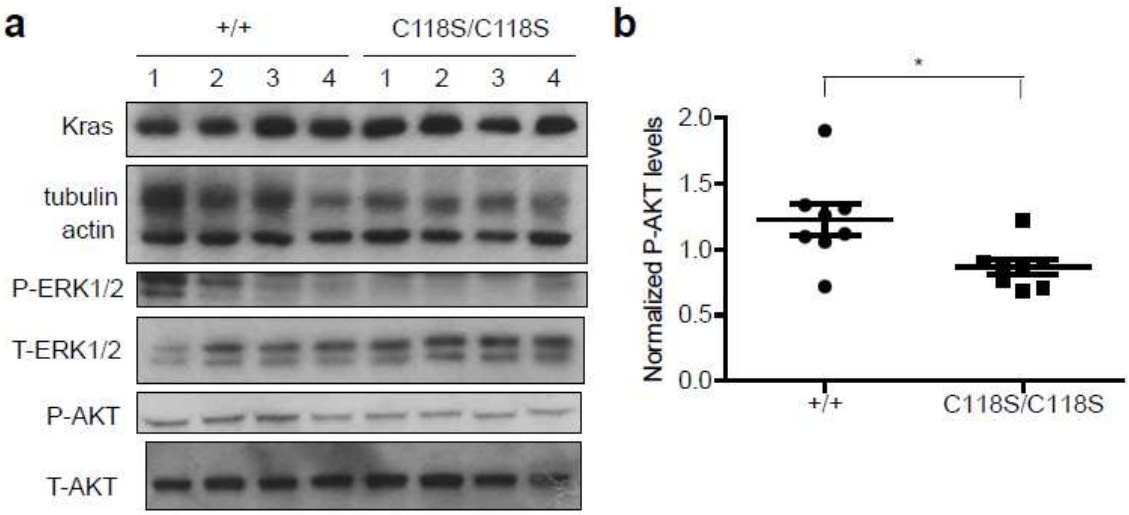

Figure 30: *Kras*$^{C118S/C118S}$ mice show decreased AKT phosphorylation.

(**a**) Equal amounts of lysates from the lungs of four *Kras*$^{+/+}$ mice and four *Kras*$^{C118S/C118S}$ mice were immunoblotted for Kras, tubulin, actin, phosphorylated (P-) ERK1/2, total (T-) ERK1/2 , phosphorylated (P-) AKT, and total (T-) AKT. (**b**) Normalized P-AKT levels (by quantification of P-AKT levels relative to T-AKT levels) from lungs of eight *Kras*$^{+/+}$ mice and eight *Kras*$^{C118S/C118S}$ mice. *: $P<0.05$, as determined by two-tailed unpaired student's *t*-test using Graphpad Prism 5.

6.3 The effect of Kras C118S mutation on tumorigenesis

6.3.1 The effect of Kras C118S mutation on carcinogen-induced tumorigenesis

In Chapter 3 (**3.2.4**), I found a decreased urethane-induced lung tumorigenesis in $Kras^{C118S/C118S}$ versus $Kras^{+/+}$ mice. To evaluate whether $Kras^{C118S/C118S}$ mice are resistant to another carcinogen, 16 $Kras^{+/+}$ and 14 $Kras^{C118S/C118S}$ mice (8-12 weeks old) were topically treated with DMBA followed by TPA twice weekly to induce skin tumors (introduced in **1.2.1.2**). Papillomas started to form at around week 12 following DMBA treatment in both groups, and increased at a similar rate at the beginning. However, the number of papillomas per mouse, as well as the percentage of mice with papillomas, differed in $Kras^{C118S/C118S}$ mice versus in $Kras^{+/+}$ mice starting from 23 weeks after DMBA treatment (Figure 31a, b), resulting in more papillomas per mouse and higher tumor incidence of the $Kras^{C118S/C118S}$ group at end point (28 weeks). Furthermore, analysis of the papillomas that developed in these mice at end point suggests no significant difference in the size of the papillomas between the two groups (Figure 31c-e). These results suggest that C118S mutation in Kras may promote the initiation of DMBA/TPA-induced skin tumorigenesis, but did not seem to affect tumor growth in this setting. It would be helpful to do histological analysis on H.E stained papillomas that developed in $Kras^{+/+}$ and $Kras^{C118S/C118S}$ mice, which would reveal the potential difference in tumor type or grade between the

two groups and would help understand whether the *Kras*^{C118S} mutation affects skin tumor progression.

I have found that *Kras*$^{C118S/C118S}$ mice developed fewer and smaller lung tumors induced by urethane but more skin papillomas upon DMBA/TPA treatment. The discrepancy in the effect of *Kras*^{C118S} mutation on tumorigenesis in the two carcinogen-induced tumor models may be explained by two possibilities. First, in the study of DMBA/TPA skin tumorigenesis, the *Kras* alleles from *Kras*$^{+/+}$ mice were from the BL6 background, while the *Kras*^{C118S} alleles from *Kras*$^{C118S/C118S}$ mice were from the 129S6 background. Since the 129S6 background has been reported to be more susceptible to cancer while the BL6 background relatively resistant (Demant 2003), it is possible that the increased skin tumor number in *Kras*$^{C118S/C118S}$ mice is due to the higher suspectibility of *Kras*^{C118S} allele in 129S6 background than the *Kras* allele in BL6 background in *Kras*$^{+/+}$ mice. To address this possibility, *Kras*$^{C118S/+}$ mice will need to be backcrossed into a 129S6 strain background, and the experiment repeated.

Second, the effect of *Kras*^{C118S} mutation on tumorigenesis may be different depending on the carcinogen, initiating oncogene, and sites of tumor development. Indeed, an intraperitoneal injection of urethane induces *Kras* mutations in the lung that lead to lung tumors, while topical treatment of DMBA/TPA induces *Hras* mutations in the skin that lead to skin tumors. The carcinogen urethane can generate nitric oxide in certain conditions (Sakano, Oikawa et al. 2002), which may account for the difference in

urethane-induced tumorigenesis between *Kras*$^{+/+}$ and *Kras*$^{C118S/+}$ or *Kras*$^{C118S/C118S}$ mice. It is possible that the decreased tumorigenesis in mice with a point mutation at C118 may be specific for tumors induced by carcinogens that can generate reactive oxygen/nitrogen species, such as urethane.

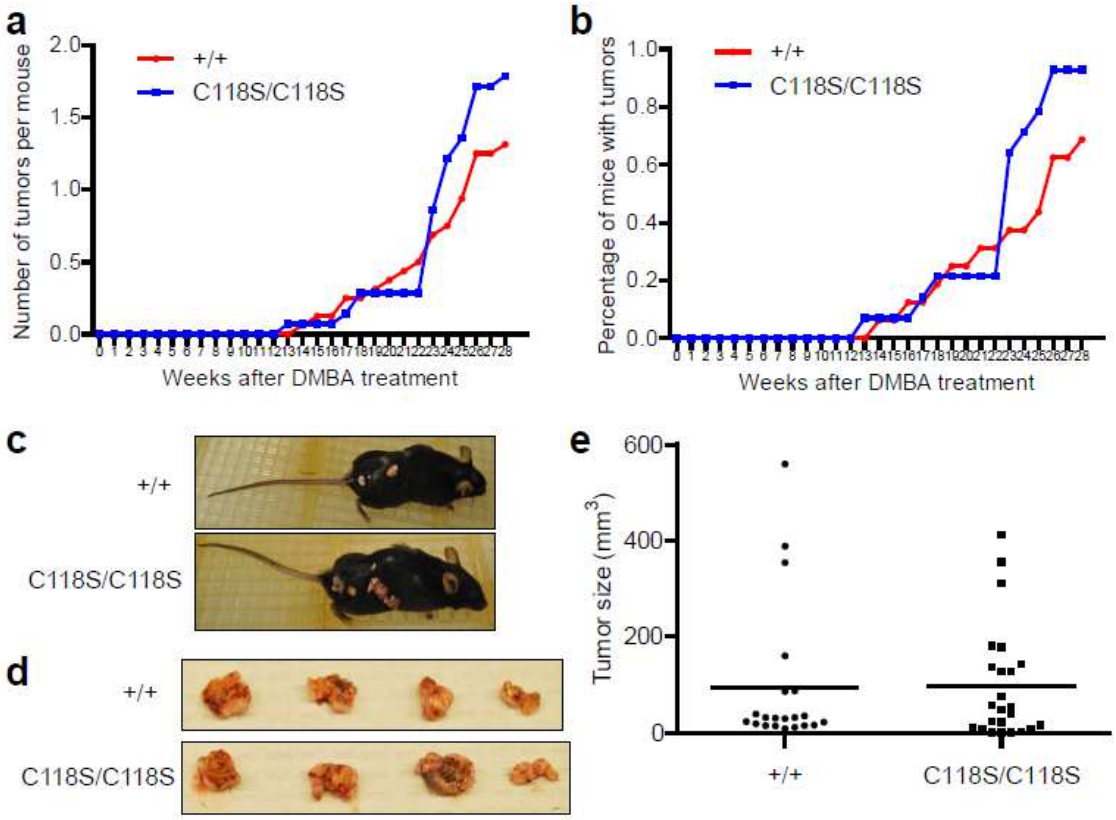

Figure 31: Skin papillomas developing in DMBA/TPA treated *Kras*$^{+/+}$ and *Kras*$^{C118S/C118S}$ mice.

16 *Kras*$^{+/+}$ and 14 *Kras*$^{C118S/C118S}$ mice were treated with DMBA at 8-12 weeks old followed by treatment with TPA twice weekly afterwards until end point. (**a**) Number of tumors per mouse and (**b**) percentage of mice with tumors at different weeks after initiation with DMBA. (**c**) Representative images of *Kras*$^{+/+}$ (+/+) and *Kras*$^{C118S/C118S}$ (C118S/C118S) mice with skin papillomas. (**d**) Representative images of skin papillomas isolated from *Kras*$^{+/+}$ (+/+) and *Kras*$^{C118S/C118S}$ (C118S/C118S) mice. (**e**) Average size of tumors developing in *Kras*$^{+/+}$ (+/+) and *Kras*$^{C118S/C118S}$ (C118S/C118S) mice. The tumor size of the two groups did not show a significant difference, as determined by two-tailed unpaired student's *t*-test using Graphpad Prism 5.

6.3.2 The effect of Kras C118S mutation on conditionally-activated $Kras^{G12D}$-driven tumorigenesis

In Chapter 3, I have found no significant difference in number, size, and burden of lung tumors between *Kras*$^{LSL\text{-}G12D/+}$ and *Kras*$^{LSL\text{-}G12D/C118S}$ mice treated with Ad-Cre, suggesting that C118S mutation in wild-type Kras does not seem to affect oncogenic $Kras^{G12D}$-driven lung tumorigenesis (**3.2.5** and Figure 9). To assess whether this result was observed in other tissues, *Kras*$^{LSL\text{-}G12D/+}$ and *Kras*$^{LSL\text{-}G12D/C118S}$ mice were crossed with *Pdx1-Cre* transgenic mice, generating *Kras*$^{LSL\text{-}G12D/+}$*; Pdx1-Cre* and *Kras*$^{LSL\text{-}G12D/C118S}$*; Pdx1-Cre* mice to induce pancreatic tumorigenesis (introduced in **1.2.2.2**). As a note, *Pdx1* promoter is "leaky", activating the *LSL-Kras*^{G12D} allele in the skin leading to facial and vulva papillomas (Gades, Ohash et al. 2008, Mazur, Gruner et al. 2010).

Both *Kras*$^{LSL\text{-}G12D/+}$*; Pdx1-Cre* and *Kras*$^{LSL\text{-}G12D/C118S}$*; Pdx1-Cre* mice developed facial and vulva papillomas (Figure 32a) and pancreatic lesions (Figure 32b) at 6 months old. The incidence of facial papillomas were two-fold higher in *Kras*$^{LSL\text{-}G12D/C118S}$*; Pdx1-Cre* mice than in *Kras*$^{LSL\text{-}G12D/+}$*; Pdx1-Cre* mice, while the incidence of vulva papillomas were similar between the two groups (Figure 32c). Quantification of the amount of normal tissue from five random fields from each H&E-stained pancreatic tissue section revealed that a huge variability from animal to animal in the amount of normal tissue (from 0 to 98%), although on average there was slightly more normal tissue remaining in *Kras*$^{LSL\text{-}G12D/C118S}$*; Pdx1-Cre* mice (Figure 32d). Nevertheless, these data argue against an effect of the C118S

mutation on wild-type Kras in now two models of conditionally activated oncogenic $Kras^{G12D}$-driven tumorigenesis.

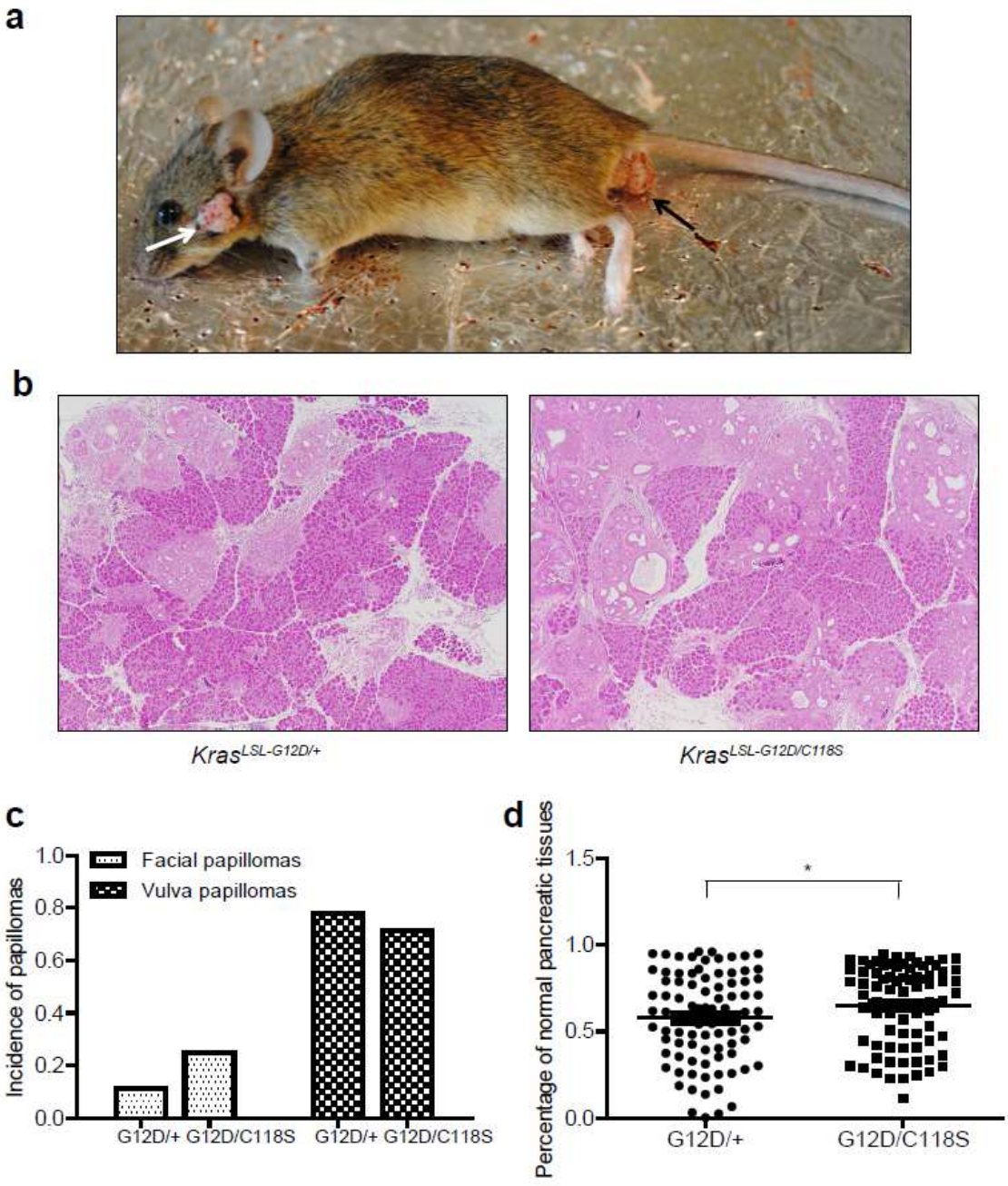

Figure 32: Papillomas and pancreatic lesions developing in *Kras*$^{LSL\text{-}G12D/+}$;*Pdx1-Cre* and *Kras*$^{LSL\text{-}G12D/C118S}$;*Pdx1-Cre* mice.

(**a**) A representative image of mice with facial (white arrows) and vulva (black arrows) papillomas. (**b**) Representative images of pancreatic tissues stained with Hematoxylin

and Eosin (H&E) at 10X. (**c**) Incidence of facial and vulva papillomas developing in 18 *Kras*$^{LSL\text{-}G12D/+}$;*Pdx1-Cre* (G12D/+) and 16 *Kras*$^{LSL\text{-}G12D/C118S}$;*Pdx1-Cre* (G12D/C118S) mice of six months old. (**d**) Percentage of normal pancreatic tissues in the pancreas of 18 *Kras*$^{LSL\text{-}G12D/+}$;*Pdx1-Cre* (G12D/+) and 16 *Kras*$^{LSL\text{-}G12D/C118S}$;*Pdx1-Cre* (G12D/C118S) mice of six months old. For H.E stained pancreatic tissues of each mouse, pictures of five random fields at 10X magnification were taken, and the normal as well as total pancreatic tissues in each picture were circled in Photoshop software, based on which the percentage of normal pancreatic tissues in each picture (represented by each dot) were calculated. *: $P<0.05$, as determined by two-tailed unpaired student's *t*-test using Graphpad Prism 5.

6.3.3 The effect of Kras C118S mutation on tumorigenesis at an early versus a late stage

The four mouse tumor models discussed so far all model *de novo* tumorigenesis, and hence are useful in studying tumor initiation and early progression. A C118S mutation in endogenous murine *Kras* impaired urethane-induced *Kras* mutation-positive lung tumorigenesis, which appeared to be linked to the oncogenic *Kras* allele (Chapter 3). On the other hand, a C118S mutation in wild-type *Kras* in the presence of a conditionally activated $Kras^{LSL\text{-}G12D}$ allele did not overtly alter oncogenic $Kras^{G12D}$-driven lung (**3.2.5**) and pancreatic tumorigenesis (**6.3.2**). In constrast, a C118S mutation in wild-type *Kras* did decrease the xenograft tumor growth of cells driven by oncogenic $HRAS^{G12V}$ (**4.2.6)** as well as $KRAS^{G12V}$ (**6.2.1**).

These results suggest that a C118S mutation in wild-type Kras can affect tumor development in some settings but not in others. One difference between these settings is that the xenograft tumor growth experiments utilize tumorigenic cells, which model later stages for tumorigenesis. Specifically, the oncogenic RAS-transformed cells used for xenograft tumor assays were immortalized with the SV40 early region including large T and small t antigen, which inactivates tumor suppressors such as p53 and p16 and activates c-Myc (Pipas 2009). In constrast, urethane-induced lung tumor model and conditionally activated $Kras^{LSL\text{-}G12D}$-driven lung and pancreatic tumor models reflect *de novo* tumorigenesis starting from an early stage.

Actually, wild-type Kras has been shown as a tumor suppressor in urethane-induced *de novo* lung tumorigenesis, since mice heterozygous for *Kras* (*Kras*$^{+/-}$ mice) developed more tumors than wild-type mice upon urethane treatment (Zhang, Wang et al. 2001, To, Rosario et al. 2013). Interestingly, in Chapter 3, I have found that mutating endogenous *Kras* cysteine 118 to serine (in order to decrease Kras activation) actually led to dereased rather than increased urethane-induced lung tumorigenesis, which indicates that the decreased tumorigenesis in *Kras*$^{C118S/+}$ and *Kras*$^{C118S/C1118S}$ mice is unlikely to be linked with an effect of the C118S mutation on the function of wild-type *Kras* allele as a tumor suppressor. Furthermore, the similar tumorigenesis between *Kras*$^{LSL\text{-}G12D/+}$ and *Kras*$^{LSL\text{-}G12D/C118S}$ mice upon activation of oncogenic Kras^{G12D} also suggests that the C118S mutation is unlikely to affect the role of wild-type Kras in *de novo* tumorigenesis. Therefore, while wild-type Kras plays a tumor suppressive role in urethane-induced *de novo* tumorigenesis (Zhang, Wang et al. 2001, To, Rosario et al. 2013) , the C118S mutation is unlikely to affect this role of wild-type Kras in this setting (early-stage tumorigenesis).

In contrast, in Chapter 4, I have found wild-type Kras to be critical for oncogenic HRAS-driven xenograft tumor growth, which models tumor development at a late stage. A C118S mutation impairs this role of wild-type Kras in the presence of constitutively active PI3K to activate Akt- eNOS cascade. Considering that a C118S mutation in wild-type HRAS has been found to reduce xenograft tumor growth of Kras mutation positive

cancer cells (Lim, Ancrile et al. 2008), I speculate that a C118S mutation in wild-type RAS proteins of any of the three isoforms may impair their critical functions in late-stage tumor development.

Taken together, considering the C118S mutation is more likely to affect oncogenic Kras in *de novo* tumorigenesis, but affects wild-type Kras in xenograft growth of transformed cells, I propose the following model. At an early stage of tumorigenesis (or tumor initiation stage), an oncogenic mutation in one *Kras* allele promotes tumorigenesis, while the remaining wild-type *Kras* allele functions as a tumor suppressor. The C118S mutation seems more likely to negatively affect the oncogenic *Kras*, resulting in decreased tumor initiation, but does not seem to affect the tumor-supressive functions of the wild-type *Kras* allele at this stage. At later stages of tumorigenesis (with accumulating oncogenic mutations and inactivated tumor suppressors), however, wild-type Kras may actually contribute to tumor development in the presence of redox environment, and the C118S mutation can decrease this activity of wild-type Kras, thus impairing tumor growth.

6.4 Concluding remarks

In the current study, I have introduced a C118S mutation into endogenous murine *Kras* and generated genetically-engineered mice with a $Kras^{C118S}$ point mutation. I have demonstrated that the $Kras^{C118S}$ mutation has a minimal effect on mice development and has a negative effect on tumor development in at least two setttings. First, $Kras^{+/C118S}$ and $Kras^{C118S/C118S}$ mice developed fewer and smaller lung tumors than $Kras^{+/+}$ mice upon treatment with urethane, which induces oncogenic Kras mutations at Q61. Second, oncogenic $HRAS^{G12V}$-transformed SV40 early region-immortalized $Kras^{C118S/C118S}$ MEFs grew as xenograft tumors more slowly than similarly transformed and immortalized $Kras^{+/+}$ MEFs. The urethane-induced lung tumor model mimics tumorigenesis starting from an ealy stage, and the decreased tumorigenesis of $Kras^{C118S/C118S}$ mice in this setting is more likely linked to an effect of C118S mutation on the oncogenic Kras. In constrast, the xenograft tumor model mimics tumorigenesis at a late stage, and the decreased xenograft tumor growth of $Kras^{C118S/C118S}$ MEFs is more related with an effect of C118S mutation on wild-type Kras.

In vitro studies on the potential mechanisms of the effect of $Kras^{C118S}$ mutation on tumorigenesis revealed that C118S mutation had a very minor, if any, effect on the activity of oncogenic $Kras^{Q61R/Q61L}$, but a moderate negative effect on oncogenic $Kras^{G13D}$ activation of the MAPK pathway. On the other hand, C118S mutation in wild-type KRAS decreases KRAS activation as well as downstream signaling, and also abolishes

wild-type KRAS-induced growth arrest. It is possible that the extent of the effect of C118S mutation on Kras is dependent upon the strength of the oncogene. The more oncogenic potential the Kras gene has, the less likely that its activity being affected by the C118S mutation. However, the exact mechanisms on the reduced urethane-induced tumorigenesis in $Kras^{+/C118S}$ and $Kras^{C118S/C118S}$ mice remain unknown. Nevertheless, my studies support the contention that redox-dependent reactions with Kras at C118 can affect tumorigenesis in some, but certainly not all settings.

References

Adachi, T., D. R. Pimentel, T. Heibeck, X. Hou, Y. J. Lee, B. Jiang, Y. Ido and R. A. Cohen (2004). "S-glutathiolation of Ras mediates redox-sensitive signaling by angiotensin II in vascular smooth muscle cells." J Biol Chem **279**(28): 29857-29862.

Ahearn, I. M., K. Haigis, D. Bar-Sagi and M. R. Philips (2012). "Regulating the regulator: post-translational modification of RAS." Nat Rev Mol Cell Biol **13**(1): 39-51.

Akhand, A. A., M. Pu, T. Senga, M. Kato, H. Suzuki, T. Miyata, M. Hamaguchi and I. Nakashima (1999). "Nitric oxide controls src kinase activity through a sulfhydryl group modification-mediated Tyr-527-independent and Tyr-416-linked mechanism." J Biol Chem **274**(36): 25821-25826.

Alderton, W. K., C. E. Cooper and R. G. Knowles (2001). "Nitric oxide synthases: structure, function and inhibition." Biochem J **357**(Pt 3): 593-615.

Anest, V., P. C. Cogswell and A. S. Baldwin, Jr. (2004). "IkappaB kinase alpha and p65/RelA contribute to optimal epidermal growth factor-induced c-fos gene expression independent of IkappaBalpha degradation." J Biol Chem **279**(30): 31183-31189.

Anest, V., J. L. Hanson, P. C. Cogswell, K. A. Steinbrecher, B. D. Strahl and A. S. Baldwin (2003). "A nucleosomal function for IkappaB kinase-alpha in NF-kappaB-dependent gene expression." Nature **423**(6940): 659-663.

Aoki, Y., T. Niihori, H. Kawame, K. Kurosawa, H. Ohashi, Y. Tanaka, M. Filocamo, K. Kato, Y. Suzuki, S. Kure and Y. Matsubara (2005). "Germline mutations in HRAS proto-oncogene cause Costello syndrome." Nat Genet **37**(10): 1038-1040.

Arozarena, I., F. Calvo and P. Crespo (2011). "Ras, an actor on many stages: posttranslational modifications, localization, and site-specified events." Genes Cancer **2**(3): 182-194.

Avanzo, J. L., M. Mesnil, F. J. Hernandez-Blazquez, Mackowiak, II, C. M. Mori, T. C. da Silva, S. C. Oloris, A. P. Garate, S. M. Massironi, H. Yamasaki and M. L. Dagli (2004). "Increased susceptibility to urethane-induced lung tumors in mice with decreased expression of connexin43." Carcinogenesis **25**(10): 1973-1982.

Barbin, A. (2000). "Etheno-adduct-forming chemicals: from mutagenicity testing to tumor mutation spectra." Mutat Res **462**(2-3): 55-69.

Batista, W., F. Ogata, M. Curcio, R. Miguel, R. Arai, A. Matsuo, M. Moraes, A. Stern and H. Monteiro (2013). "S-nitrosoglutathione and endothelial nitric oxide synthase-derived nitric oxide regulate compartmentalized ras S-nitrosylation and stimulate cell proliferation." Antioxidants & redox signaling **18**(3): 221-238.

Bonavida, B. and S. Baritaki (2011). "Dual role of NO donors in the reversal of tumor cell resistance and EMT: Downregulation of the NF-kappaB/Snail/YY1/RKIP circuitry." Nitric Oxide **24**(1): 1-7.

Bos, J. L., H. Rehmann and A. Wittinghofer (2007). "GEFs and GAPs: critical elements in the control of small G proteins." Cell **129**(5): 865-877.

Brady, D. C., M. S. Crowe, M. L. Turski, G. A. Hobbs, X. Yao, A. Chaikuad, S. Knapp, K. Xiao, S. L. Campbell, D. J. Thiele and C. M. Counter (2014). "Copper is required for oncogenic BRAF signalling and tumorigenesis." Nature **509**(7501): 492-496.

Braig, M. and C. A. Schmitt (2006). "Oncogene-induced senescence: putting the brakes on tumor development." Cancer Res **66**(6): 2881-2884.

Castellano, E. and J. Downward (2011). "RAS Interaction with PI3K: More Than Just Another Effector Pathway." Genes Cancer **2**(3): 261-274.

Castellano, E. and E. Santos (2011). "Functional specificity of ras isoforms: so similar but so different." Genes Cancer **2**(3): 216-231.

Chen, X., N. Mitsutake, K. LaPerle, N. Akeno, P. Zanzonico, V. A. Longo, S. Mitsutake, E. T. Kimura, H. Geiger, E. Santos, H. G. Wendel, A. Franco, J. A. Knauf and J. A. Fagin (2009). "Endogenous expression of Hras(G12V) induces developmental defects and neoplasms with copy number imbalances of the oncogene." Proc Natl Acad Sci U S A **106**(19): 7979-7984.

Chin, L., A. Tam, J. Pomerantz, M. Wong, J. Holash, N. Bardeesy, Q. Shen, R. O'Hagan, J. Pantginis, H. Zhou, J. W. Horner, 2nd, C. Cordon-Cardo, G. D. Yancopoulos and R. A. DePinho (1999). "Essential role for oncogenic Ras in tumour maintenance." Nature **400**(6743): 468-472.

Cho, D. H., T. Nakamura, J. Fang, P. Cieplak, A. Godzik, Z. Gu and S. A. Lipton (2009). "S-nitrosylation of Drp1 mediates beta-amyloid-related mitochondrial fission and neuronal injury." Science **324**(5923): 102-105.

Clavreul, N., T. Adachi, D. R. Pimental, Y. Ido, C. Schoneich and R. A. Cohen (2006). "S-glutathiolation by peroxynitrite of p21ras at cysteine-118 mediates its direct activation and downstream signaling in endothelial cells." FASEB J **20**(3): 518-520.

Cox, A. D., S. W. Fesik, A. C. Kimmelman, J. Luo and C. J. Der (2014). "Drugging the undruggable RAS: Mission Possible?" Nat Rev Drug Discov **13**(11): 828-851.

Cully, M., H. You, A. J. Levine and T. W. Mak (2006). "Beyond PTEN mutations: the PI3K pathway as an integrator of multiple inputs during tumorigenesis." Nat Rev Cancer **6**(3): 184-192.

de Rooij, J. and J. L. Bos (1997). "Minimal Ras-binding domain of Raf1 can be used as an activation-specific probe for Ras." Oncogene **14**(5): 623-625.

Dejardin, E. (2006). "The alternative NF-kappaB pathway from biochemistry to biology: pitfalls and promises for future drug development." Biochem Pharmacol **72**(9): 1161-1179.

Demant, P. (2003). "Cancer susceptibility in the mouse: genetics, biology and implications for human cancer." Nat Rev Genet **4**(9): 721-734.

Descargues, P., A. K. Sil and M. Karin (2008). "IKKalpha, a critical regulator of epidermal differentiation and a suppressor of skin cancer." Embo J **27**(20): 2639-2647.

Deschenes-Simard, X., F. Kottakis, S. Meloche and G. Ferbeyre (2014). "ERKs in cancer: friends or foes?" Cancer Res **74**(2): 412-419.

Dimmeler, S., I. Fleming, B. Fisslthaler, C. Hermann, R. Busse and A. M. Zeiher (1999). "Activation of nitric oxide synthase in endothelial cells by Akt-dependent phosphorylation." Nature **399**(6736): 601-605.

Ding, L., G. Getz, D. A. Wheeler, E. R. Mardis, M. D. McLellan, K. Cibulskis, C. Sougnez, H. Greulich, D. M. Muzny, M. B. Morgan, L. Fulton, R. S. Fulton, Q. Zhang, M. C. Wendl, M. S. Lawrence, D. E. Larson, K. Chen, D. J. Dooling, A. Sabo, A. C. Hawes, H. Shen, S. N. Jhangiani, L. R. Lewis, O. Hall, Y. Zhu, T. Mathew, Y. Ren, J. Yao, S. E. Scherer, K. Clerc, G. A. Metcalf, B. Ng, A. Milosavljevic, M. L. Gonzalez-Garay, J. R. Osborne, R. Meyer, X. Shi, Y. Tang, D. C. Koboldt, L. Lin, R. Abbott, T. L. Miner, C. Pohl, G. Fewell, C. Haipek, H. Schmidt, B. H. Dunford-Shore, A. Kraja, S. D. Crosby, C. S. Sawyer, T. Vickery, S. Sander, J. Robinson, W. Winckler, J. Baldwin, L. R. Chirieac, A. Dutt, T. Fennell, M. Hanna, B. E. Johnson, R. C. Onofrio, R. K. Thomas, G. Tonon, B. A.

Weir, X. Zhao, L. Ziaugra, M. C. Zody, T. Giordano, M. B. Orringer, J. A. Roth, M. R. Spitz, Wistuba, II, B. Ozenberger, P. J. Good, A. C. Chang, D. G. Beer, M. A. Watson, M. Ladanyi, S. Broderick, A. Yoshizawa, W. D. Travis, W. Pao, M. A. Province, G. M. Weinstock, H. E. Varmus, S. B. Gabriel, E. S. Lander, R. A. Gibbs, M. Meyerson and R. K. Wilson (2008). "Somatic mutations affect key pathways in lung adenocarcinoma." Nature **455**(7216): 1069-1075.

Donovan, S., K. M. Shannon and G. Bollag (2002). "GTPase activating proteins: critical regulators of intracellular signaling." Biochim Biophys Acta **1602**(1): 23-45.

Downward, J. (2003). "Targeting RAS signalling pathways in cancer therapy." Nat Rev Cancer **3**(1): 11-22.

Dudzinski, D. M., J. Igarashi, D. Greif and T. Michel (2006). "The regulation and pharmacology of endothelial nitric oxide synthase." Annu Rev Pharmacol Toxicol **46**: 235-276.

Dudzinski, D. M. and T. Michel (2007). "Life history of eNOS: partners and pathways." Cardiovasc Res **75**(2): 247-260.

Elmets, C. A., M. Athar, K. A. Tubesing, D. Rothaupt, H. Xu and H. Mukhtar (1998). "Susceptibility to the biological effects of polyaromatic hydrocarbons is influenced by genes of the major histocompatibility complex." Proc Natl Acad Sci U S A **95**(25): 14915-14919.

Engelman, J. A. (2009). "Targeting PI3K signalling in cancer: opportunities, challenges and limitations." Nat Rev Cancer **9**(8): 550-562.

Esteban, L. M., C. Vicario-Abejon, P. Fernandez-Salguero, A. Fernandez-Medarde, N. Swaminathan, K. Yienger, E. Lopez, M. Malumbres, R. McKay, J. M. Ward, A. Pellicer and E. Santos (2001). "Targeted genomic disruption of H-ras and N-ras, individually or in combination, reveals the dispensability of both loci for mouse growth and development." Mol Cell Biol **21**(5): 1444-1452.

Feig, L. A. (2003). "Ral-GTPases: approaching their 15 minutes of fame." Trends Cell Biol **13**(8): 419-425.

Filler, R. B., S. J. Roberts and M. Girardi (2007). "Cutaneous two-stage chemical carcinogenesis." CSH Protoc **2007**: pdb prot4837.

Forrester, M. T., M. W. Foster, M. Benhar and J. S. Stamler (2009). "Detection of protein S-nitrosylation with the biotin-switch technique." Free Radic Biol Med **46**(2): 119-126.

Forrester, M. T., M. W. Foster and J. S. Stamler (2007). "Assessment and application of the biotin switch technique for examining protein S-nitrosylation under conditions of pharmacologically induced oxidative stress." J Biol Chem **282**(19): 13977-13983.

Foster, M. W., D. T. Hess and J. S. Stamler (2009). "Protein S-nitrosylation in health and disease: a current perspective." Trends Mol Med **15**(9): 391-404.

Fukumura, D., S. Kashiwagi and R. K. Jain (2006). "The role of nitric oxide in tumour progression." Nat Rev Cancer **6**(7): 521-534.

Fulton, D., J. P. Gratton, T. J. McCabe, J. Fontana, Y. Fujio, K. Walsh, T. F. Franke, A. Papapetropoulos and W. C. Sessa (1999). "Regulation of endothelium-derived nitric oxide production by the protein kinase Akt." Nature **399**(6736): 597-601.

Gades, N. M., A. Ohash, L. D. Mills, M. A. Rowley, K. S. Predmore, R. J. Marler and F. J. Couch (2008). "Spontaneous vulvar papillomas in a colony of mice used for pancreatic cancer research." Comp Med **58**(3): 271-275.

Geller, D. A. and T. R. Billiar (1998). "Molecular biology of nitric oxide synthases." Cancer Metastasis Rev **17**(1): 7-23.

Ghosh, S. and M. Karin (2002). "Missing pieces in the NF-kappaB puzzle." Cell **109 Suppl**: S81-96.

Gilmore, T. D. (2006). "Introduction to NF-kappaB: players, pathways, perspectives." Oncogene **25**(51): 6680-6684.

Gonzalez, E., R. Kou, A. J. Lin, D. E. Golan and T. Michel (2002). "Subcellular targeting and agonist-induced site-specific phosphorylation of endothelial nitric-oxide synthase." J Biol Chem **277**(42): 39554-39560.

Grabocka, E., Y. Pylayeva-Gupta, M. J. Jones, V. Lubkov, E. Yemanaberhan, L. Taylor, H. H. Jeng and D. Bar-Sagi (2014). "Wild-type H- and N-Ras promote mutant K-Ras-driven tumorigenesis by modulating the DNA damage response." Cancer Cell **25**(2): 243-256.

Gysin, S., M. Salt, A. Young and F. McCormick (2011). "Therapeutic strategies for targeting ras proteins." Genes Cancer **2**(3): 359-372.

Hancock, J. F. (2003). "Ras proteins: different signals from different locations." Nat Rev Mol Cell Biol **4**(5): 373-384.

Harrison, D. G. (1997). "Cellular and molecular mechanisms of endothelial cell dysfunction." J Clin Invest **100**(9): 2153-2157.

Hayden, M. S. and S. Ghosh (2008). "Shared principles in NF-kappaB signaling." Cell **132**(3): 344-362.

Hecker, E. (1987). "Three stage carcinogenesis in mouse skin--recent results and present status of an advanced model system of chemical carcinogenesis." Toxicol Pathol **15**(2): 245-258.

Henis, Y. I., J. F. Hancock and I. A. Prior (2009). "Ras acylation, compartmentalization and signaling nanoclusters (Review)." Mol Membr Biol **26**(1): 80-92.

Hennings, H., A. B. Glick, D. T. Lowry, L. S. Krsmanovic, L. M. Sly and S. H. Yuspa (1993). "FVB/N mice: an inbred strain sensitive to the chemical induction of squamous cell carcinomas in the skin." Carcinogenesis **14**(11): 2353-2358.

Heo, J. and S. L. Campbell (2004). "Mechanism of p21Ras S-nitrosylation and kinetics of nitric oxide-mediated guanine nucleotide exchange." Biochemistry **43**(8): 2314-2322.

Hess, D. T., A. Matsumoto, S. O. Kim, H. E. Marshall and J. S. Stamler (2005). "Protein S-nitrosylation: purview and parameters." Nat Rev Mol Cell Biol **6**(2): 150-166.

Hill, B. G. and A. Bhatnagar (2012). "Protein S-glutathiolation: redox-sensitive regulation of protein function." J Mol Cell Cardiol **52**(3): 559-567.

Hingorani, S. R., E. F. Petricoin, A. Maitra, V. Rajapakse, C. King, M. A. Jacobetz, S. Ross, T. P. Conrads, T. D. Veenstra, B. A. Hitt, Y. Kawaguchi, D. Johann, L. A. Liotta, H. C. Crawford, M. E. Putt, T. Jacks, C. V. Wright, R. H. Hruban, A. M. Lowy and D. A. Tuveson (2003). "Preinvasive and invasive ductal pancreatic cancer and its early detection in the mouse." Cancer Cell **4**(6): 437-450.

Hirst, D. G. and T. Robson (2011). "Nitric oxide physiology and pathology." Methods Mol Biol **704**: 1-13.

Hobbs, G. A., M. G. Bonini, H. P. Gunawardena, X. Chen and S. L. Campbell (2013). "Glutathiolated Ras: characterization and implications for Ras activation." Free Radic Biol Med **57**: 221-229.

Hoberg, J. E., A. E. Popko, C. S. Ramsey and M. W. Mayo (2006). "IkappaB kinase alpha-mediated derepression of SMRT potentiates acetylation of RelA/p65 by p300." Mol Cell Biol **26**(2): 457-471.

Hocker, H. J., K. J. Cho, C. Y. Chen, N. Rambahal, S. R. Sagineedu, K. Shaari, J. Stanslas, J. F. Hancock and A. A. Gorfe (2013). "Andrographolide derivatives inhibit guanine nucleotide exchange and abrogate oncogenic Ras function." Proc Natl Acad Sci U S A **110**(25): 10201-10206.

Huang, H., J. Daniluk, Y. Liu, J. Chu, Z. Li, B. Ji and C. D. Logsdon (2014). "Oncogenic K-Ras requires activation for enhanced activity." Oncogene **33**(4): 532-535.

Huang, L., J. Carney, D. M. Cardona and C. M. Counter (2014). "Decreased tumorigenesis in mice with a Kras point mutation at C118." Nat Commun **5**: 5410.

Ibiza, S., A. Perez-Rodriguez, A. Ortega, A. Martinez-Ruiz, O. Barreiro, C. A. Garcia-Dominguez, V. M. Victor, J. V. Esplugues, J. M. Rojas, F. Sanchez-Madrid and J. M. Serrador (2008). "Endothelial nitric oxide synthase regulates N-Ras activation on the Golgi complex of antigen-stimulated T cells." Proc Natl Acad Sci U S A **105**(30): 10507-10512.

Ichikawa, T., Y. Yano, M. Uchida, S. Otani, K. Hagiwara and T. Yano (1996). "The activation of K-ras gene at an early stage of lung tumorigenesis in mice." Cancer Lett **107**(2): 165-170.

Ise, K., K. Nakamura, K. Nakao, S. Shimizu, H. Harada, T. Ichise, J. Miyoshi, Y. Gondo, T. Ishikawa, A. Aiba and M. Katsuki (2000). "Targeted deletion of the H-ras gene decreases tumor formation in mouse skin carcinogenesis." Oncogene **19**(26): 2951-2956.

Jackson, E. L., N. Willis, K. Mercer, R. T. Bronson, D. Crowley, R. Montoya, T. Jacks and D. A. Tuveson (2001). "Analysis of lung tumor initiation and progression using conditional expression of oncogenic K-ras." Genes Dev **15**(24): 3243-3248.

Jaffrey, S. R. and S. H. Snyder (2001). "The biotin switch method for the detection of S-nitrosylated proteins." Sci STKE **2001**(86): pl1.

James, G. L., J. L. Goldstein and M. S. Brown (1995). "Polylysine and CVIM sequences of K-RasB dictate specificity of prenylation and confer resistance to benzodiazepine peptidomimetic in vitro." J Biol Chem **270**(11): 6221-6226.

Jeng, H. H., L. J. Taylor and D. Bar-Sagi (2012). "Sos-mediated cross-activation of wild-type Ras by oncogenic Ras is essential for tumorigenesis." Nat Commun **3**: 1168.

Johnson, L., D. Greenbaum, K. Cichowski, K. Mercer, E. Murphy, E. Schmitt, R. T. Bronson, H. Umanoff, W. Edelmann, R. Kucherlapati and T. Jacks (1997). "K-ras is an essential gene in the mouse with partial functional overlap with N-ras." Genes Dev **11**(19): 2468-2481.

Johnson, L., K. Mercer, D. Greenbaum, R. T. Bronson, D. Crowley, D. A. Tuveson and T. Jacks (2001). "Somatic activation of the K-ras oncogene causes early onset lung cancer in mice." Nature **410**(6832): 1111-1116.

Kallianos, A., S. Tsimpoukis, P. Zarogoulidis, K. Darwiche, A. Charpidou, I. Tsioulis, G. Trakada, K. Porpodis, D. Spyratos, A. Panoutsopoulos, L. Veletza, K. Kostopoulos, C. Kostopoulos, I. Karapantzos, K. Tsakiridis, W. Hohenforst-Schmidt, K. Zarogoulidis, A. Rapti and K. Syrigos (2013). "Measurement of exhaled alveolar nitrogen oxide in patients with lung cancer: a friend from the past still precious today." Onco Targets Ther **6**: 609-613.

Karnoub, A. E. and R. A. Weinberg (2008). "Ras oncogenes: split personalities." Nat Rev Mol Cell Biol **9**(7): 517-531.

Kashatus, D. F., K. H. Lim, D. C. Brady, N. L. Pershing, A. D. Cox and C. M. Counter (2011). "RALA and RALBP1 regulate mitochondrial fission at mitosis." Nat Cell Biol **13**(9): 1108-1115.

Kisley, L. R., B. S. Barrett, A. K. Bauer, L. D. Dwyer-Nield, B. Barthel, A. M. Meyer, D. C. Thompson and A. M. Malkinson (2002). "Genetic ablation of inducible nitric oxide synthase decreases mouse lung tumorigenesis." Cancer Res **62**(23): 6850-6856.

Koera, K., K. Nakamura, K. Nakao, J. Miyoshi, K. Toyoshima, T. Hatta, H. Otani, A. Aiba and M. Katsuki (1997). "K-ras is essential for the development of the mouse embryo." Oncogene **15**(10): 1151-1159.

Kohl, N. E., C. A. Omer, M. W. Conner, N. J. Anthony, J. P. Davide, S. J. deSolms, E. A. Giuliani, R. P. Gomez, S. L. Graham, K. Hamilton and et al. (1995). "Inhibition of

farnesyltransferase induces regression of mammary and salivary carcinomas in ras transgenic mice." Nat Med **1**(8): 792-797.

Kratz, C. P., S. Schubbert, G. Bollag, C. M. Niemeyer, K. M. Shannon and M. Zenker (2006). "Germline mutations in components of the Ras signaling pathway in Noonan syndrome and related disorders." Cell Cycle **5**(15): 1607-1611.

Lampson, B., N. Pershing, J. Prinz, J. Lacsina, W. Marzluff, C. Nicchitta, D. MacAlpine and C. Counter (2013). "Rare codons regulate KRas oncogenesis." Current biology : CB **23**(1): 70-75.

Lampson, B. L., S. D. Kendall, B. B. Ancrile, M. M. Morrison, M. J. Shealy, K. S. Barrientos, M. S. Crowe, D. F. Kashatus, R. R. White, S. B. Gurley, D. M. Cardona and C. M. Counter (2012). "Targeting eNOS in pancreatic cancer." Cancer Res **72**(17): 4472-4482.

Lancaster, J. R., Jr. (2008). "Protein cysteine thiol nitrosation: maker or marker of reactive nitrogen species-induced nonerythroid cellular signaling?" Nitric Oxide **19**(2): 68-72.

Lander, H. M., D. P. Hajjar, B. L. Hempstead, U. A. Mirza, B. T. Chait, S. Campbell and L. A. Quilliam (1997). "A molecular redox switch on p21(ras). Structural basis for the nitric oxide-p21(ras) interaction." J Biol Chem **272**(7): 4323-4326.

Lander, H. M., A. T. Jacovina, R. J. Davis and J. M. Tauras (1996). "Differential activation of mitogen-activated protein kinases by nitric oxide-related species." J Biol Chem **271**(33): 19705-19709.

Lander, H. M., A. J. Milbank, J. M. Tauras, D. P. Hajjar, B. L. Hempstead, G. D. Schwartz, R. T. Kraemer, U. A. Mirza, B. T. Chait, S. C. Burk and L. A. Quilliam (1996). "Redox regulation of cell signalling." Nature **381**(6581): 380-381.

Lee, M. and J. C. Choy (2013). "Positive feedback regulation of human inducible nitric-oxide synthase expression by Ras protein S-nitrosylation." J Biol Chem **288**(22): 15677-15686.

Lim, K. H., B. B. Ancrile, D. F. Kashatus and C. M. Counter (2008). "Tumour maintenance is mediated by eNOS." Nature **452**(7187): 646-649.

Lim, K. H., A. T. Baines, J. J. Fiordalisi, M. Shipitsin, L. A. Feig, A. D. Cox, C. J. Der and C. M. Counter (2005). "Activation of RalA is critical for Ras-induced tumorigenesis of human cells." Cancer Cell **7**(6): 533-545.

Lim, K. H. and C. M. Counter (2005). "Reduction in the requirement of oncogenic Ras signaling to activation of PI3K/AKT pathway during tumor maintenance." Cancer Cell **8**(5): 381-392.

Lim, K. H., K. O'Hayer, S. J. Adam, S. D. Kendall, P. M. Campbell, C. J. Der and C. M. Counter (2006). "Divergent roles for RalA and RalB in malignant growth of human pancreatic carcinoma cells." Curr Biol **16**(24): 2385-2394.

Lin, Y. F., K. Raab-Graham, Y. N. Jan and L. Y. Jan (2004). "NO stimulation of ATP-sensitive potassium channels: Involvement of Ras/mitogen-activated protein kinase pathway and contribution to neuroprotection." Proc Natl Acad Sci U S A **101**(20): 7799-7804.

Madge, L. A. and M. J. May (2010). "Classical NF-kappaB activation negatively regulates noncanonical NF-kappaB-dependent CXCL12 expression." J Biol Chem **285**(49): 38069-38077.

Maher, J., D. A. Baker, M. Manning, N. J. Dibb and I. A. Roberts (1995). "Evidence for cell-specific differences in transformation by N-, H- and K-ras." Oncogene **11**(8): 1639-1647.

Malkinson, A. M. (1989). "The genetic basis of susceptibility to lung tumors in mice." Toxicology **54**(3): 241-271.

Mallis, R. J., J. E. Buss and J. A. Thomas (2001). "Oxidative modification of H-ras: S-thiolation and S-nitrosylation of reactive cysteines." Biochem J **355**(Pt 1): 145-153.
Malumbres, M. and M. Barbacid (2003). "RAS oncogenes: the first 30 years." Nat Rev Cancer **3**(6): 459-465.

Manenti, G., F. Galbiati, R. Gianni-Barrera, A. Pettinicchio, A. Acevedo and T. A. Dragani (2004). "Haplotype sharing suggests that a genomic segment containing six genes accounts for the pulmonary adenoma susceptibility 1 (Pas1) locus activity in mice." Oncogene **23**(25): 4495-4504.

Mannick, J. B., C. Schonhoff, N. Papeta, P. Ghafourifar, M. Szibor, K. Fang and B. Gaston (2001). "S-Nitrosylation of mitochondrial caspases." J Cell Biol **154**(6): 1111-1116.
Mannick, J. B. and C. M. Schonhoff (2002). "Nitrosylation: the next phosphorylation?" Arch Biochem Biophys **408**(1): 1-6.

Marshall, H. E., D. T. Hess and J. S. Stamler (2004). "S-nitrosylation: physiological regulation of NF-kappaB." Proc Natl Acad Sci U S A **101**(24): 8841-8842.

Masri, F. A., S. A. Comhair, T. Koeck, W. Xu, A. Janocha, S. Ghosh, R. A. Dweik, J. Golish, M. Kinter, D. J. Stuehr, S. C. Erzurum and K. S. Aulak (2005). "Abnormalities in nitric oxide and its derivatives in lung cancer." Am J Respir Crit Care Med **172**(5): 597-605.

Matallanas, D., D. Romano, F. Al-Mulla, E. O'Neill, W. Al-Ali, P. Crespo, B. Doyle, C. Nixon, O. Sansom, M. Drosten, M. Barbacid and W. Kolch (2011). "Mutant K-Ras activation of the proapoptotic MST2 pathway is antagonized by wild-type K-Ras." Mol Cell **44**(6): 893-906.

Matzinger, S. A., B. Chen, Y. Wang, K. A. Crist, G. D. Stoner, G. J. Kelloff, R. A. Lubet and M. You (1997). "Tissue-specific expression of the K-ras allele from the A/J parent in (A/J x TSG-p53) F1 mice." Gene **188**(2): 261-269.

Mazur, P. K., B. M. Gruner, H. Nakhai, B. Sipos, U. Zimber-Strobl, L. J. Strobl, F. Radtke, R. M. Schmid and J. T. Siveke (2010). "Identification of epidermal Pdx1 expression discloses different roles of Notch1 and Notch2 in murine Kras(G12D)-induced skin carcinogenesis in vivo." PLoS One **5**(10): e13578.

Michel, T. and O. Feron (1997). "Nitric oxide synthases: which, where, how, and why?" J Clin Invest **100**(9): 2146-2152.

Michell, B. J., J. E. Griffiths, K. I. Mitchelhill, I. Rodriguez-Crespo, T. Tiganis, S. Bozinovski, P. R. de Montellano, B. E. Kemp and R. B. Pearson (1999). "The Akt kinase signals directly to endothelial nitric oxide synthase." Curr Biol **9**(15): 845-848.

Moncada, S. and A. Higgs (1993). "The L-arginine-nitric oxide pathway." N Engl J Med **329**(27): 2002-2012.

Mooi, W. J. and D. S. Peeper (2006). "Oncogene-induced cell senescence--halting on the road to cancer." N Engl J Med **355**(10): 1037-1046.

Mott, H. R., J. W. Carpenter and S. L. Campbell (1997). "Structural and functional analysis of a mutant Ras protein that is insensitive to nitric oxide activation." Biochemistry **36**(12): 3640-3644.

Nakamura, K., H. Ichise, K. Nakao, T. Hatta, H. Otani, H. Sakagami, H. Kondo and M. Katsuki (2008). "Partial functional overlap of the three ras genes in mouse embryonic development." Oncogene **27**(21): 2961-2968.

Nathan, C. and Q. W. Xie (1994). "Nitric oxide synthases: roles, tolls, and controls." Cell **78**(6): 915-918.

Nuzum, E. O., A. M. Malkinson and D. G. Beer (1990). "Specific Ki-ras codon 61 mutations may determine the development of urethan-induced mouse lung adenomas or adenocarcinomas." Mol Carcinog **3**(5): 287-295.

O'Hayer, K. M. and C. M. Counter (2006). "A genetically defined normal human somatic cell system to study ras oncogenesis in vivo and in vitro." Methods Enzymol **407**: 637-647.

Oliveira, J. B., N. Bidere, J. E. Niemela, L. Zheng, K. Sakai, C. P. Nix, R. L. Danner, J. Barb, P. J. Munson, J. M. Puck, J. Dale, S. E. Straus, T. A. Fleisher and M. J. Lenardo (2007). "NRAS mutation causes a human autoimmune lymphoproliferative syndrome." Proc Natl Acad Sci U S A **104**(21): 8953-8958.

Patek, C. E., M. J. Arends, W. A. Wallace, F. Luo, S. Hagan, D. G. Brownstein, L. Rose, P. S. Devenney, M. Walker, S. J. Plowman, R. L. Berry, W. Kolch, O. J. Sansom, D. J. Harrison and M. L. Hooper (2008). "Mutationally activated K-ras 4A and 4B both mediate lung carcinogenesis." Exp Cell Res **314**(5): 1105-1114.

Pignatelli, B., C. Q. Li, P. Boffetta, Q. Chen, W. Ahrens, F. Nyberg, A. Mukeria, I. Bruske-Hohlfeld, C. Fortes, V. Constantinescu, H. Ischiropoulos and H. Ohshima (2001). "Nitrated and oxidized plasma proteins in smokers and lung cancer patients." Cancer Res **61**(2): 778-784.

Pipas, J. M. (2009). "SV40: Cell transformation and tumorigenesis." Virology **384**(2): 294-303.

Plowman, S. J., D. J. Williamson, M. J. O'Sullivan, J. Doig, A. M. Ritchie, D. J. Harrison, D. W. Melton, M. J. Arends, M. L. Hooper and C. E. Patek (2003). "While K-ras is essential for mouse development, expression of the K-ras 4A splice variant is dispensable." Mol Cell Biol **23**(24): 9245-9250.

Prior, I. A., P. D. Lewis and C. Mattos (2012). "A comprehensive survey of Ras mutations in cancer." Cancer Res **72**(10): 2457-2467.

Puhakka, A., V. Kinnula, U. Napankangas, M. Saily, P. Koistinen, P. Paakko and Y. Soini (2003). "High expression of nitric oxide synthases is a favorable prognostic sign in non-small cell lung carcinoma." APMIS **111**(12): 1137-1146.

Pylayeva-Gupta, Y., E. Grabocka and D. Bar-Sagi (2011). "RAS oncogenes: weaving a tumorigenic web." Nat Rev Cancer **11**(11): 761-774.

Quilliam, L. A., J. F. Rebhun and A. F. Castro (2002). "A growing family of guanine nucleotide exchange factors is responsible for activation of Ras-family GTPases." Prog Nucleic Acid Res Mol Biol **71**: 391-444.

Quintanilla, M., K. Brown, M. Ramsden and A. Balmain (1986). "Carcinogen-specific mutation and amplification of Ha-ras during mouse skin carcinogenesis." Nature **322**(6074): 78-80.

Raines, K. W., M. G. Bonini and S. L. Campbell (2007). "Nitric oxide cell signaling: S-nitrosation of Ras superfamily GTPases." Cardiovasc Res **75**(2): 229-239.

Raines, K. W., G. L. Cao, E. K. Lee, G. M. Rosen and P. Shapiro (2006). "Neuronal nitric oxide synthase-induced S-nitrosylation of H-Ras inhibits calcium ionophore-mediated extracellular-signal-regulated kinase activity." Biochem J **397**(2): 329-336.

Razzaque, M. A., Y. Komoike, T. Nishizawa, K. Inai, M. Furutani, T. Higashinakagawa and R. Matsuoka (2012). "Characterization of a novel KRAS mutation identified in Noonan syndrome." Am J Med Genet A **158A**(3): 524-532.

Reynaert, N. L., K. Ckless, S. H. Korn, N. Vos, A. S. Guala, E. F. Wouters, A. van der Vliet and Y. M. Janssen-Heininger (2004). "Nitric oxide represses inhibitory kappaB kinase through S-nitrosylation." Proc Natl Acad Sci U S A **101**(24): 8945-8950.

Roberts, P. J. and C. J. Der (2007). "Targeting the Raf-MEK-ERK mitogen-activated protein kinase cascade for the treatment of cancer." Oncogene **26**(22): 3291-3310.

Rothwarf, D. M. and M. Karin (1999). "The NF-kappa B activation pathway: a paradigm in information transfer from membrane to nucleus." Sci STKE **1999**(5): RE1.

Sakano, K., S. Oikawa, Y. Hiraku and S. Kawanishi (2002). "Metabolism of carcinogenic urethane to nitric oxide is involved in oxidative DNA damage." Free Radic Biol Med **33**(5): 703-714.

Sarkisian, C. J., B. A. Keister, D. B. Stairs, R. B. Boxer, S. E. Moody and L. A. Chodosh (2007). "Dose-dependent oncogene-induced senescence in vivo and its evasion during mammary tumorigenesis." Nat Cell Biol **9**(5): 493-505.

Schubbert, S., K. Shannon and G. Bollag (2007). "Hyperactive Ras in developmental disorders and cancer." Nat Rev Cancer **7**(4): 295-308.

Schuhmacher, A. J., C. Guerra, V. Sauzeau, M. Canamero, X. R. Bustelo and M. Barbacid (2008). "A mouse model for Costello syndrome reveals an Ang II-mediated hypertensive condition." J Clin Invest **118**(6): 2169-2179.

Serrano, M., A. W. Lin, M. E. McCurrach, D. Beach and S. W. Lowe (1997). "Oncogenic ras provokes premature cell senescence associated with accumulation of p53 and p16INK4a." Cell **88**(5): 593-602.

Sethi, G., B. Sung and B. B. Aggarwal (2008). "Nuclear factor-kappaB activation: from bench to bedside." Exp Biol Med (Maywood) **233**(1): 21-31.

Shen, H. M. and V. Tergaonkar (2009). "NFkappaB signaling in carcinogenesis and as a potential molecular target for cancer therapy." Apoptosis **14**(4): 348-363.

Singh, S. and A. K. Gupta (2011). "Nitric oxide: role in tumour biology and iNOS/NO-based anticancer therapies." Cancer Chemother Pharmacol **67**(6): 1211-1224.

Smith, M. J., B. G. Neel and M. Ikura (2013). "NMR-based functional profiling of RASopathies and oncogenic RAS mutations." Proc Natl Acad Sci U S A **110**(12): 4574-4579.

Stamler, J. S., S. Lamas and F. C. Fang (2001). "Nitrosylation. the prototypic redox-based signaling mechanism." Cell **106**(6): 675-683.

Stathopoulos, G. T., T. P. Sherrill, D. S. Cheng, R. M. Scoggins, W. Han, V. V. Polosukhin, L. Connelly, F. E. Yull, B. Fingleton and T. S. Blackwell (2007). "Epithelial NF-kappaB activation promotes urethane-induced lung carcinogenesis." Proc Natl Acad Sci U S A **104**(47): 18514-18519.

Stites E. C. doi: http://dx.doi.org/10.1101/005397

Switzer, C. H., R. Y. Cheng, L. A. Ridnour, S. A. Glynn, S. Ambs and D. A. Wink (2012). "Ets-1 is a transcriptional mediator of oncogenic nitric oxide signaling in estrogen receptor-negative breast cancer." Breast Cancer Res **14**(5): R125.

Takai, Y., T. Sasaki and T. Matozaki (2001). "Small GTP-binding proteins." Physiol Rev **81**(1): 153-208.

To, M., R. Rosario, P. Westcott, K. Banta and A. Balmain (2013). "Interactions between wild-type and mutant Ras genes in lung and skin carcinogenesis." Oncogene **32**(34): 4028-4033.

To, M. D., C. E. Wong, A. N. Karnezis, R. Del Rosario, R. Di Lauro and A. Balmain (2008). "Kras regulatory elements and exon 4A determine mutation specificity in lung cancer." Nat Genet **40**(10): 1240-1244.

Tuveson, D. A., A. T. Shaw, N. A. Willis, D. P. Silver, E. L. Jackson, S. Chang, K. L. Mercer, R. Grochow, H. Hock, D. Crowley, S. R. Hingorani, T. Zaks, C. King, M. A. Jacobetz, L. Wang, R. T. Bronson, S. H. Orkin, R. A. DePinho and T. Jacks (2004). "Endogenous oncogenic K-ras(G12D) stimulates proliferation and widespread neoplastic and developmental defects." Cancer Cell **5**(4): 375-387.

Umanoff, H., W. Edelmann, A. Pellicer and R. Kucherlapati (1995). "The murine N-ras gene is not essential for growth and development." Proc Natl Acad Sci U S A **92**(5): 1709-1713.

Vigil, D., J. Cherfils, K. L. Rossman and C. J. Der (2010). "Ras superfamily GEFs and GAPs: validated and tractable targets for cancer therapy?" Nat Rev Cancer **10**(12): 842-857.

Voice, J. K., R. L. Klemke, A. Le and J. H. Jackson (1999). "Four human ras homologs differ in their abilities to activate Raf-1, induce transformation, and stimulate cell motility." J Biol Chem **274**(24): 17164-17170.

Whyte, D. B., P. Kirschmeier, T. N. Hockenberry, I. Nunez-Oliva, L. James, J. J. Catino, W. R. Bishop and J. K. Pai (1997). "K- and N-Ras are geranylgeranylated in cells treated with farnesyl protein transferase inhibitors." J Biol Chem **272**(22): 14459-14464.
Williams, J. G., K. Pappu and S. L. Campbell (2003). "Structural and biochemical studies of p21Ras S-nitrosylation and nitric oxide-mediated guanine nucleotide exchange." Proc Natl Acad Sci U S A **100**(11): 6376-6381.

Willumsen, B. M., K. Norris, A. G. Papageorge, N. L. Hubbert and D. R. Lowy (1984). "Harvey murine sarcoma virus p21 ras protein: biological and biochemical significance of the cysteine nearest the carboxy terminus." EMBO J **3**(11): 2581-2585.

Wink, D. A., H. B. Hines, R. Y. Cheng, C. H. Switzer, W. Flores-Santana, M. P. Vitek, L. A. Ridnour and C. A. Colton (2011). "Nitric oxide and redox mechanisms in the immune response." J Leukoc Biol **89**(6): 873-891.

Woodworth, C. D., E. Michael, L. Smith, K. Vijayachandra, A. Glick, H. Hennings and S. H. Yuspa (2004). "Strain-dependent differences in malignant conversion of mouse skin tumors is an inherent property of the epidermal keratinocyte." Carcinogenesis **25**(9): 1771-1778.

Xiao, G., A. B. Rabson, W. Young, G. Qing and Z. Qu (2006). "Alternative pathways of NF-kappaB activation: a double-edged sword in health and disease." Cytokine Growth Factor Rev **17**(4): 281-293.

Xu, J. (2005). "Preparation, culture, and immortalization of mouse embryonic fibroblasts." Curr Protoc Mol Biol **Chapter 28**: Unit 28 21.

Yan, J., S. Roy, A. Apolloni, A. Lane and J. F. Hancock (1998). "Ras isoforms vary in their ability to activate Raf-1 and phosphoinositide 3-kinase." J Biol Chem **273**(37): 24052-24056.

Yang, G. Y., S. Taboada and J. Liao (2009). "Induced nitric oxide synthase as a major player in the oncogenic transformation of inflamed tissue." Methods Mol Biol **512**: 119-156.

You, M., U. Candrian, R. R. Maronpot, G. D. Stoner and M. W. Anderson (1989). "Activation of the Ki-ras protooncogene in spontaneously occurring and chemically induced lung tumors of the strain A mouse." Proc Natl Acad Sci U S A **86**(9): 3070-3074.

Young, A., D. Lou and F. McCormick (2013). "Oncogenic and wild-type Ras play divergent roles in the regulation of mitogen-activated protein kinase signaling." Cancer Discov **3**(1): 112-123.

Yu, C. X., S. Li and A. R. Whorton (2005). "Redox regulation of PTEN by S-nitrosothiols." Mol Pharmacol **68**(3): 847-854.

Yumi Yamamoto, U. N. V., Shashi Prajapati, Youn-Tae Kwak and R. B. Gaynor (2003). "histone H3 phosphorylation by IKKalpha is critical for cytokine-induced gene expression." Nature **243**: 655-659.

Zandi, E., D. M. Rothwarf, M. Delhase, M. Hayakawa and M. Karin (1997). "The IkappaB kinase complex (IKK) contains two kinase subunits, IKKalpha and IKKbeta, necessary for IkappaB phosphorylation and NF-kappaB activation." Cell **91**(2): 243-252.

Zhang, F. L., P. Kirschmeier, D. Carr, L. James, R. W. Bond, L. Wang, R. Patton, W. T. Windsor, R. Syto, R. Zhang and W. R. Bishop (1997). "Characterization of Ha-ras, N-ras, Ki-Ras4A, and Ki-Ras4B as in vitro substrates for farnesyl protein transferase and geranylgeranyl protein transferase type I." J Biol Chem **272**(15): 10232-10239.

Zhang, Y., A. Keszler, K. A. Broniowska and N. Hogg (2005). "Characterization and application of the biotin-switch assay for the identification of S-nitrosated proteins." Free Radic Biol Med **38**(7): 874-881.

Zhang, Z., Y. Wang, H. G. Vikis, L. Johnson, G. Liu, J. Li, M. W. Anderson, R. C. Sills, H. L. Hong, T. R. Devereux, T. Jacks, K. L. Guan and M. You (2001). "Wildtype Kras2 can inhibit lung carcinogenesis in mice." Nat Genet **29**(1): 25-33.

Biography

I was born on February 22nd, 1985 in Nanchang City, Jiangxi Province, China. I matriculated at East China Normal University in Shanghai in 2001 and graduated with a Bachelor of Science degree in biotechnology in 2005. Then I spent three years as a graduate student in Professor Jinglun Xue's Gene Therapy Group in Fudan University, and received my Master of Science degree in genetics in 2008. I came to the United States and became a graduate student in PhD program of Molecular Cancer Biology at Duke University in August 2008. After rotations in three labs, I joined the lab of Professor Christopher Counter in May 2009, where I began my investigation on RAS tumorigenesis and the role of protein *S*-nitrosylation in tumorigenesis.

Selected Publications:

Huang, L. and Counter C. M. (2015) Reduced $HRAS^{G12V}$-driven tumorigenesis of cells expressing $KRAS^{C118S}$. *PLoS ONE. In minor revision.*

Huang, L., Carney, J., Cardona, D. M., and Counter C. M. (2014) Decreased tumorigenesis in mice with a *Kras* point mutation at C118. *Nature Communications*. 5:5410

Huang, L., Xu, G., Zhang, J., Tian, L., Xue, J., Chen, J., and Jia, W. (2008) Daxx interacts with HIV-1 integrase and inhibits lentiviral gene expression. *Biochemical and Biophysical Research Communications* **373:** 241-245